Interdigital Dielectrometry Based Detection and Identification of Dangerous Materials for Security Applications

by

Jason Sears

B.A.Sc., University of Toronto (2001)
Submitted to the Department of Electrical Engineering and Computer Science
in partial fulfillment of the requirements for the degree of

Master of Science

at the

MASSACHUSETTS INSTITUTE OF TECHNOLOGY

August 2003

Signature of Author .....
Department of Electrical Engineering and Computer Science
29 August 2003

Certified by .....
Markus Zahn
Professor of Electrical Engineering
Thesis Supervisor

Accepted by .....
Arthur C. Smith
Chairman, Committee on Graduate Students

Interdigital Dielectrometry Based Detection and Identification of Dangerous Materials for Security Applications

by

Jason Sears

Submitted to the Department of Electrical Engineering and Computer Science
on 29 August 2003, in partial fulfillment of the
requirements for the degree of
Master of Science

Abstract

Recent terrorist threats have increased the attention paid to searching airline passengers for dangerous and explosive materials. In particular, the possibility that terrorists might hide explosives in shoes has prompted most airline screening stations to require that shoes be removed for x-ray inspection. This thesis is a preliminary investigation of an interdigital dielectrometry based method that could safely and accurately determine the material content within shoes while they are worn. Theoretical modeling of the sensor and the representative materials under test were conducted with the finite element analysis package Maxwell from Ansoft Corp. and analytic/numerical mathematical models for material property estimation. The studies show that dangerous materials hidden in the sole of a shoe could be detected and identified if they lie within the penetration depth of the sensor and if they are sufficiently different in their complex dielectric properties from the normal shoe material. Perliminary finite element computer simulations were also performed to show the effects of sensing electrode segmentation on improving the penetration depth of the electric field, but at the cost of reduced signal strength. Experiments using interdigital sensors with wavelengths ranging from 1 mm to 40 mm in the frequency range of 0.005 Hz to 10 kHz first on homogeneous materials such as air, sand, sugar, salt, wood, Lexan, Teflon, and paper and later on actual shoes with cavities containing foreign materials show that the materials can be identified based on their complex dielectric properties as extracted from experimental data using an inverse parameter solver for material property estimation. The ability of the dielectrometry system to precisely identify materials from a database is presenty limited by measurement noise, contact quality and sample placement inconsistency. Likewise, variations due to moisture content and other contamination present challenges to future development of the technology.

Thesis Supervisor: Markus Zahn
Title: Professor of Electrical Engineering

Acknowledgments

I am indebted to Professor Markus Zahn, my research supervisor, for his enthusiasm and patience with me in my first year at MIT. I thank him for his passionate interest in the subject and the friendly way that he teaches. I thank my family for their support and their good advice. I am grateful for my friendship with Evelyn, who provided more motivation than she knows for me to finish this work. Finally I thank all the members of the MIT Cycling Team and my roommates at the Pirate House for the distractions they created.

Contents

List of Figures

Part I

Introduction to Dielectrometry Technology

Chapter 1

Introduction

1.1 Introduction to Dielectrometry

Interdigital dielectrometry is a method of measuring the electric properties of dielectric materials. An electric field is imposed in the material under test (MUT) by a pair of electrodes, and the transcapacitance and transconductance between the electrode pair is measured. An analytical/numerical model of the sensor system is used to solve for such unknown quantities as material thickness and material complex dielectric constant from the measured impedance or admittance values.

The electrodes of the dielectrometry sensor are spatially periodic coplanar metal traces on an insulating substrate, arranged side-by-side and separated by a fixed spacing. The electrode pair is made to cover a substantial area by connecting many repeated fingers such that two interleaved comb patterns are formed, as illustrated in Figure 1-1.

The sensor pad containing the driving/sensing electrode pair is placed in proximity to the material sample and driven by a sinusoidal voltage over a controlled frequency range. The resulting electric field is spatially periodic in the plane of the sensor with fundamental wavelength λ, due to the repetition of the electrode fingers, and decays exponentially away from the sensor surface, penetrating the material sample to a limited depth that is proportional to the spatial wavelength of the electrodes. The drive voltage is sinusoidal in time and generally all materials are linear but lossy dielectrics. The sensing electrode voltage or current is at the frequency of the driving voltage but is out of phase for lossy dielectrics. The electric field is governed

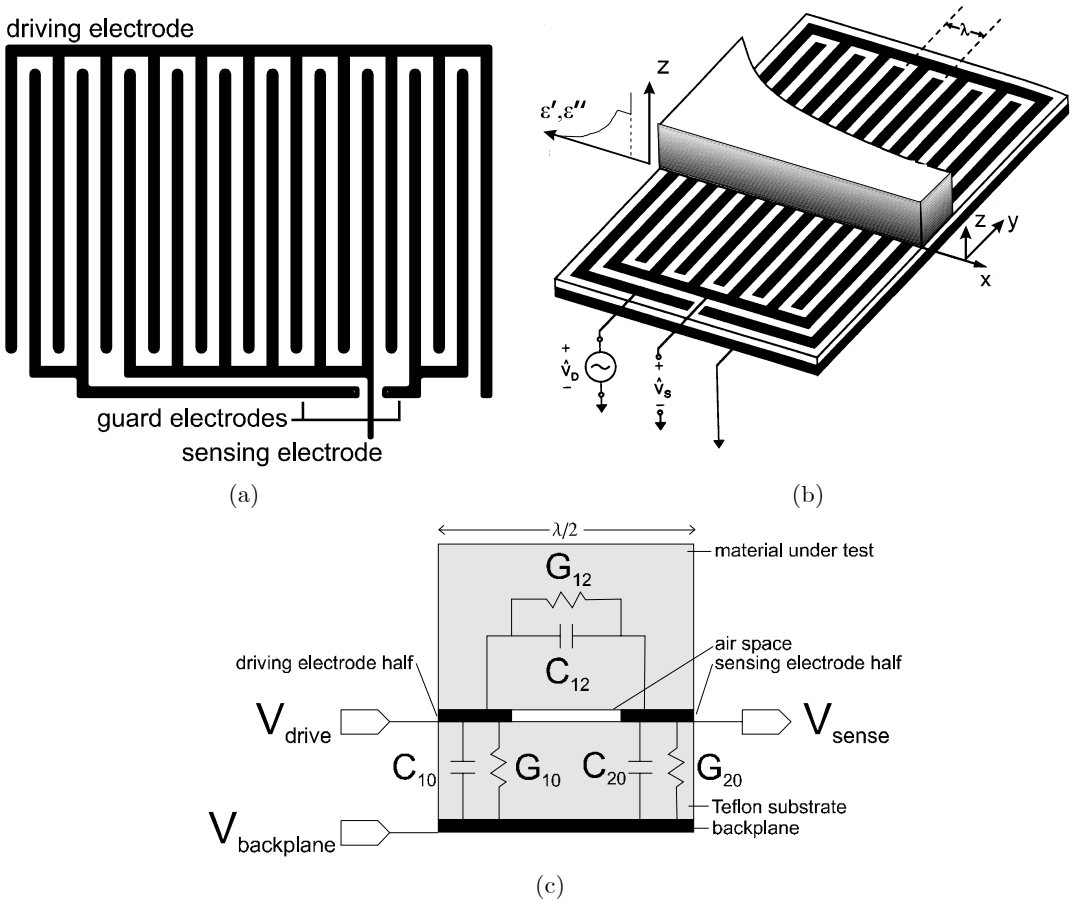

Figure 1-1: *The interdigital electrode pair (a) shows two interleaved combs that increase the surface area covered by the electrodes. A schematic with a representative material sample under test (b) shows the electrical connections to the sensor and the exponential decay of the electric field as it penetrates the material. One wavelength of the sensor is defined as the fundamental spatial period between a pair of driving or sensing electrode fingers. A one half wavelength section of the sensor, (c), shows the drive, sense and backplane electrodes together with the electrical equivalent circuit for the transconductance and transcapacitance for the material under test and for the substrate.*

by the dielectric property profiles and geometry of the material under test. As a result the transcapacitance and transconductance of the electrodes are related to the material sample's complex dielectric constant. An analytical/computational model of the sensor and material sample is used to calculate the complex dielectric constant as a function of frequency and the thickness of the material sample from the measured capacitance and conductance.

The nominal value and frequency dispersive nature of the complex dielectric constant are unique indicators of a material's identity. Given the complex dielectric constant as a function of frequency derived from the interdigital dieletrometry measurements, and a knowledge base of the electric character of all candidate materials, the particular sample material(s) can be identified.

If several sensors of differing spatial periodicity are used, then the added measurement data can be used to compute the thicknesses and properties of each of the multiple layers of differing materials. One sensor is required for each data quantity that is to be computed. Thus, if both the thickness and the complex dielectric constant of a material under test are desired, then data from at least two sensors of different spatial periods are required. Using more sensors than are required over-constrains the computation and a least-squares best fit can be applied to refine the output. If the material under test instead has a smoothly varying dielectric profile for which a parametric function is known, the measured data can be applied to the function to solve for the parameters. For example, one application of dielectrometry is to measure the moisture concentration profile in transformer pressboard [12]. A physical model based on diffusion laws describes the possible profiles of moisture concentration as a function of several parameters. Measuring the pressboard with a three wavelength sensor allows three parameters to be solved for and thus the moisture profile to be known in a smoothed stepwise layer approximation. This measurement would be difficult to do otherwise because the pressboard is only millimeters thick.

The dielectrometry sensor can be connected to the sensing electronics in several ways, pictured in Figure 1-2. These configurations have been studied and redesigned in the past because when they are done correctly, stray capacitances can be eliminated from the measurement. All three methods described in this thesis incorporate a metal backplane below the sensor substrate (pictured in Figure 1-1(c) and guard fingers at the side of the sensor that resemble the

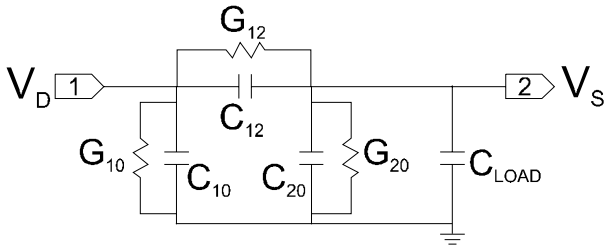

(a) The backplane and guard fingers are grounded, so an unwanted admittance with conductance G_{20} and capacitance C_{20} exists between them and the sensing electrode.

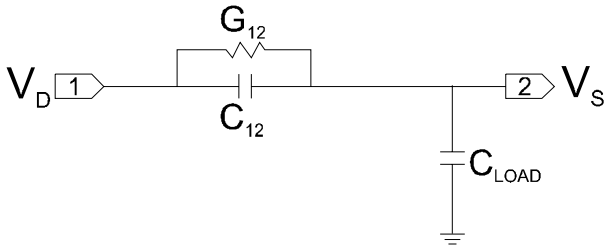

(b) The Floating Voltage with Guard Plane Mode method (abbreviated FVGPM) eliminates the admittance between the backplane and the sensing electrode by driving the backplane and guard fingers at the sensing electrode potential with a voltage follower.

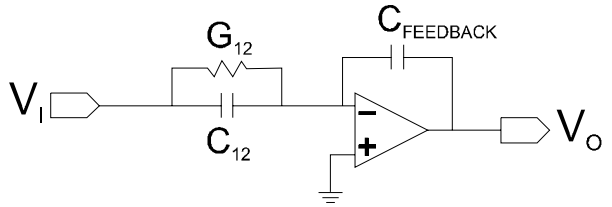

(c) The Short Circuit Current Mode (abbreviated SCCM) method eliminates the admittance between the backplane and sensing electrode and also has the convenience of a grounded backplane and guard fingers.

Figure 1-2: *Three methods for connecting the dielectrometry sensor electrodes to voltage signal sensing electronics.*

sensing fingers but are electrically isolated from them (pictured in Figure 1-1(a)). The backplane reduces the contribution to the measurement of materials below the sensor plane, while the guard fingers serve to improve the approximation that the sensor extends infinitely in the plane. The first connection method is to ground the backplane and guard fingers and allow the sensing electrode potential to float while measuring it. There exists an undesired admittance between the backplane/guard finger node and the sensing electrode which affects the measurement. The second method eliminates this undesired admittance by driving the backplane and guard fingers at the sensing electrode voltage using a voltage follower. This method is known as the Floating Voltage with Guard Plane Mode, or FVGPM, and minimizes the effect of substrate properties. The last method simplifies the electronics by grounding the backplane and guard fingers, and virtually grounding the sensing electrode but measuring the current through it. The current measurement is achieved by charging the feedback capacitor of an integrating opamp and measuring its output voltage. This method has the advantage that the admittance between the backplane, guard fingers and sensing electrode is eliminated, with the convenience of a grounded backplane and guard fingers to enhance shielding from noise. This method is called the Short Circuit Current Mode, or SCCM. These three methods are described in detail in Section 5.2.

1.2 Background of Dielectrometry Research Applications at MIT

Early research in interdigital dielectrometry at MIT under Professor S.D. Senturia was based on sensors printed with integrated circuit technology. The "microsensors" had very small wavelengths of order 1 μm and were applied to measure the properties of moisture sensitive thin film polyethylene oxide ([1], 1980) or the cure state of epoxy resin ([2], 1982; [4], 1985). In [4] Coln described a virtually grounded sensing electrode that is similar to the short circuit current sensor used for much of the experimentation in this thesis. The early research focused primarily on the transistor level design of the sensing and driving electronics that interfaced to the interdigital dielectrometry electrodes.

Sensors with longer wavelengths of order 1 mm were investigated by students under Professor J.R. Melcher, generally with the focus on monitoring transformer oil and electrical insulation

materials. This research provided the fundamental basis for subsequent dielectrometry research conducted to the present at the Laboratory for Electromagnetic and Electronic Systems. M.C. Zaretsky in ([5], 1987) introduced a continuum model that can be solved inversely to find continuum parameters from experimental data, which formed the basis for the present mathematical models. Zaretsky also introduced the notion of ω-κ imposed dielectrometry by using 50 μm and 1 mm wavelength sensors to estimate spatial distributions in heterogeneous material. He also described the π network equivalent circuit that approximates the circuit topology of the dielectrometry sensor. P. Li interpreted the shape of the gain and phase responses versus frequency as they reflect the permittivity, conductivity and dispersive properties of homogeneous and heterogeneous material layers in ([6], 1987).

Tragically Professor Melcher passed away in 1991. The dielectrometry research was carried on by Professor M. Zahn and his students. P.A. von Guggenberg, Y. Sheiretov and later Y. Du studied the measurement of transformer pressboard moisture content using the three wavelength sensor originally developed by von Guggenberg in ([7], 1993; [8], 1994 and [12], 1999). Von Guggenberg's three wavelength sensor used a Kapton substrate. Since Kapton is hydrophilic, the ambient humidity affected the sensor's permittivity and conductivity. To avoid this, the sensor had to be coated with Parylene. A. Mamishev, working with Du, developed the hydrophobic Teflon substrate three wavelength sensor which did not require a Parylene coating. Mamishev ([10], 1999) and Lu ([11], 1999) applied dielectrometry sensor technology to landmine detection.

A student beginning research in the field of dielectrometry would benefit greatly by reading the theses [1] to [4] and especially [5] to [12], and the published papers [13] to [24], while being introduced to the dielectrometry measurement equipment but before beginning serious experimental analysis.

Model based interdigital dielectrometry developed in the Laboratory for Electromagnetic and Electronic Systems at MIT for non-destructive testing and evaluation measurements in electric power apparatus use spatially periodic electrodes and windings excited by sinusoidal time varying signals to generate spatially and temporally periodic electric and magnetic fields. Dielectrometry is the science of measurement of material properties that govern the quasistatic distribution of electric field within a weakly conducting dielectric material excited by charged

metallic electrodes.

Previous electromagnetic modeling has developed continuum models for quasistatic interdigital capacitive sensors. The detection method measures the electrode or winding impedance or admittance as a function of radian frequency and sensor position to measure spatial profiles of dielectric permittivity and electrical conductivity. From changes in signal response with sensor position and from frequency spectroscopy signatures of materials it is possible to identify the presence and location of objects and to identify specific materials from the change in the materials electrical properties with frequency. Originally, dielectrometers utilized a voltage stressed parallel plate electrode structure that applied the electric field from both sides of a lossy dielectric. These arrangements have been improved with MIT developed coplanar electrode arrangements that permit measurements to be made from a single side. These interdigital geometries allow model based predictive capability from physical, analytical, and numerical models that greatly reduces the effort required to design an optimal sensor for a particular application and has the interpretative capability to permit determination of material property profiles as a function of time and space with reduced dependence on empirical calibration standards. Figure 2 shows the MIT designed and tested three wavelength dielectrometry sensor on a Teflon substrate used in successful moisture diffusion measurements in transformer board. Such a sensor structure is inexpensive and lightweight because it is nothing more than etched copper on a Teflon substrate from commercially available Teflon that is copper coated on both sides.

Because of the model-based nature of the sensor technology it is possible to pre-compute many possible material combinations and configurations and store the results in look-up tables for quick computer assessment, display, and decision making.

Significant general applications of these dielectric sensors include material characterization; non-destructive testing and evaluation; health monitoring of electric power apparatus and civil and aerospace structures (e.g., moisture, corrosion, cracks, etc.), and sub-surface detection of buried objects (e.g., landmines, UXOs).

The proposed security application concept is motivated by the recent event of Richard Reid hiding explosive material in his sneakers on American Airlines 63 on Dec. 22, 2001 and then boarding a plane undetected. This event now causes special and time consuming attention

to footwear at airport security stations and results in inconvenience to all passengers. To improve the quality and speed of footwear detection this proposal envisions a security floor-pad embedded with dielectrometry and magnetometry sensors that every air passenger stands on passing through the security gate. A frequency sweep of sensors determines in a fraction of a second whether the shoe contains dangerous materials as identified by signatures in dielectric, conductivity, and magnetic spectroscopy measurements. Such a floor-pad could also include an overlay that completely surrounds a shoe like a glove to more thoroughly test the entire volume of a shoe and its contents for dangerous materials. To minimize air-gap effects, vacuum can be used so that the sensor overlay hugs the shoe so that the sensors have intimate contact with the shoe. This detection method can be similarly performed over the entire body of a person by using a closely-fitting body-suit or surrounding cage structure well-instrumented with dielectrometry and magnetometry sensors. Such measurements can be used, for example, to detect and identify hidden explosives, illegal drugs, as well as conventional forbidden items such as guns and knives. With the anticipated operation of these sensors at frequencies above 1 kHz, the entire measurement interval from initiation of a frequency sweep to deciding if concealed dangerous materials are present can be done in a fraction of a second.

Figure 1-3 shows the present generation of MIT hardware with a computerized controller, interface box, and three wavelength sensor to perform dielectrometry measurements on the heel of a shoe under test. New sensors produced as part of the work for this thesis are shown next to the existing three wavelength sensors and a sample shoe in Figure 1-4.

1.3 Scope of the Thesis

This thesis is divided into four parts. The first part is the Introduction. The second part, Theory of Dielectrometry, contains a discussion of the interdigital sensor's equivalent circuit in Chapter 2 with a comparison to sample cases of common combinations of layered materials under test. Chapter 3 describes a procedure for solving for the admittance matrix of the sensor using Ansoft's Maxwell 2D field simulator and gives the results from simulations of segmented sensors. Chapter 4 compares measurements to the results of forward parameter solver GETGP3 which calculates the sensing voltage or current gain and phase from material

Figure 1-3: *The three wavelength sensor measuring the material of a shoe, connected to the sensing electronics and a PC used for logging data. A second three wavelength sensor stands next to the interface box to show the sensor's appearance.*

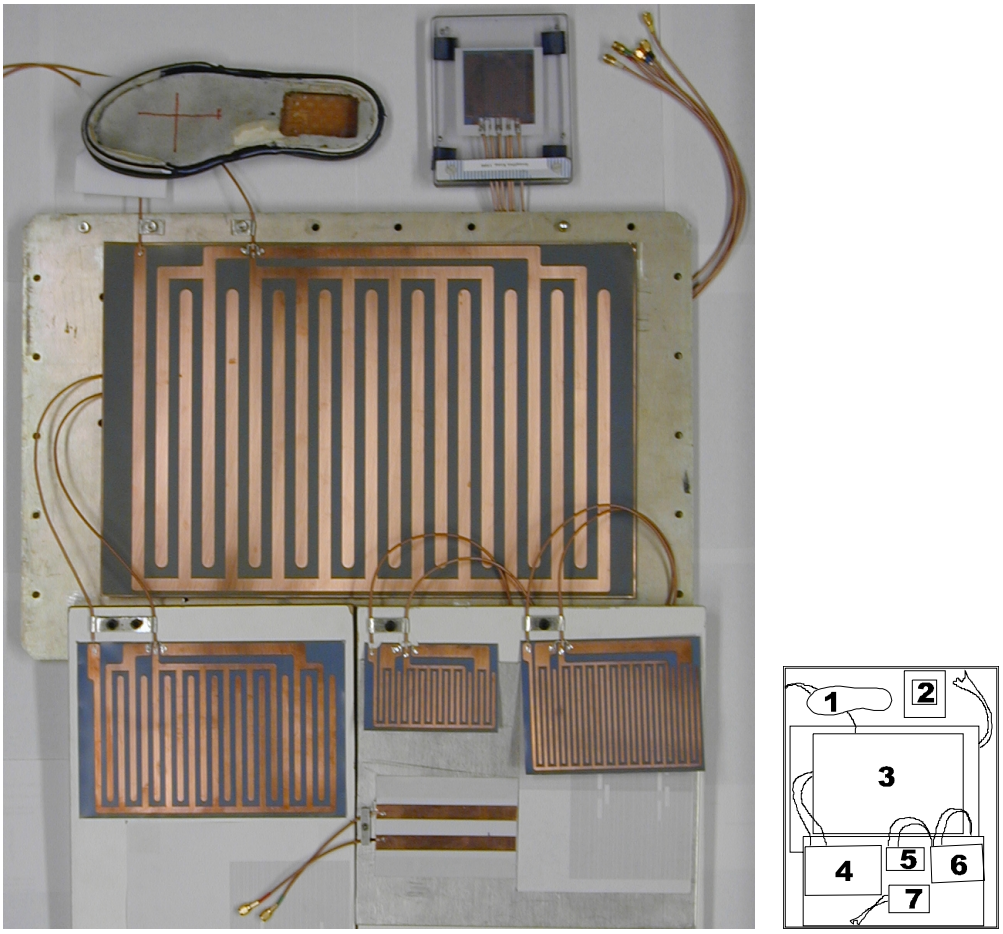

(a) (b)

Figure 1-4: *1. Sample shoe with heel cavity for placing materials under test; 2. Three wavelength sensor with wavelengths of 1 mm, 2.5 mm and 5 mm; 3. 40 mm wavelength sensor; 4. 20 mm wavlength sensor; 5. small area 10 mm wavelength sensor; 6. large area 10 mm wavelength sensor; 7. two strip sensor with wavelength approximately 50 mm.*

properties and geometry, and to the inverse parameter solver ESTLSQ, which calculates the complex permittivity geometry from gain and phase values. The third part of this thesis is Experiments. In Chapter 5, three measurement methods are described in detail, and the testing of the equipment to make sure it is working properly is outlined. Chapter 6 describes the results of dielectrometry experiments on samples-under-test including basic homogeneous materials and then actual cutout shoes filled with various materials, as simulated explosives. The fourth part, Summary and Future Work, gives suggestions for continuing the development of detection and identification of dangerous materials for security applications.

Part II

Theory of Dielectrometry

Chapter 2

The Equivalent Circuit

2.1 General Equivalent Circuit

The interdigital dielectrometry sensor can be modelled as the discrete circuit of Figure 2-1(b) where the conductance $G_{12}(\omega)$ and capacitance $C_{12}(\omega)$ are functions of frequency, and either of them may have negative values at some frequencies. Neither the conductance nor the capacitance between the sensing and driving electrodes need be constant with frequency because the interdigital dielectrometry sensor and material under test do not usually consist of one homogeneous material ([10], pp 241). This is true even when the complex dielectric constants of all materials in the problem are not functions of frequency (i.e., the materials are non-dispersive). Importantly, the plots of gain and phase versus frequency produced by a frequency sweep of the dielectrometry sensor can have quite distinct features (extrema and breakpoints) that are caused entirely by the combination of non-dispersive materials on top of the sensor and not by frequency dependent complex dielectric constants. In general for non-dispersive materials, the sensor can only be represented by a distributed circuit of an infinite number of frequency-independent capacitive and conductive elements in a two-dimensional ladder network such as the one illustrated in Figure 2-1(a). The distributed circuit can be reduced to the simple capacitive and conductive networks of Figures 2-1(b) and 2-1(c) where the transcapacitance $C_{12}(\omega)$ and transconductance $G_{12}(\omega)$ are frequency-dependent ([10], pp. 246).

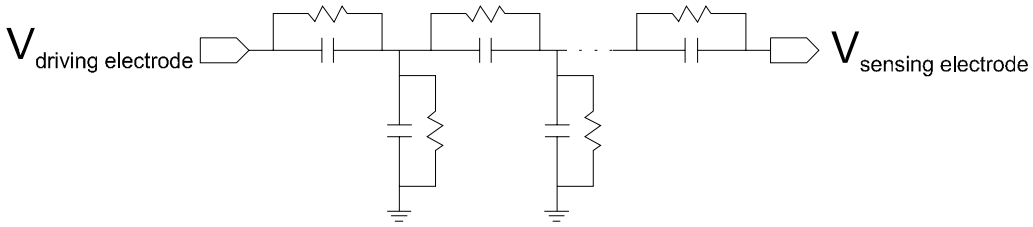

(a) The general distributed circuit of frequency independent elements representing an interdigital dielectrometry sensor. The shunt elements to ground are due to current flow through and capacitance of the surface charge distribution along the interface between drive and sense electrodes and between the dielectric under test and substrate.

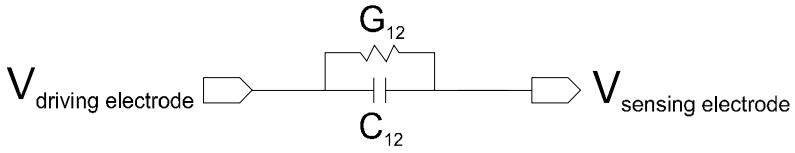

(b) The general equivalent circuit for an interdigital dielectrometry sensor. Sensing electronics attached to the sensing electrode terminal contribute to the voltage gain's transfer function, so their configuration is important.

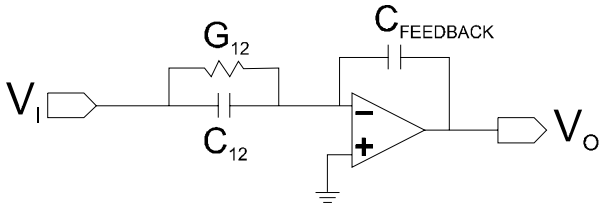

(c) The general equivalent circuit of a interdigital dielectrometry sensor, hooked up to a short circuit current mode (SCCM) signal sensing circuit.

Figure 2-1: *The general equivalent circuit of the sensor by itself and attached to a voltage or current sensing circuit.*

2.2 Mathematical Model Solvers: GETGP3, ESTLSQ, EST3

The dielectrometry sensor and material under test can also be modeled mathematically as a quasi-static electric fields problem. Three computer programs called GETGP3, ESTLSQ and EST3 that utilize such a model to relate the voltage gain transfer function to the material under test complex dielectric constants and layer thicknesses have been created by former students.

The GETGP3 parameter estimator is a software package created by former student Yanko Sheiretov (now Ian Shay). The software simulates the potential profile of the interdigitated dielectrometry sensors and returns the gain and phase of the voltage signal on the sensing electrode as a function of AC steady state frequency. It uses a mathematical continuum model and numerical techniques to calculate the electric field in the vicinity of the sensor. Some idealized assumptions are made in the model [27]. The program does not support dispersive sample materials per se, although such materials can be simulated by running it multiple times across a range of frequencies and substituting the appropriate values of the dispersive complex dielectric constant each time. The program almost always converges on a solution.

ESTLSQ is a companion package to GETGP3 and it solves the same problem but inversely. Given a gain∠phase measurement at a particular frequency, ESTLSQ calculates the complex dielectric constant and the thickness of the sample layers. ESTLSQ runs the forward model used in GETGP3 iteratively and finds a solution using a multidimensional Newton's method. It optimizes the solution using a least squares fit. The program can solve for up to as many variables (complex permittivity or layer thickness) as there are sensors. Additional variables must be known and given as inputs. It considers data points at distinct frequencies separately. EST3 is a subset of ESTLSQ that is capable of estimating a given number of parameters from gain-phase measurements taken with the *same number* of different sensors. EST3 sometimes does not converge on a solution.

2.3 Solutions from a mathematical model of the sensor

$G_{12}(\omega)$ and $C_{12}(\omega)$ of the general equivalent circuits in Figures 2-1(b) and 2-1(c) are almost always frequency dependent components. One special case where they are frequency-independent exists for a lossless substrate and material under test. The circuit forms a capacitive impedance

	Units	Single layer case	Two layer case
Top layer relative permittivity	-	-	5
Top layer conductivity	$\frac{\mu S}{m}$	-	10
Top layer thickness	mm	-	5000
Bottom layer relative permittivity	-	1,2,5	1,2,5
Bottom layer conductivity	$\frac{\mu S}{m}$	0,1,100	0,1,100
Bottom layer thickness	mm	50	5
Sensor wavelength λ	mm	5	5
Sensor substrate relative permittivity	-	2.1	2.1
Sensor substrate conductivity	$\frac{\mu S}{m}$	0	0
Sensor substrate normalized thickness $\frac{t}{\lambda}$	-	0.0508	0.0508
Normalized feedback capacitance $\frac{C_F}{M_L \epsilon_{substrate}}$	-	609	609

Table 2.1: The parameters used for the simulations of the one and two layer material under test cases in Figures 2-2 and 2-3 where sensor wavelength λ is the spatial periodicity of the sensor, t is the thickness and $\epsilon_{substrate}$ is the total permittivity of the substrate, C_F is the SCCM feedback capacitor and M_L is the total sensing electrode meander length equal to the length of each sensing electrode finger times the number of fingers.

divider with the voltage gain transfer function, $\widehat{G} = \frac{V_o}{V_i} = -\frac{C_{12}}{C_F}$. Both legs of the impedance divider are purely imaginary, and the frequency dependence of the capacitors cancels so that the response is independent of frequency. The Bode plot for this case is shown in Figure 2-2(a) for three permittivities with $\sigma = 0$. For single layers of a lossy material under test the equivalent capacitance and conductance are functions of frequency, as seen in the same Figure. The parameters of the material under test and of the sensor used in the simulations are given in Table 2.1. For configurations where the material under test consists of two distinct (possibly lossy) layers, the components $G_{12}(\omega)$ and $C_{12}(\omega)$ are also frequency dependent and exhibit breakpoints at two frequencies corresponding to weighted combinations of the two materials' properties and thicknesses. Figures 2-3(a) and 2-3(b) show the gain and phase components of Bode plots calculated using the forward solver GETGP3 for the two layer material under the test configurations of Figure 2-3(c). The test material consists of two layers capped by a grounded conducting plane. The curves for a conducting bottom layer show a behavior for a frequency dependent capacitance and conductance. Note that the frequency break point is increased by two decades when the conductivity of the bottom layer is increased by two orders of magnitude, demonstrating that those breakpoints are due to the conductivity of the bottom layer.

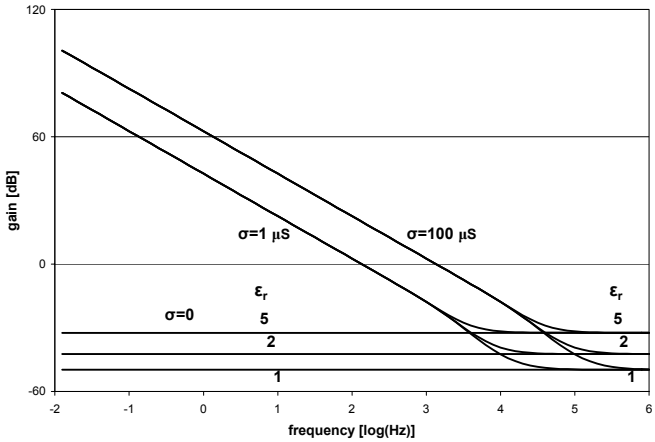

(a) The gain for nine cases of a single layer sample under test.

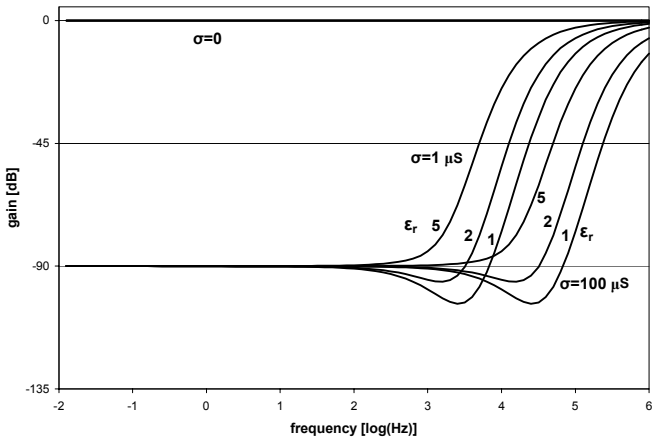

(b) The phase for nine cases of a single layer sample under test.

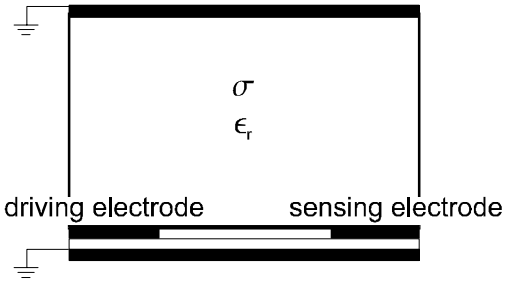

(c) A single layer sample under test where the complex dielectric constant is varied.

Figure 2-2: *A survey of calculated gain and phase responses using GETGP3 for a single layer of material under test that has three values of relative permittivity {1, 2, 5} and three values of conductivity {0, 1, 100} [uS/m], for a total of nine cases.*

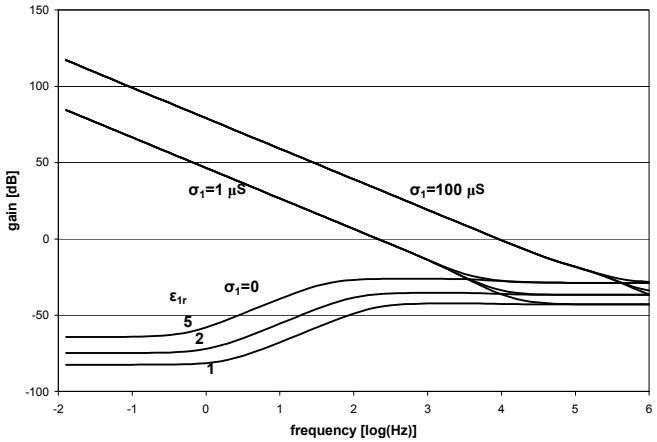

(a) The gain for nine cases of a two layer sample under test.

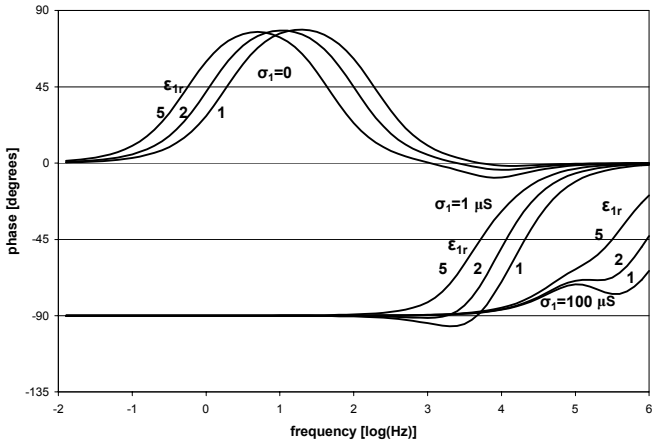

(b) The phase for nine cases of a two layer sample under test.

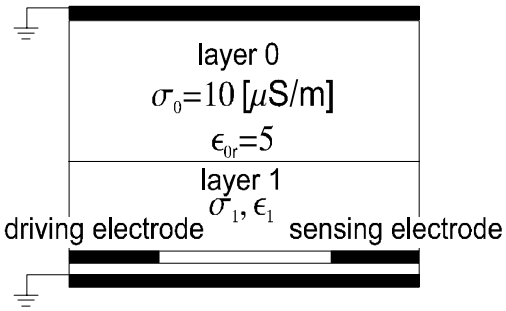

(c) A two layer sample under test where the bottom layer's complex dielectric constant is varied.

Figure 2-3: *A survey of calculated gain and phase responses using GETGP3 for two layers of material under test where the top layer has relative permittivity of 5 and conductivity of 10 [uS/m], and the bottom layer has three values of relative permittivity {1, 2, 5} and three values of conductivity {0, 1, 100} [uS/m], for a total of nine cases.*

2.4 Equivalent Circuits of Real Measurements

A simplified interdigital dielectrometry sensor can be made by placing two strips of conducting copper shielding adhesive tape side by side on a sheet of Teflon. While one strip (the driving electrode) is driven at a variable frequency sinusoidal voltage, the other strip (the sensing electrode) is attached to the inverting input of an integrating opamp which has a capacitor as its feedback path. The sensing electrode is held at ground potential by the opamp and the voltage output of the opamp is proportional to and lags by $\frac{\pi}{2}$ the sinusoidal current that is drawn from the sensing electrode. This sensing method is known as the short circuit current mode or SCCM. The sensor is placed with the copper strips facing up on a grounded plane and materials to be tested are set on top of the sensor. Such a sensor behaves approximately like the multi-fingered interdigital dielectrometry sensors that are used throughout this thesis, and is described in more detail in Section 6.6.3.

The simple material under test configurations of Section 2.3 can be used to understand frequency-dependent behavior in real measurements by using distinctly insulating and slightly conducting materials. A Staedtler rubber eraser is a good slightly conducting material, while a sheet of Teflon is almost a perfect insulator. The two materials were set up in four configurations on the simplified two strip sensor to represent the cases studied above. The configurations were air only; a layer of Teflon above the eraser; layers of Teflon above and below the eraser; and a layer of Teflon below the eraser. The gain and phase responses of these setups are illustrated in Figures 2-4(a) and 2-4(b), respectively. The measurement of air represents the purely capacitive circuit for a lossless substrate and material under test and has flat gain and a phase of zero that is not dependent on frequency. The measurement of the eraser with a Teflon layer above it represents the case for $\sigma_1 = 1$ or $\sigma_1 = 100$ from the previous section. The gain flattens at lower frequencies due to saturation of the integrating op amp, but would otherwise continue rising as the frequency decreases. The eraser with a Teflon layer both on top and below it behaves like the case where $\sigma_1 = 0$ in Figure 2-3 and also shows the predicted response, with a pole caused by the capacitance of the insulating Teflon layer at a frequency just below the zero. Finally the case of the eraser with a Teflon layer under it but not on top represents a circuit that is different from the cases analyzed in the previous section, because it has a connection to ground via the top grounded plate.

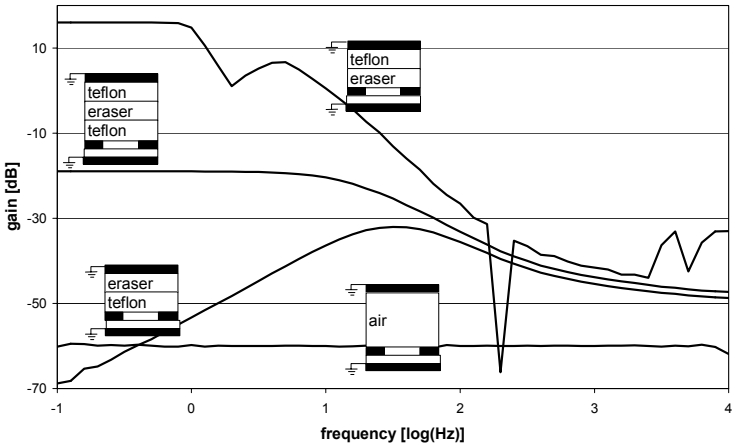

(a) Measured gain for various configurations of a Staedtler rubber eraser, a slight conductor, and Teflon, an insulator.

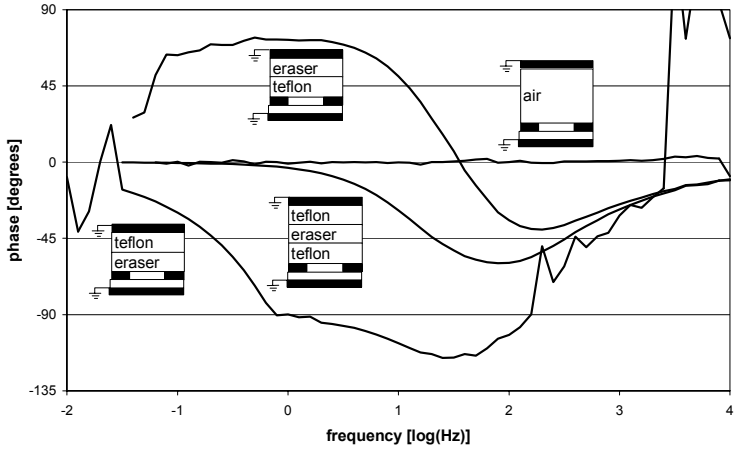

(b) Measured phase for various configurations of Staedtler rubber eraser, a slight conductor, and Teflon, an insulator.

Figure 2-4: *Different combinations of a good insulator (Teflon sheet) and a slight conductor (a Staedtler rubber eraser) produce measured gain and phase responses that are represented by the equivalent circuits studied in the previous section. The measurement suffered from noise especially in the case where the eraser rubber was in contact with the sensor electrodes. At high frequencies the phase is prone to be noisy because small time errors correspond to large phase errors. At frequencies below 1 Hz, the integrator is saturated, so measurements are meaningless. The cause of the large spike at 200 Hz is unknown.*

Chapter 3

Maxwell 2D^{TM} Numerical Simulations

3.1 Introduction to Maxwell 2D

Ansoft's Maxwell 2D finite element modeling software is a valuable tool for solving field problems in electric, magnetic and electromechanical systems. In this research, Maxwell 2D has been used to confirm the accuracy of the GETGP3 forward problem solver. Both software packages perform the same task of extracting electrode transimpedance per length from a 2D description of the physical setup of the sensor. While GETGP3 does this calculation using a Fourier series of analytical solutions, Maxwell 2D uses finite element mathematics to break the problem space into triangles and solves simultaneous boundary conditions at the adjacent edges of every triangle pair. Although neither method is exact, they should converge to the correct answer with arbitrary accuracy because they start from the same governing equations: Maxwell's equations and the constitutive relations. The impedance values resulting from Maxwell 2D's calculations were converted to gain and phase values that could be compared directly to the gain and phase output of GETGP3. As expected, the output of the two programs did converge.

While GETGP3 is limited to solving for the gain and phase of the signal from a traditional interdigital electrode pair, Maxwell 2D is a more versatile program because any geometry can be defined for its input. As an example, the sensing electrode can be segmented along its length, essentially forming multiple thin electrodes whose total area is equivalent to the traditional

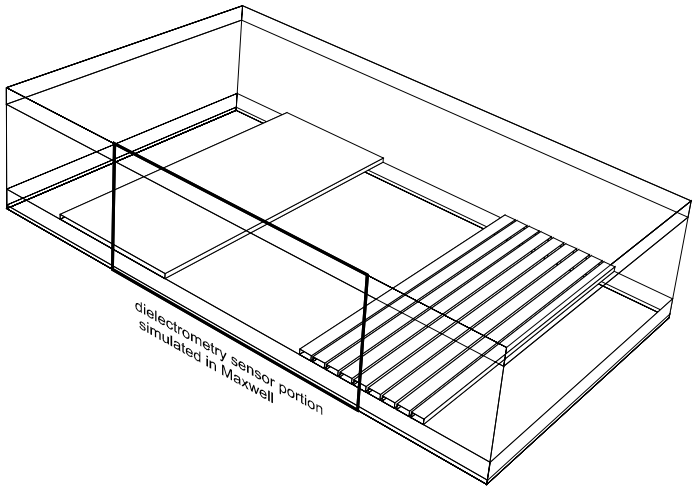

Figure 3-1: *A section of an interdigital dielectrometry sensor in which the sensing electrode, at the right, has been segmented. All the segments are virtually grounded, and the current from each segment can be monitored separately to yield more information about the layers of a material under test.*

sense electrode's area. A cross section of a segmented sensing electrode dielectrometry sensor is illustrated in Figure 3-1. A second study was performed using Maxwell 2D to determine the advantage that segmenting the sense electrode could provide on electric field penetration depth. Hypothetically, the center segment will be the termination of the most deeply penetrating electric field lines, while the more shallow field lines will terminate at the outer segments, as illustrated in Figure 3-2. As a result the signal on the center segmented sensor electrode will be more strongly influenced by materials further away from the sensor pad, but will also be weaker because the area of the center electrode will be only a fraction of the total. Maxwell 2D can help to find an optimum balance between these two trade offs.

In this chapter, a step-by-step procedure for solving a conductance and capacitance problem in Maxwell 2D is given. Important theory is discussed along the way. Next, Maxwell 2D is used to simulate the same problem that had already been solved by GETGP3, and the two program results are shown to agree. Finally, results for the segmented electrode study are presented and discussed.

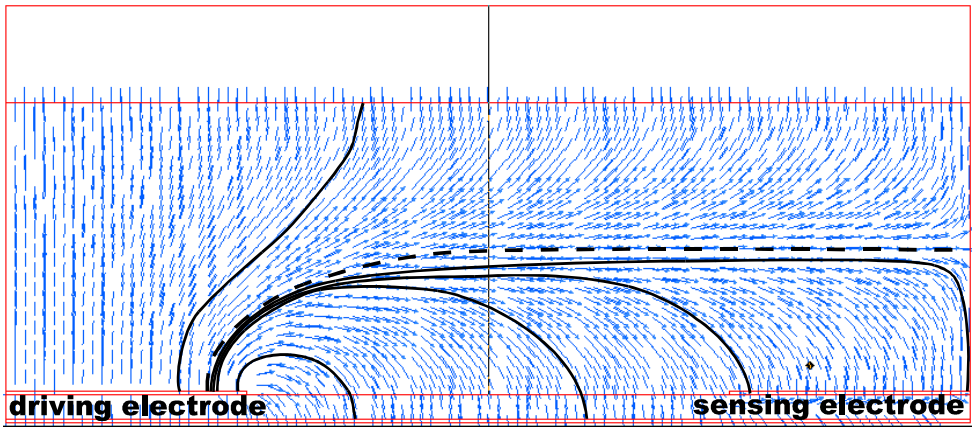

Figure 3-2: *A cross section of half a segmented sensing electrode and half of the adjacent driving electrode. The field lines from the center of the sensing electrode penetrate the deepest into the material under test, and can be measured separately due to the segmentations of the sensing electrode.*

3.2 Setting up a problem in Maxwell 2D

3.2.1 Beginning a Project

This procedure for completing a solution in Maxwell 2D assumes no experience of the reader. In most cases the steps appear in the Maxwell 2D environment from top to bottom in the order they will be completed. The procedure describes the steps taken for the particular research of this thesis. For more general information, open the help application from the bottom of the project window. Occasionally the FrameViewer application has trouble opening the help menu. If this happens, go to the blank FrameViewer application that has opened and choose File/Index.

To begin a new project, open Maxwell 2D, select Projects, open a New Project and name it. The project window for your new project will automatically open.

Select the type of solver to use. For calculating conductance and capacitance, use AC Conduction.

3.2.2 Drawing the Model

Select Define Model/Draw Model and draw your model of electrodes, grounds, substrate, materials under test etc., in the graphics window that appears. Be sure to set the units to the desired scale. For better precision, you can specify coordinates by typing in the boxes below the drawing window. Follow the prompts below the drawing window while performing a routine, such as editing a vertex. Maxwell 2D assumes that closed paths represent solid material and refers to them as Objects. Objects are given a name when you create them, and are assigned a material later in the design process. The area within the drawing boundary that is not filled with Objects is automatically recognized as its own Object named Background, and can be assigned a material later. Open paths are distinguished from closed ones in that they are not considered Objects and cannot be assigned a material. However, open paths are still useful in a model because they can be used to define boundaries and as paths along which to find solutions.

You may want to sweep the dimension of an object and have Maxwell 2D solve the problem at incremental values of the dimension. If so, include that object in the drawing. If the object you will vary is meant to be in direct contact with other objects, it is a good idea to draw them initially with a space in between. This allows you to unambiguously select constraint points when you get to that step. Later when you set the values of the constraints, you can set them so the space between the objects goes to zero.

To prepare an object's dimension to be swept, or simply to make that dimension easy to modify in the future, select Constraint/Add/Point-to-Point Distance. Click on the point that you wish to be an anchor, and then on the point you wish to constrain. Both points must be on object boundaries: they cannot be floating. If the anchor and constrained points are on the same object, the object will change size. If they are on different objects, the object will move without changing size. Note also that the constrained point can move only along the direction of the constraining vector when you sweep the value of this constraint. Now give your constraint a Name and an Expr (Expr is just another name for 'value'). Do not select 'Enforce' until all of your constraints are set up. Enforce causes a constraint to be effected. Selecting enforce on one constraint causes all constraints to be enforced.

The nomenclature used in Maxwell 2D for the constraint system is not entirely rigorous. A

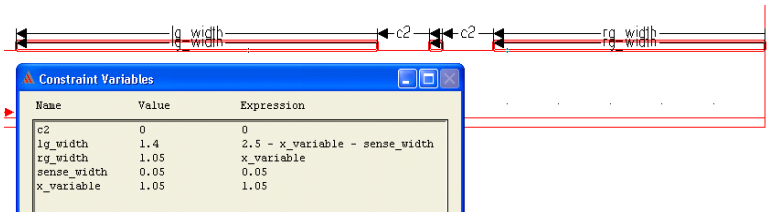

Figure 3-3: *A screenshot of the constraint setup on the sensing electrode segments before enforcing. Note the gaps labelled c2 between electrode segments to make point selection easier.*

rigorous system would be as follows: A constraint defines the geometric distance between two points (or angle between lines or the length of an arc, depending on the constraint type), and hence should be considered a relationship with no numeric value. A variable is the numeric value assigned to a constraint. For example, here is how the terms 'variable' and 'constraint' should be applied: 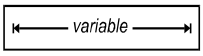

. Maxwell 2D follows this nomenclature but also allows a constraint name to be used as a variable, with a value equal to the value given to that constraint. Thus if the constraint named 'mid_distance' has a value of 5, setting the value of the constraint named 'top_distance' as 'mid_distance' is allowed and gives 'top_distance' a value of 5. For example, if you've made a constraint like this, 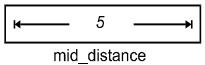

then you can make another one like this 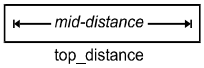

and it will have a value of 5. When sweeping the geometry, both constraints and variables are eligible for sweeping. With this in mind, add constraints to your objects to fully define the geometry that you want to sweep. Be sure that you select anchor and constraint points where you actually want them to avoid overlapping objects when you try to enforce your constraints. This is why it's a good idea to separate the objects when you initially draw them, as shown in Figure 3-3. Figure 3-4 shows how the gap is removed after the constraint is enforced. When the last constraint is in place, select Constraint/Enforce. The geometry of your drawing should now change to correspond to the values of the constraints that you have set up. This geometric version of your model is called the 'Nominal Problem'.

Save your work, and exit from Define Model.

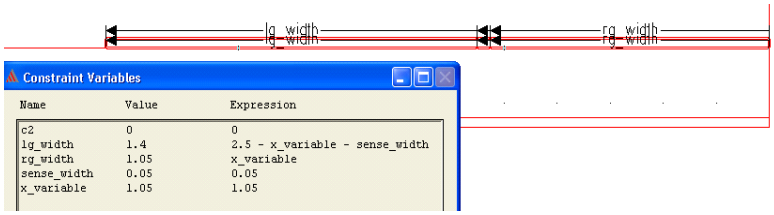

Figure 3-4: *Constraint setup after enforcing. All dimensions change to their constrained values. This geometry is called the nominal problem.*

3.2.3 Defining the Materials

Choose Setup Materials. In the window, select an object that you wish to define from the top list on the left, or by clicking on it in the model window. Then select a material from the bottom list, and click the Assign button between the two lists. If you want to create your own material characteristics, select Material/Add or Material/Derive and fill in the dielectric parameters that are available. Assign materials to all of your model objects and to the background. Save and exit from Setup Materials.

3.2.4 Setting Up Potentials

Choose Setup Boundaries/Sources. Here you will declare which objects or surfaces behave as voltage or charge sources in your problem. To select objects in this step, you must use Edit/Select instead of simply clicking on the desired line. Choose a method for selecting an object that will become a source and make the selection. Now choose Assign/Source and declare the values for the source.

Because some real problems do not have well defined boundaries, they cannot be drawn accurately on a real sheet of paper. For example, the field of a point charge extends to infinity, but no drawing area is large enough to show that there is nothing between the point charge and infinity. In this window, you will be able to indicate in the finite drawing area how the artificial drawing boundaries should be interpreted. Select Assign/Boundaries/Balloon to model the area outside of your drawing space as nearly infinite, isolating your model from all other objects. The potential goes to zero at infinity. You can also declare edges interior to the drawing to map onto other non-adjacent edges, by using the Master/Slave options. To create an infinite

periodic structure that is symmetrical, you can define opposite edges of the drawing to be symmetry axes in Setup Boundaries/Sources. To create an infinite periodic structure that is not symmetrical, you must use the Master/Slave boundaries.

3.2.5 Declaring Executive Parameters

This section discusses admittance, a property of AC circuits. Signals are marked with a tilde (e.g., $\widetilde{V}$) to indicate that they are AC and of a single frequency. Differentiation is carried out by multiplying a signal by $j\omega$.

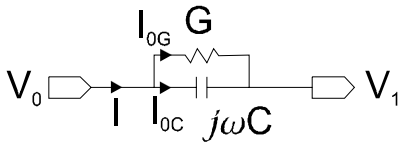

Figure 3-5: *The admittance between two nodes is the reciprocal of impedance. Admittance is a characteristic of AC circuits.*

Finding the admittance of a conductance G in parallel with a capacitance C ($Y = G + j\omega C$ [Siemens]) between exactly two nodes is an easy problem to visualize, as in Figure 3-5. When a potential is applied between the two nodes, they will hold opposite charges, and a current will flow between them. The amount of charge that node 0 will hold is expressed by the definition of capacitance:

$$\widetilde{Q}_0 = C(\widetilde{V}_0 - \widetilde{V}_1) \tag{3.1}$$

or after differentiating,

$$j\omega\widetilde{Q}_0 = \widetilde{I}_{0C} = j\omega C(\widetilde{V}_0 - \widetilde{V}_1) \tag{3.2}$$

The amount of current that will flow out of node 0 is expressed by Ohm's law,

$$\widetilde{I}_{0G} = G(\widetilde{V}_0 - \widetilde{V}_1) \tag{3.3}$$

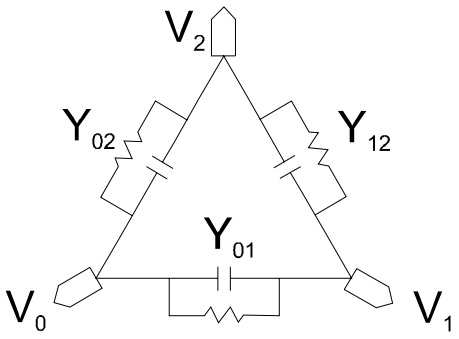

Figure 3-6: *The admittance between three nodes is the superposition of the admittance between each pair of nodes.*

Combining these equations we can write

$$\widetilde{I} = \widetilde{I}_{0C} + \widetilde{I}_{0G} = (G + j\omega C)(\widetilde{V}_0 - \widetilde{V}_1) = Y(\widetilde{V}_0 - \widetilde{V}_1) \text{ [A]} \tag{3.4}$$

where admittance, Y, is,

$$Y = G + j\omega C \text{ [S]} \tag{3.5}$$

conductance, G, is,

$$G = \frac{1}{R} \text{ [S]} \tag{3.6}$$

and susceptance, B, is,

$$\omega C = B[S] \tag{3.7}$$

When there are *more* than two nodes, the problem is simply a linear superposition of all the possible two-node combinations. This can be represented succinctly in a matrix. For example, given a system such as in Figure 3-6 with three nodes labeled $0, 1$ and 2, the current leaving node 0 is expanded from Equation 3.1 as

$$\widetilde{I}_0 = (Y_{01} + Y_{02})\widetilde{V}_0 - Y_{01}\widetilde{V}_1 - Y_{02}\widetilde{V}_2 \tag{3.8}$$

or in matrix form

$$\widetilde{I}_0 = \begin{bmatrix} Y_{01}+Y_{02} & -Y_{01} & -Y_{02} \end{bmatrix} \begin{bmatrix} \widetilde{V}_0 \\ \widetilde{V}_1 \\ \widetilde{V}_2 \end{bmatrix} \tag{3.9}$$

The full matrix is

$$\begin{bmatrix} \widetilde{I}_0 \\ \widetilde{I}_1 \\ \widetilde{I}_2 \end{bmatrix} = \begin{bmatrix} Y_{01}+Y_{02} & -Y_{01} & -Y_{02} \\ -Y_{10} & Y_{10}+Y_{12} & -Y_{12} \\ -Y_{20} & -Y_{21} & Y_{20}+Y_{21} \end{bmatrix} \begin{bmatrix} \widetilde{V}_0 \\ \widetilde{V}_1 \\ \widetilde{V}_2 \end{bmatrix} \tag{3.10}$$

The diagonal entries in the matrix represent the self admittance of a node and are numerically equal to the current that will flow from it if it is set to 1 volt and all other nodes are set to zero volts. The off-diagonal entries represent the mutual admittances between nodes and are numerically equal to the current that will flow from each of the other nodes when one node is set to 1 volt and all other nodes are set to zero.

Now consider that if all potentials are referenced to node 0, $\tilde{\mathrm{V}}_0$ is identically zero, and no ambiguity is lost. We can eliminate the zeroth column from the matrix because it now contributes nothing to the current. And if we don't care to know what current is flowing from node 0, we can eliminate the zeroth row from the matrix as well, resulting in an abbreviated matrix:

$$\begin{bmatrix} \widetilde{I}_1 \\ \widetilde{I}_2 \end{bmatrix} = \begin{bmatrix} Y_{10}+Y_{12} & -Y_{12} \\ -Y_{21} & Y_{20}+Y_{21} \end{bmatrix} \begin{bmatrix} \widetilde{V}_1 \\ \widetilde{V}_2 \end{bmatrix} \tag{3.11}$$

Note that node 0 still affects the matrix in the diagonal entries, because it contributes to each node's self admittance.

In Maxwell 2D, to define the objects in your problem between which you want to find the complex admittance, choose Executive Parameters/Matrix. Select an object from your model that you wish to appear in the matrix, and assign it to be either a Signal Line or a Ground. Ground corresponds to node 0 described above, and is simply a special case of a Signal Line whose row and column have been eliminated from the admittance matrix. Only one node or group can be identified as a Ground, and it is not necessary to identify any node as a Ground.

Maxwell 2D will calculate the admittance matrix for the nominal problem only. To calculate

admittance entries for a parametric sweep, choose Setup Executive Parameters/Select Matrix Entries. The entries you choose will be solved for every variation in the parametric sweep. Maxwell 2D displays admittance as (conductance per unit length, capacitance per unit length) in units of [S/m, F/m] where susceptance per unit length has been converted automatically to capacitance per unit length, $C = \frac{B}{\omega}$.

3.2.6 Setting Up the Solution

Choose Setup Solution/Options to fine-tune the way Maxwell 2D will solve the problem. First select Manual Mesh to refine the mesh that divides the problem space into triangles. In this option, clear the automatic mesh by using Mesh/Delete, then create your own by specifying the number of triangles to start with in each object of your drawing. Select Refine/Object, click on an object, fill in the Refine Number box and choose Accept. When you have specified the number of triangles you want in each object, choose Ok and a new mesh will be generated and displayed. Exit from the Meshmaker.

Edit the variables in the Solve Setup screen as desired. Be sure to leave Starting Mesh on Current instead of Initial, so that the mesh you just generated will be used. A reasonable error to achieve in the problems presented here is 0.01% after several adaptive passes. When finished, select Ok.

If you would like to run a parametric solution, choose Setup Solution/Variables. Choose Variables/Add, and select the variable that you wish to sweep from the list that is presented. This variable will be added to the existing parameters in the table's header. Choose Data/Sweep, and click on the variable you wish to sweep. To create a linear sweep, leave the function val(t) as t, and set t_start and t_end to the extremums of your sweeping range. To create a functional sweep, such as logarithmic frequency, set val(t) to a function of t using the special function characters that are described in the sweep window's help button, and set t_start and t_end to the values which will correspond to the extremums of your sweeping range. The setup for a logarithmic frequency sweep is illustrated in Figure 3-7. Select Accept and then Ok. When you select Ok, a row will be created for each value of the swept parameter. Each row has a specific setup name, and each setup will be simulated one at a time when you choose Solve/Variables later. Exit Setup Solution.

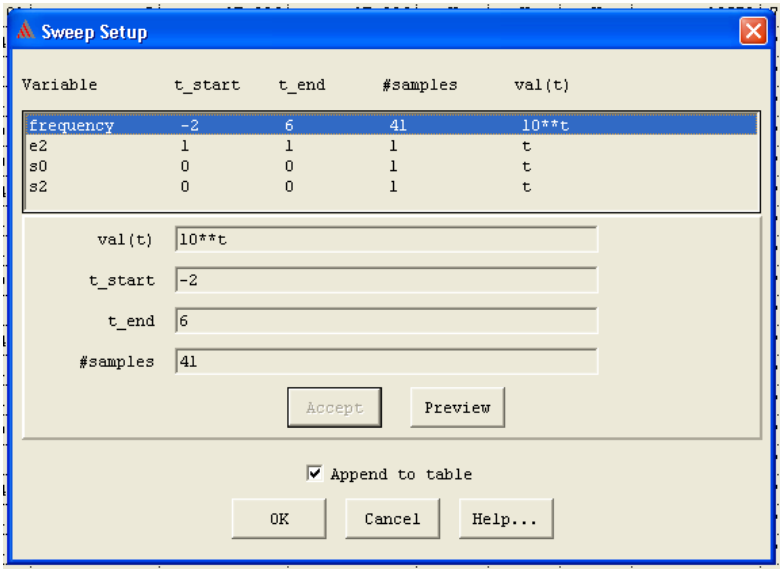

(a) The function and starting and ending values setup for a logarithmic frequency sweep. 'e2 and 's2' are the permittivity and conductivity of layer 2 that will be varied in a sweep of their own. 's0' is the conductivity of layer 0. Note the unconventional notation used for exponentiation, described under Help.

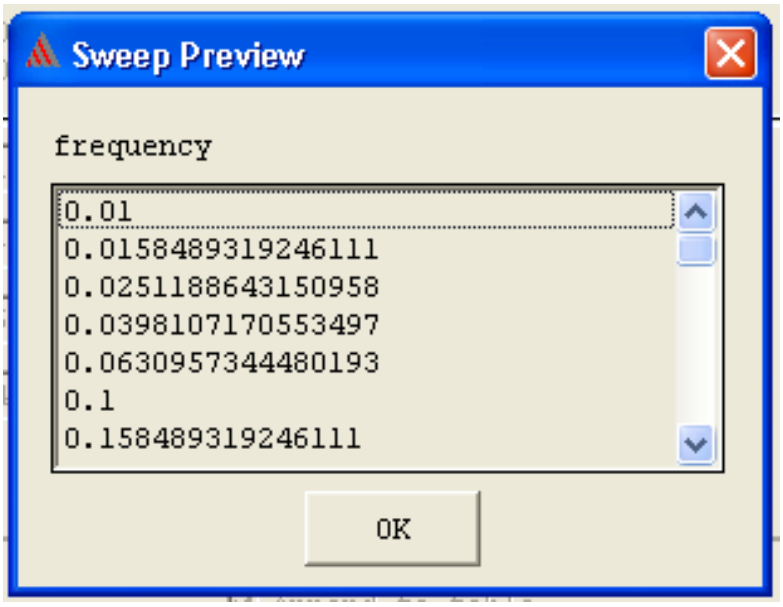

(b) The frequency values generated by the function val(t).

Figure 3-7: *Screenshots showing the syntax for setting up a logarithmic frequency sweep from 0.01 Hz to 1MHz with five steps per decade, and the resulting frequency values that will be applied one at a time to the problem during the solution process.*

3.2.7 Solving

Select Solve/Nominal Problem to have Maxwell 2D solve the nominal problem (that is, the model with all variables set to their original values when they were created). If you declared admittance matrix Signal Line objects, the admittance matrix will be computed now. Maxwell 2D will solve the problem repeatedly, refining the mesh in the triangles of greatest error, up to the maximum number of passes that you specified in Setup Solution/Options or until the energy error target you specified is reached.

Select Solve/Variables to have Maxwell 2D solve the parametric model (that is, the model for which you defined multiple values for variables under Setup Solution/Variables.) If any of the variables of your model are dimensions, Maxwell 2D will start solving each setup using the initial mesh. This is because some of the mesh seed points change every time the dimension changes, making the current mesh incompatible with the new dimensions. To gain some control over the mesh in this situation, you can add seed points in the Meshmaker window under Mesh/Seed, and then save them using Mesh/Seed/SaveSeed. These seeds will be used to create the initial mesh every time a parameter changes. You cannot include any other mesh refinements, such as Refine/Object, in a parametric solution. If none of your variables are dimensions, then Maxwell 2D can use the same mesh for every parameter value, as long as you specify Mesh/Current (not Mesh/Initial) in Setup Solution/Options.

3.2.8 Post Process

To view the field and potential solutions for your problem, select Post Process/Nominal Problem. In this window you can plot various field quantities and adjust the way they are displayed, under Plot/Field. You can also create an animation to view the field as it changes over a cycle. There is a very versatile tool under Data/Calculator. Although it is fairly difficult to use, and follows the rules of Reverse Polish Notation, it allows you to plot virtually any function of the field solution. For example, you can find the potential along a path that you have previously defined. A useful capability of Calculator lets you export to file the numerical value of a field quantity at all the points on a user-specified grid. Follow these steps in calculator to export the x component of the electric field on a grid:

1. Input/Quantity/E
2. Input/Num/Scalar/type in the desired phase for the exported field
3. General/Cmplx/AtPhase
4. Input/Geom/Area/All
5. General/Domain
6. Vector/Scal?/ScalarX
7. Export/On Grid/type in the desired grid parameters and file name, and choose Ok.

Post Process cannot plot electric field lines. Instead, it plots arrows on a grid. Unfortunately, when printing the electric field arrows, Maxwell 2D seems to convert the screen image to a bitmap, so the arrows print wide and fuzzy and the high resolution of a laser printer is lost. Printed electric fields plots from Maxwell 2D are not fantastic.

To view the admittance matrix for the nominal problem, choose Solutions/Matrix at the top of the main screen. The admittance matrix can then be exported by choosing Operations/Export and specifying a path.

If you have completed a parametric solution, you cannot view any of the fields nor any of the admittance matrices. These are calculated for the nominal problem only. Open Post Process/Variables to view the variables that you had asked to be calculated during the parametric solution, such as the admittance between two particular nodes. To export the Variables, choose File/Export.

3.3 Results

Maxwell 2D was first used to calculate the same gain and phase values that had been calculated by GETGP3 for a 20 mm wavelength sensor to compare the accuracy of the two programs. Four interesting sample material configurations were chosen for test cases and input into each program for simulation. The sample cases are illustrated in Figure 3-8. The simulations were conducted in Maxwell 2D as a parametric problem. A generic model was drawn with the three layers of fixed thickness (0.1 mm, 0.9 mm and 2 mm), so that one mesh could be used for all

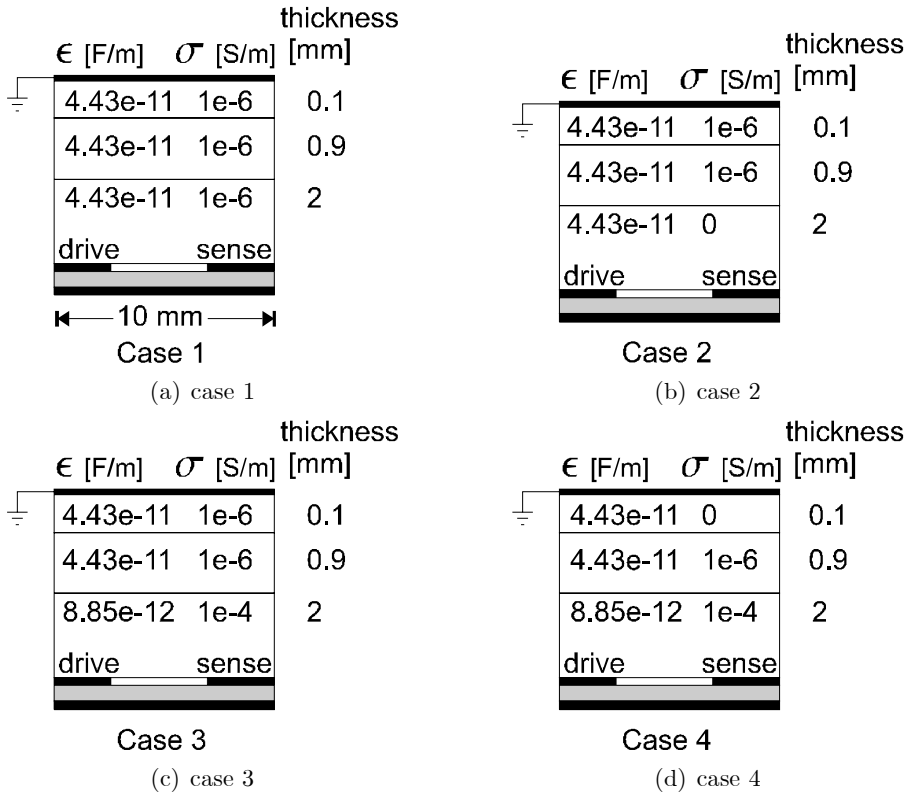

(a) case 1 (b) case 2

(c) case 3 (d) case 4

Figure 3-8: *Four configurations of perfectly insulating and slightly conducting layers of dielectric, simulated in Maxwell and also in GETGP3, for comparison.*

of the setups and the time for mesh generation would be eliminated. The model drawing is shown in Figure 3-9(a). The dielectric constant and conductivity of each layer were defined as parameters rather than constants in Setup Materials. This allowed the dielectric constant and conductivity to be varied in Setup Solution/Variables. Each of the four material configurations was set up to be simulated on a logarithmic range of frequencies from 0.01Hz to 1MHz with five steps per decade, totalling 41 setups per configuration, or 164 setups in total. Each setup took approximately four minutes to solve. The mesh that was used was produced by first refining the number of triangles in each of the sample layers and in the substrate, and then letting Maxwell 2D refine the resulting mesh three times to a final error of 0.0126% and 19578 triangles by running the nominal problem. The final mesh is shown in Figure 3-9(b). Since the geometry remained constant for all 164 setups, the mesh did not have to be regenerated, so the same one was used for all of the setups. Each setup of the parametric problem was allowed only one pass to avoid mesh refinement. The simulation was conducted in GETGP3 as four separate problems, each solving one of the four material configurations and using the parameters of a 20 mm wavelength sensor and a 1 nF feedback capacitor. The GETGP3 input files are listed in Table 3.1. The output file from GETGP3 was a list of gain and phase values at ten frequencies per decade between 0.01 Hz and 1 MHz. Next, the capacitance and conductance calculated by Maxwell 2D were converted to the gain and phase that would be measured by a sensor with a 1 m meander length and a 1 nF feedback capacitor. The capacitance and conductance from Maxwell 2D must be multiplied by 2 because only half of each electrode is represented in the model.

$$Gain = 20 \log \left(\frac{2\sqrt{(\omega C_{12})^2 + G_{12}^2}}{\omega C_F} \right) \tag{3.12}$$

$$Phase = \arctan \left(\frac{G_{12}}{-\omega C_{12}} \right) \tag{3.13}$$

$$C_F = 1 \text{ [nF]} \tag{3.14}$$

The gain and phase from the two programs are compared in Figures 3-10 and 3-11, and it is evident that the two programs converge to the same result. Note also that curves representing the gain and phase response that would result from a circuit consisting of a discrete capacitor in parallel with a resistor are included in the plots. It is interesting to compare the response of

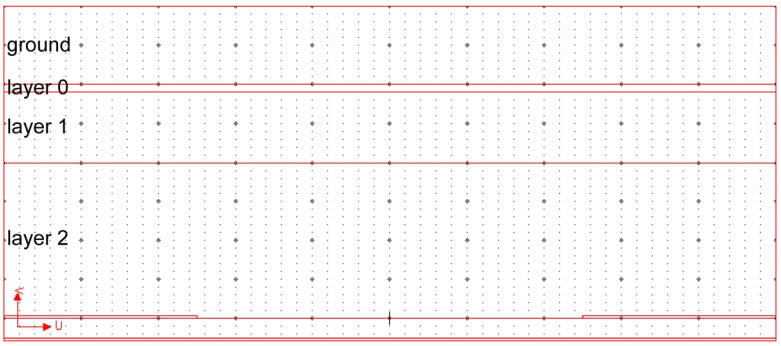

(a) A three layer Maxwell model where the dielectric constant of each layer was varied in a parametric sweep to simulate the four cases of Figure 3-8 .

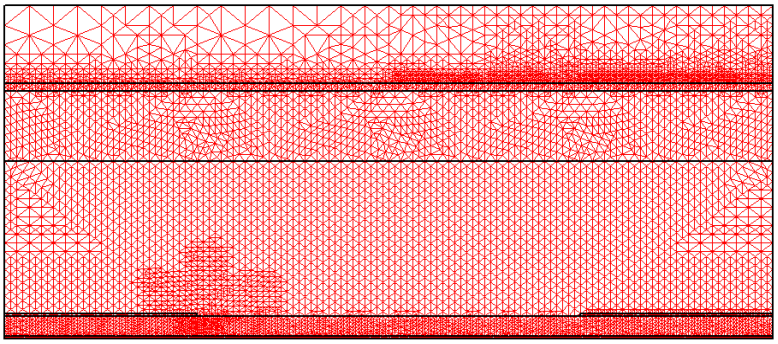

(b) The mesh generated for the model contains 19578 triangles and resulted in a final energy error of 0.0126% .

Figure 3-9: *The three layer model and the mesh used for the simulations of the four cases of Figure 3-8 .*

input parameters				
	Case 1	Case 2	Case 3	Case 4
output file name	ggp_x100.txt	ggp_x101.txt	ggp_x102.txt	ggp_x103.txt
mode	3	3	3	3
surface permittivity	0	0	0	0
fourier terms	250	250	250	250
number of layers	1	2	2	2
number of sensors	1	1	1	1
take these params:	-	-	-	-
wavelength	2.00E-02	2.00E-02	2.00E-02	2.00E-02
substrate permittivity	1.86E-11	1.86E-11	1.86E-11	1.86E-11
substrate thickness	0.0127	0.0127	0.0127	0.0127
electrode spacing	0.25	0.25	0.25	0.25
normalized C_F	53.76	53.76	53.76	53.76
layer 0 thickness	0.003	0.001	0.001	0.001
layer 0 perm, cond	(4.43e-11,1e-6)	(4.43e-11,1e-6)	(4.43e-11,1e-6)	(4.43e-11,1e-6)
layer 0 surf perm, cond	(0,0)	(0,0)	(0,0)	(0,0)
layer 1 thickness	-	0.002	0.002	0.0009
layer 1 perm, cond	-	(4.43e-11,0)	(8.85e-12,1e-4)	(4.43e-11,1e-6)
layer 1 surf perm, cond	-	(0,0)	(0,0)	(0,0)
layer 2 thickness	-	-	-	0.002
layer 2 perm, cond	-	-	-	(8.85e-12,1e-4)
layer 2 surf perm, cond	-	-	-	(0,0)
upper freq	1.00E+06	1.00E+06	1.00E+06	1.00E+06
lower freq	1.00E-02	1.00E-02	1.00E-02	1.00E-02

Table 3.1: *Input parameters for GETGP3 for the four cases that are simulated by GETGP3 and Maxwell 2D for comparison. Input files can be used to provide the sensor specifications by replacing the dash - in the 'take these params' row with the file name.*

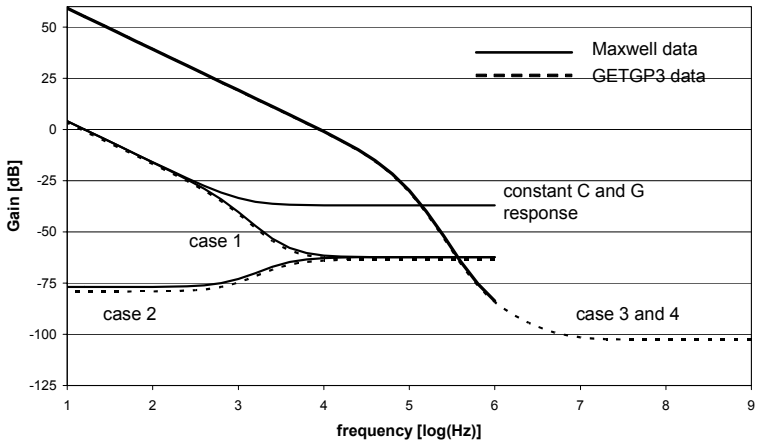

Figure 3-10: *Gain derived from the capacitance and conductance calculated by Maxwell compared to the gain calculated by GETGP3 for a 20mm wavelength sensor and four sample geometries. A curve for constant conductance and capacitance values that uses the low frequency values of case 1 shows how C and G are frequency dependent.*

the dielectrometry sensor to the constant component response, and to develop one's intuition about what causes the features of each response.

3.3.1 Electrode Segmentation

The next exercise with Maxwell 2D was to determine the effect of segmenting the sensing electrode. Hypothetically, a segmented electrode provides greater penetration depth while sacrificing signal strength. The capacitance per unit width of the sense electrode as a function of the distance from its axis was determined. This can be used to calculate the capacitance of any section of the electrode, allowing many segmentation schemes to be analyzed.

The sense electrode half was broken into two segments, both at zero volts, in the model, as shown in Figure 3-12. The capacitance between each segment and the drive electrode was calculated by Maxwell 2D. While the combined width of the two segments remained constant, the width of each segment was varied from zero to the full half width of the electrode. Since the geometry changed, the series could not be executed as a parametric solution. Each segment width was setup manually and simulated as a nominal problem. The complete series was run

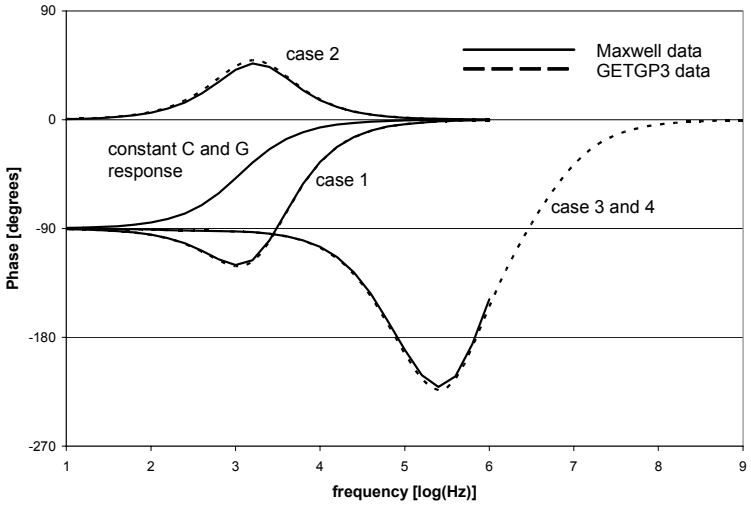

Figure 3-11: *Phase derived from the capacitance and conductance calculated by Maxwell compared to the phase calculated by GETGP3 for a 20mm wavelength sensor and four sample geometries.*

for three different heights of the ground plane above the sensor: 0.5 mm, 3 mm and 20 mm. A drawing of the 3 mm model with a split sensing electrode is shown in Figure 3-12, and a mesh for the 3 mm model is shown in Figure 3-13. A relation between the capacitance per unit width and the distance from the electrode axis was established, and is plotted in Figure 3-14.

3.3.2 Optimum Segmentation Width

Determining the optimum segmentation width is not an easy problem. A narrower sensing electrode terminates fewer of the shallow-penetrating field lines and thus produces a signal that represents a deeper section of the material. A wider sensing electrode intercepts more field lines from the driving electrode and thus produces a higher signal strength, and thus a higher signal to noise ratio. The analysis should consider the noise characteristic of the device used to amplify the received signal versus the depth of electric field penetration. The optimal width is the one which produces the least error margin in the derived values for the sample's complex dielectric constant and thickness.

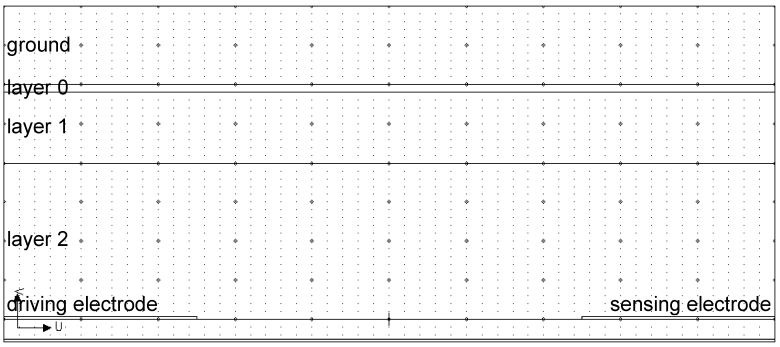

Figure 3-12: *The model used to calculate the capacitance per unit width of the sense electrode, showing the constraints on the width of the sense electrode segment and on the height of the ground plane above the sensor, presently set to 3mm. The width of the model is 10mm.*

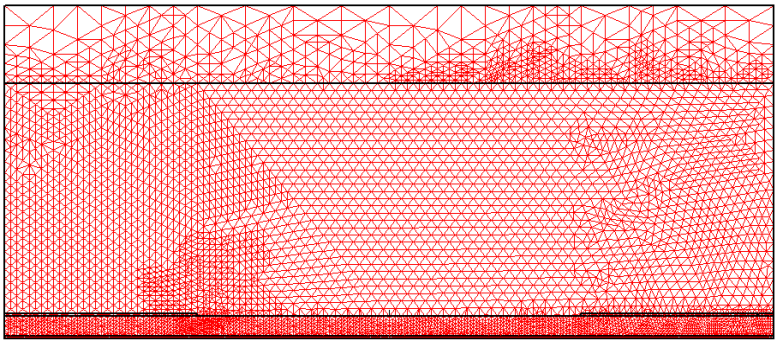

Figure 3-13: *The mesh generated by Maxwell after three passes starting from 5000 triangles in the air-filled area and 3000 in the substrate. Note the increased triangle density in the areas of high field intensity, especially at the corner of the driving electrode.*

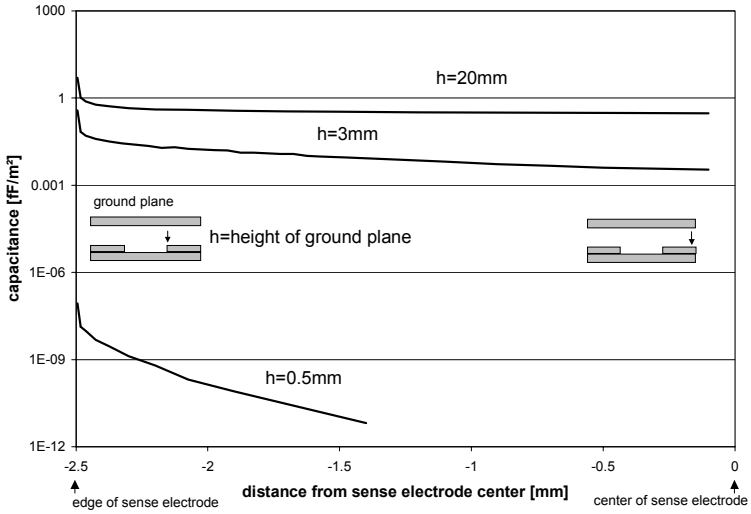

Figure 3-14: *The capacitance per unit area of a 20mm wavelength sensor, from the sensing electrode to the driving electrode with the ground plane at various heights. The capacitance towards the middle of the sensing electrode is more severely decreased for a lower ground plane, because more field lines are intercepted by the ground plane. The capacitance per unit width near the sensing electrode center was near zero for the 0.5mm high ground plane, so it could not be plotted on a logarithmic scale.*

Chapter 4

GETGP3 Forward Solver and ESTLSQ Inverse Solver

4.1 GETGP3 Forward Solver

The GETGP3 parameter estimator is a software package created by former student Yanko Sheiretov (now Ian Shay). The software simulates the potential profile of the interdigitated dielectrometry sensors and returns the gain and phase of the voltage signal on the sensing electrode as a function of AC steady state frequency. It uses a mathematical continuum model and numerical techniques to calculate the electric field in the vicinity of the sensor. Some idealized assumptions are made in the model, including that the electrode structure extends to infinity in both planar directions; the interdigitated electrodes have zero thickness; the material under study consists of a finite number of homogeneous layers which extend to infinity in the horizontal directions and have dielectric properties that are independent of spatial position; the topmost layer is in contact with a conducting grounded plane; at any given excitation frequency, the dielectric properties of all materials are linear, so that if the input is a pure sinusoid, the resulting output is also sinusoidal [27]. The input to the program consists of a text file, stored in the same directory, in which the relevant parameters of the sensor and the material under test are listed in a predefined order. The input file does not contain field headings. The program does not support dispersive sample materials per se, although such materials can be simulated by running it multiple times across a range of frequencies and substituting the appropriate values

of the dispersive complex dielectric constant each time. The program almost always converges on a solution. One way to judge its performance is to compare it to real measurements.

4.2 Comparison of Forward Simulations to Measurements

The results of GETGP3 simulations were compared to actual measurements to verify their accuracy. Measurements from the short circuit current mdoe (SCCM) method and the Hewlett-Packard 4192A Impedance Analyzer using the three wavelength sensor with 5 mm, 2.5 mm and 1 mm wavelengths were compared to simulations of three different sample materials: air, Lexan$^{\mathrm{TM}}$ and Teflon$^{\mathrm{TM}}$. The input parameters for the simulation, summarized in Table 4.2, were the measured thickness of the plastic samples and their dielectric constants ([32], [30], [31]), and the known geometry of the three-wavelength sensor.

The correlation of the simulation to measurements should be very close since the simulation is analytical and can be made arbitrarily exact. However, the physical setup is not perfect. Parameters that affect the accuracy of the measurements but are difficult to quantify are: air layer thickness between the sensor surface and the sample material; surface finish of the sample; contact quality; and actual interelectrode spacing. The air layer between the sensor and the material under test was included in the model to compensate for all of the unknown parameters. The thickness of the air layer was adjsuted to optimize the agreement between the simulations and measurements for Lexan$^{\mathrm{TM}}$.

To compare the data among the three methods, the gain$\angle$phase values from the GETGP3 output have been converted into capacitance values using the expression

$$C_{12} = -C_L 10^{\frac{|\hat{G}|}{20}} \cos\phi \tag{4.1}$$

for FVGPM measurements and from the SCCM measurements with the expression

$$C_{12} = C_F 10^{\frac{|\hat{G}|}{20}-1} \cos\phi \tag{4.2}$$

where a compensation of (-1) in the exponent has been made for a $-10\times$ amplification introduced in the SCCM interface box by an additional 10x inverting amplifier to increase the signal

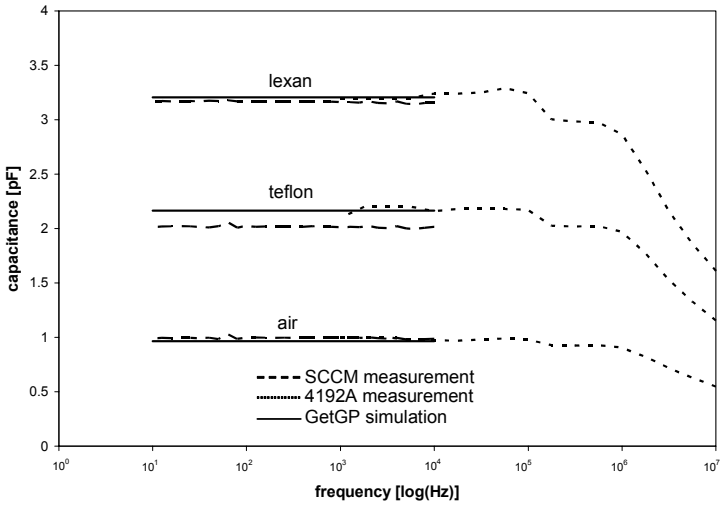

Figure 4-1: *Capacitance of the 5 mm wavelength sensor when measuring air, Teflon and Lexan, comparing the data from the Short Circuit Current Mode, the HP 4192A impedance analyzer, and the GETGP3 forward problem solver.*

Wavelength [mm]	amplifying board	C_F [nF]	meander length [m]	$\epsilon_{substrate}[F/m]$	$\widetilde{C_F}$
5.0	1.2	2.89	0.255	$1.86E-11$	609
2.5	1.3	2.91	0.253	$1.86E-11$	618
1.0	1.1	9.81	0.251	$1.86E-11$	2101

Table 4.1: *The amplifier boards used in the experiment with their respective feedback capacitances listed, and the meander lengths for each wavelength. Normalized feedback capacitance is calculated according to Equation 4.3.*

strength. Table 4.2 lists the input parameters for each simulation; the columns of that Table can be used as the input files to GETGP3 by interspersing the sensor parameters from Table 4.3. Note that normalized feedback capacitance is calculated as

$$\widetilde{C_F} = \frac{C_F}{meanderlength \times \epsilon_{substrate}} \tag{4.3}$$

The feedback capacitance and meander length values for each wavelength are taken from Table B.4 and are summarized in Table 4.1.

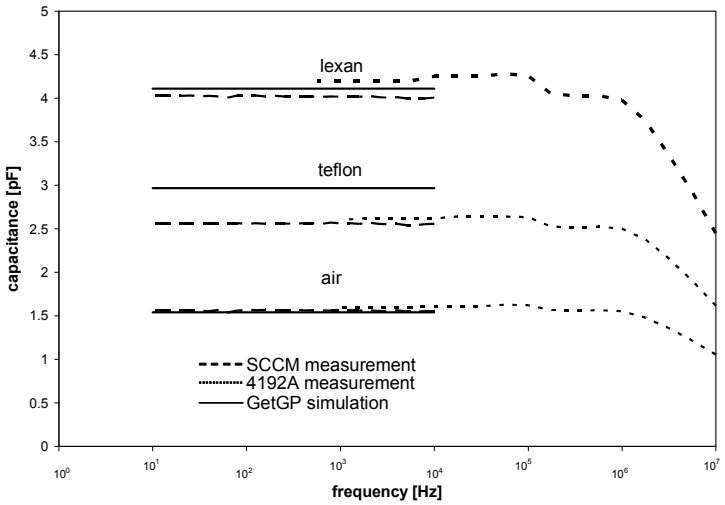

Figure 4-2: *Capacitance of the 2.5 mm wavelength sensor when measuring air, Teflon and Lexan, comparing the data from the Short Circuit Current Mode, the HP 4192A impedance analyzer, and the GETGP3 forward problem solver.*

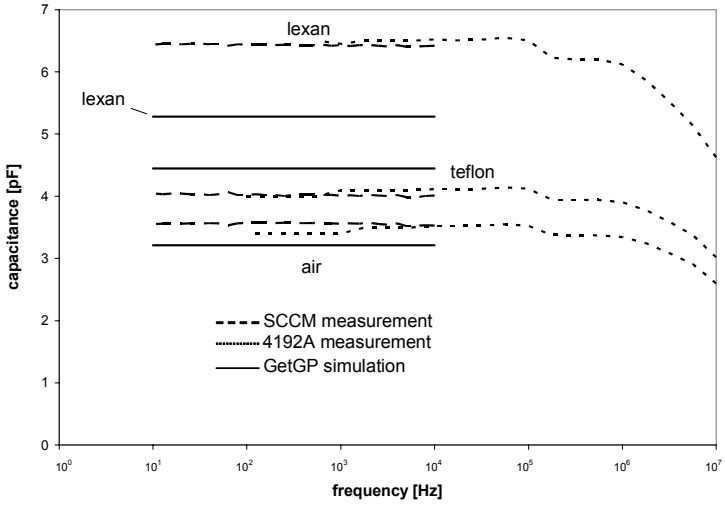

Figure 4-3: *Capacitance of the 1 mm wavelength sensor when measuring air, Teflon and Lexan, comparing the data from the Short Circuit Current Mode, the HP 4192A impedance analyzer, and the GETGP3 forward problem solver.*

material	air	Lexan™	Teflon™
input file parameters			
output file name	ggp_ou1b.dat	ggp_ou3c.dat	ggp_ou5d.txt
mode	3	3	3
surface permittivity	0	0	0
fourier terms	250	250	250
number of layers	1	2	2
number of sensors	3	3	3
sensor specs	(see Table 4.3 for specs of 5 mm, 2.5 mm and 1 mm sensors)		
layer 0 thickness	1000	0.01768	0.06
layer 0 (perm,cond)	(8.85e-12,0)	(2.8e-11,0)	(1.86e-11,0)
layer 0 surf (perm,cond)	(0,0)	(0,0)	(0,0)
layer 1 thickness	-	0.00003	0.00003
layer 1 (perm,cond)	-	(8.85e-12,0)	(8.85e-12,0)
layer 1 surf (perm,cond)	-	(0,0)	(0,0)
upper freq	10000	10000	10000
lower freq	1000	1000	1000
simulated gain [dB] (not including +20dB from inverting opamp); phase = -180 for all cases			
5 mm	-69.5172	-59.1014	-62.5149
2.5 mm	-65.5119	-56.9981	-59.8332
1 mm	-69.6953	-65.375	-66.8673
simulated capacitance [nF]			
5 mm	0.97	3.20	2.16
2.5 mm	1.54	4.11	2.97
1 mm	3.21	5.28	4.45

Table 4.2: *The input files used to simulate measurements of infinite half-spaces of air, Teflon and Lexan, with the gain results (note that phase is -180 degrees for any perfectly insulating material), and the corresponding capacitance of each sensor wavelength.*

sensor #0 parameters	-
spatial wavelength [m]	0.005
substrate permittivity [F/m]	1.86e-11
normalized substrate thickness	0.0508
normalized interelectrode spacing	0.25
normalized feedback capacitance	609
sensor #1 parameters	-
spatial wavelength [m]	0.0025
substrate permittivity [F/m]	1.86e-11
normalized substrate thickness	0.102
normalized interelectrode spacing	0.25
normalized feedback capacitance	618
sensor #2 parameters	-
spatial wavelength [m]	0.001
substrate permittivity [F/m]	1.86e-11
normalized substrate thickness	0.254
normalized interelectrode spacing	0.25
normalized feedback capacitance	2101

Table 4.3: *The sensor specs for the 5 mm, 2.5 mm and 1 mm Teflon substrate sensors to be inserted in Table 4.2 as input to GETGP3.*

4.2.1 Discussion of Results

The air gap thickness was set at 30 μm to optimize the agreement between the simulation and the measurements for Lexan. This value for air gap does not necessarily represent the true thickness of the layer of air, since it compensates also for the air cavity between the 17.8 μm thick electrodes, inaccurate interelectrode spacing, and surface roughness of the sample. It is better called the equivalent air gap. With this correction, the GETGP3 data have excellent agreement with the measured values for the 5 mm wavelength sensor in Figure 4-1 and the 2.5 mm wavelength sensor in Figure 4-2. The largest discrepancy is in the 1 mm wavelength sensor for Lexan, in Figure 4-3, which may be due to contact quality or interelectrode spacing. It is noted in ([10], pp. 218) that equivalent air gaps must be treated as separate parameters for each wavelength of a three wavelength sensor, though here they have all been made the same for simplicity.

Some steps can be taken to refine the comparison between measurement and model. A 20 lb lead weight should always be place on top of the material under test to maximize contact quality by minimizing air gap thickness between the sensor and the material under test, and the sample

should be consistently placed for every measurement. The contact quality could be further improved by depositing the sensor on the actual sample. Also the sample parameter space should be enlarged by using other materials (preferably not granular or hydrophilic because they are affected by compaction and ambient humidity respectively) and including the new 10 mm, 20 mm and 40 mm wavelength sensors.

4.3 ESTLSQ Inverse Estimator

ESTLSQ is a companion package to GETGP3 and it solves the same problem but inversely. Given a gain∠phase measurement at a particular frequency, ESTLSQ calculates the complex dielectric constant and the thickness of the sample layers. ESTLSQ runs the forward model used in GETGP3 iteratively and finds a solution using a multidimensional Newton's method. It optimizes the solution using a least squares fit. The program can solve for up to as many variables (complex permittivity or layer thickness) as there are sensors. Additional variables must be known and given as inputs. It considers data points at distinct frequencies separately. ESTLSQ uses the same phase convention as GETGP3: phase should be specified in the range $-180^\circ \leq \phi < 180^\circ$; a perfect insulator would result in a phase measurement of $\phi = -180^\circ$ while a poor conductor would result in a phase measurement of $\phi \lesssim 180^\circ$. If a phase outside of the range $-180^\circ \leq \phi < 180^\circ$ is given, the program will add or subtract multiples of 360° until it is inside the range.

Newton's method suffers from the tendency to get stuck in local minima without finding the global minimum. Although ESTLSQ uses methods to find good initial guesses near the global minimum, it still reflects this flaw.

A subset of ESTLSQ is the program EST3, which must be given data from the same number of sensors as there are variables (complex permittivity or layer thickness) to be solved for. EST3 sometimes does not converge on a solution.

4.3.1 Comparison of Inverse Simulations to Measurements

The inverse estimator ESTLSQ can be evaluated by comparing its results to the known complex dielectric constants and thicknesses of the samples under test. The same three material config-

urations used for investigating the forward system are used here: air, Lexan^{TM} and Teflon^{TM}. The measurements from the SCCM method are used as input parameters to the program (listed in Table 4.5), and the desired output is the dielectric constant and the thickness of the material. The ESTLSQ input files form the columns of Table 4.4 while the sensor parameters are listed in Table 4.3.

The accuracy of ESTLSQ is hindered by the uncertainty over the air gap thickness, or contact quality. This is especially true for the 1 mm wavelength sensor that has the smallest penetration depth of all the sensors, because it has the greatest portion of electric field energy in the air gap. Fortunately, the program considers all wavelengths simultaneously in attaining a least squares best fit, so the error of the 1 mm sensor is averaged out with the relative accuracy of the longer wavelength sensors.

The parameter estimates for air are quite accurate, and are summarized in Table 4.6. The permittivity/conductivity pair represents one unknown complex variable, since together they are equivalent to the complex dielectric constant. The negative conductivity is due to a phase measurement $\phi > -180°$, and should be considered a result of noise since the average phase measurement is so close to -180°.

The two trials for Lexan 1 and Lexan 2 are identical except for the initial guess that was supplied to ESTLSQ for the permittivity of Lexan and for the thickness of the air gap. See Table 4.4 for the initial values. In the first trial, Lexan 1, the initial guesses were 2.8e-11 $\frac{F}{m}$ and 30 μm respectively, and the results agreed quite closely with these values. See Table 4.6 for the results. In the second trial, Lexan 2, the initial guesses were deliberately moved away from the correct values, to 2e-11 $\frac{F}{m}$ for the permittivity of Lexan and 50 μm for the air gap thickness, respectively. Again, the results agreed quite closely with the initial guess rather than with the true value of the unknowns. This reflects a tendency of the Newton's root finding method to get stuck in local minima. Importantly, the gain error was roughly 0.1 (quite small) for the first trial that provided accurate results, and roughly 0.43 (four times larger) for the second trial that was less accurate. So although ESTLSQ suffers from this root finding problem, it is able to indicate with good accuracy how well its results fit the input data points.

However, ESTLSQ's accuracy may be over represented in the data of Table 4.6 due to the following phenomenon. If the program is allowed to determine two parameters, then it is able

to vary one of them in order to fit the other one well. For example, in the Lexan 2 case at 10 Hz, the program has determined a very accurate value of 2.83e-11 $\frac{F}{m}$ for the permittivity of Lexan by giving the air gap a negative thickness. Giving the program the ability to choose air gap thickness in the simulations for Lexan and Teflon may explain why these simulations have very consistent, accurate results for permittivity, while the air gap thickness it determines may in fact be very inaccurate. Significantly, since the measurement is very sensitive to the air gap thickness, the permittivity estimates would be much less accurate if the air gap thickness was known and was not allowed to vary in ESTLSQ simulations.

material	air	Lexan 1	Lexan 2	Teflon
input file parameters				
output file name	lsq_o07b.txt	lsq_o08b.txt	lsq_o08e.txt	lsq_o09b.txt
mode	3	3	3	3
surface permittivity	(0,0)	(0,0)	(0,0)	(0,0)
fourier terms	250	250	250	250
number of layers	1	2	2	2
number of sensors	3	3	3	3
number of unknowns	1	2	2	2
unknown parameters	0,b	0,b,1,t	0,b,1,t	0,b,1,t
sensor specs	(see Table 4.3 for specs of 5 mm, 2.5 mm and 1 mm sensors)			
layer 0 thickness	1	0.01768	0.01768	0.06
layer 0 (perm,cond)	(8.85e-12,0)	(2.8e-11,0)	(2e-11,0)	(1.86e-11,0)
layer 0 surf (perm,cond)	(0,0)	(0,0)	(0,0)	(0,0)
layer 1 thickness		0.00003	0.00005	0.00003
layer 1 (perm,cond)		(8.85e-12,0)	(8.85e-12,0)	(8.85e-12,0)
layer 1 surf (perm,cond)		(0,0)	(0,0)	(0,0)
number of data points	12	12	12	12
collocation point technique?	yes	yes	yes	yes

Table 4.4: *The input files for ESTLSQ simulations of measurements on half spaces of air, Lexan, and Teflon. The two cases for Lexan differ in the initial guesses of permittivity of Lexan and air gap thickness.*

4.4 Future Work on the Parameter Estimator

The accuracy of GETGP3 in predicting the gain and phase of a particular measurement is limited by the physical assumptions that are made about the measurement setup. The most

material	data point set
air	10000(-69.32,-179.8) 10000(-65.45,-179.6) 10000(-68.88,-178.7)
	1000(-69.26,-179.9) 1000(-65.41,-179.9) 1000(-68.81,-179.8)
	100(-69.23,-180.2) 100(-65.37,-180.2) 100(-68.76,-180.1)
	10(-69.28,-180) 10(-65.43,-180.1) 10(-68.86,-180)
Lexan 1 and Lexan 2	10000(-59.24,179.98) 10000(-57.22,180.05) 10000(-63.68,180.42)
	1000(-59.22,179.44) 1000(-57.2,179.7) 1000(-63.67,179.9)
	100(-59.2,176.69) 100(-57.17,178.67) 100(-63.66,179.31)
	10(-59.19,179.93) 10(-57.17,179.95) 10(-63.66,179.75)
Teflon	10000(-63.13,180.25) 10000(-61.13,180.18) 10000(-67.77,180.37)
	1000(-63.14,180.28) 1000(-61.1,179.89) 1000(-67.77,180.08)
	100(-63.09,180.03) 100(-61.11,179.76) 100(-67.75,179.97)
	10(-63.13,179.97) 10(-61.1,179.33) 10(-67.69,179.65)

Table 4.5: *Data points taken from measurements to be appended to the columns of Table 4.4 when used as input files to ESTLSQ. ESTLSQ treats each wavelength separately, and knows to parse the points in the order that they are listed in Table 4.3, namely (5 mm, 2.5 mm, 1 mm).*

significant of these assumptions are: the claimed dielectric constant of the material under test, which can be unknowingly affected by moisture in hydrophilic specimens such as paper, grain size in non-solid specimens such as sugar, and temperature; and the air gap between the sensor electrodes and the specimen, which presently incorporates the effect of the air between the electrodes themselves since they are assumed to have zero thickness in the model, and which is difficult to duplicate between measurements. The limits on the accuracy of GETGP3 in turn affect the accuracy of ESTLSQ, which uses GETGP3 iteratively to solve for unknown physical parameter(s). Ultimately the usefulness of dielectrometry is due to the ability of the inverse problem solver to estimate physical properties that cannot be measured directly. Parameters that the system is sensitive to, such as uncertainty in known dielectric constants and in layer thickness, will have to be controlled or strategically eliminated to achieve the best results.

material	frequency [kHz]	permittivity	conductivity	thickness of air layer	gain error
air	10	9.06e-12	-4.7e-9	-	4.07e-2
	1	9.12e-12	-1.1e-10	-	4.21e-2
	0.1	9.16e-12	1.8e-11	-	4.35e-2
	0.01	9.09e-12	5.7e-13	-	4.01e-2
Lexan 1	10	2.80E-11	5.02E-10	2.94E-05	6.49E-02
	1	2.79E-11	7.10E-10	2.79E-05	6.35E-02
	0.1	2.78E-11	4.10E-11	7.90E-06	1.35E-01
	0.01	2.83E-11	-8.03E-14	-1.32E-06	2.53E-01
Lexan 2	10	2.00E-11	-3.23E-12	4.70E-05	4.28E-01
	1	2.00E-11	3.37E-12	4.70E-05	4.31E-01
	0.1	2.00E-11	1.78E-12	4.70E-05	4.37E-01
	0.01	2.00E-11	5.67E-15	4.70E-05	4.35E-01
Teflon	10	1.82e-11	-5.4e-9	7.03e-5	2.08e-2
	1	1.83e-11	-4.6e-11	7.00e-5	1.92e-2
	0.1	1.83e-11	2.2e-11	6.89e-5	2.19e-2
	0.01	1.83e-11	6.3e-12	6.76e-5	2.26e-2

Table 4.6: *Output from ESTLSQ simulations. Note that results are different for the two Lexan cases that had identical input data points but different initial guesses. This means the initial guess matters (it should not) and that ESTLSQ tends to get stuck in local minimums when finding roots. Lexan 1 yields the more accurate result and thus has a smaller gain error.*

Part III

Experiments

Chapter 5

Experimental Procedure

5.1 Introduction

Within the method of dielectrometry, there are several variations on the measuring technique. Fundamentally, dielectrometry is the measurement of the capacitance and conductance between two electrodes that are in proximity to a material whose dielectric constant is the quantity to be determined. The measured capacitance and conductance are then related to the material's complex dielectric constant by a mathematical model of the system. In the simplest case the electrodes form a parallel plate capacitor with capacitance C and conductance G and plates of area A a distance d apart. The model of the system is then

$$\varepsilon = \frac{Cd}{A} \tag{5.1}$$

$$\sigma = \frac{Gd}{A} \tag{5.2}$$

Interdigital dielectrometry has the benefit that the sensor lies all in one plane and so can be applied to a sample material from just one side, instead of having to sandwich the sample. This comes at the cost of having a more complex model relating the permittivity and conductivity to the measured quantities of capacitance and conductance which are generally functions of frequency. Although the math becomes more complex, the procedure is the same: measure the capacitance and conductance between the two electrodes; develop a model that relates

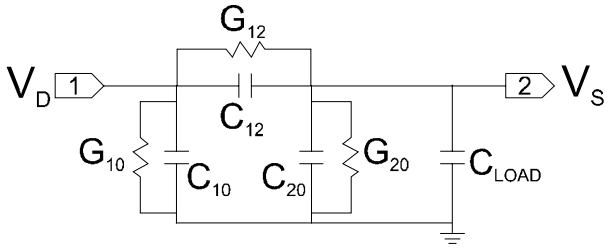

Figure 5-1: *The equivalent circuit for the floating voltage with ground plane mode measurement method.*

capacitance and conductance to the complex dielectric constant of the sample material; solve for the complex dielectric constant using the model.

The research for this thesis has employed three methods for measuring the impedance between the sensor's electrodes: the Short Circuit Current Mode (SCCM), the Floating Voltage Guard Plane Mode (FVGPM), and a commercial Hewlett-Packard Impedance Analyzer. For each method, the procedure is described first. Preliminary testing of all the equipment is described next. Results of the measurements are then presented. Some improvements to the method are described, and the results using the improved method are presented.

5.2 Measurement Methods

Floating Voltage with Ground Plane Mode

The original dielectrometry sensors at MIT consist of a driving electrode to which a sinusoidal voltage of constant amplitude is applied (the driving signal), a sensing electrode loaded by a known capacitance C_L whose potential is measured, and a grounded backplane that eliminates contributions to the signal from the back side of the sensor. The equivalent circuit of the sensor is shown in Figure 5-1.

The complex gain between the sensing and driving electrodes is given by

$$\widehat{G} = \frac{V_S}{V_D} = \frac{G_{12} + j\omega C_{12}}{G_{12} + G_{20} + jw(C_{12} + C_{20}) + j\omega(C_L)} \tag{5.3}$$

This equation involves the unknown components C_{12} and G_{12} which we would like to know,

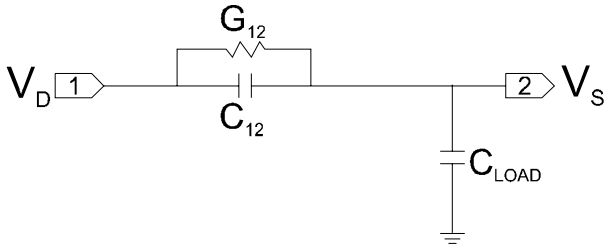

Figure 5-2: *The equivalent circuit for the floating voltage with guard plane mode measurement method.*

as well as C_{20} and G_{20} which are not useful because they are simply properties of the sensor and not of the material under test. All of these elements are frequency dependent, it should be noted, because they represent a circuit that differs topologically from the actual sensor ([10], pp125). Alternatively, the actual sensor could be represented by a discrete circuit of elements that are not dependent on frequency, but such a circuit would require an infinite number of discrete elements. Equation 5.3, which is in the complex domain, can be solved for at most 2 variables, yet there are four that we do not know: G_{12}, C_{12}, G_{20} and C_{20}.

A solution to this problem is to eliminate C_{20} and G_{20} by driving the backplane at the same potential as the sensing electrode, described next.

Floating Voltage with Guard Plane Mode

A potential equal to that of the sensing electrode is applied to the guard fingers and the backplane, eliminating the contribution of these conductors to the self capacitance of the sensing electrode. The equivalent circuit for this configuration is shown in Figure 5-2.

The complex gain is now given by Equation 5.4

$$\widehat{G} = \frac{V_S}{V_D} = \frac{j\omega C_{12} + G_{12}}{j\omega C_{12} + j\omega C_L + G_{12}} = \left|\widehat{G}\right| \cos\theta + j \left|\widehat{G}\right| \sin\theta \tag{5.4}$$

where the explicit solution of G_{12} and C_{12} is:

$$C_{12}(\omega) = -\frac{C_L \left|\widehat{G}\right| (\left|\widehat{G}\right| - \cos\theta)}{1 + \left|\widehat{G}\right|^2 - 2\left|\widehat{G}\right| \cos\theta} \tag{5.5}$$

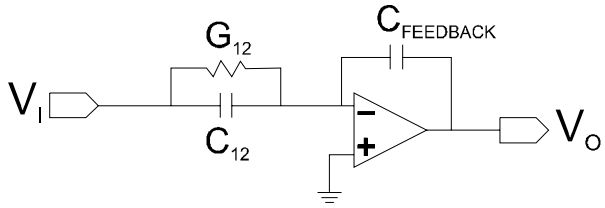

Figure 5-3: *The equivalent circuit for the short circuit current mode measurement method.*

$$G_{12}(\omega) = -\frac{\omega C_L \left|\widehat{G}\right| \sin\theta}{1 + \left|\widehat{G}\right|^2 - 2\left|\widehat{G}\right| \cos\theta} \tag{5.6}$$

As a consequence of driving the backplane at the sensing electrode voltage, the backplanes of each wavelength on a three wavelength sensor must be separated. Also, all grounded conductors must be placed sufficiently far away from the sensing electrode so that the elimination of C_{20} is valid. This requires that the ground plane above the sample material be driven at the sensing electrode potential as well.

Short Circuit Current Mode

The advantage of a simplified equivalent circuit and the convenience of a grounded backplane are combined in the design of the Short Circuit Current Mode. The equivalent circuit is shown in Figure 5-3 and the complex gain is

$$\widehat{G} = \frac{V_S}{V_D} = -\frac{G_{12} + j\omega C_{12}}{j\omega C_F} = \left|\widehat{G}\right| \cos\theta + j\left|\widehat{G}\right| \sin\theta \tag{5.7}$$

where G_{12} and C_{12} can be explicitly solved for and are:

$$C_{12}(\omega) = -\left|\widehat{G}\right| C_F \cos\phi = -\operatorname{Re}\left\{\widehat{G}\right\} C_F \tag{5.8}$$

$$G_{12}(\omega) = \omega C_F \left|\widehat{G}\right| \sin\phi = \operatorname{Im}\left\{\widehat{G}\right\} \omega C_F \tag{5.9}$$

One should remember that these are frequency dependent because they do not represent the actual circuit topology.

5.2.1 The Floating Voltage Guard Plane Mode System (FVGPM)

Because the Short Circuit Current Mode (SCCM) is used almost exclusively in the research for this thesis, and because the procedure for SCCM is a little more detailed than for FVGPM, the procedure is described in full under the Short Circuit Current Mode section that follows. A few notes specific to FVGPM are included here.

Required Equipment

- Controller Box (labelled {A,B,C,D,E})
- Interface Box (FVGPM's labelled {6,7})
- Sensor (Zahn 2 for FVGPM)
- Controller Box to Serial Port cable
- Takedata.exe (preferred) or a terminal program such as Kermit or Hyperterminal

Setting up the Equipment

To use the equipment, follow this procedure:

Attach the interface box to the controller box making sure to use the middle circular bulkhead connector on the controller box as shown in Figure 5-4. The FVGPM interface box has only one driving electrode output, but three sensing electrode inputs corresponding to the three wavelengths of a three wavelength sensor, as pictured in Figure 5-5. It can also be used reliably with a single wavelength sensor plugged into any one of the input channels.

5.2.2 The Short Circuit Current Mode System

The sensor is connected to a system of electronics which sends the driving voltage signal, receives the transmitted voltage signal from the sensing electrode, processes the signal, and stores the data. The system consists of the sensor, an interface box, a controller box, and a PC, and is illustrated in Figure 5-6.

Figure 5-4: *The connection of the FVGPM interface box to the controller box uses the middle circular bulkhead connector.*

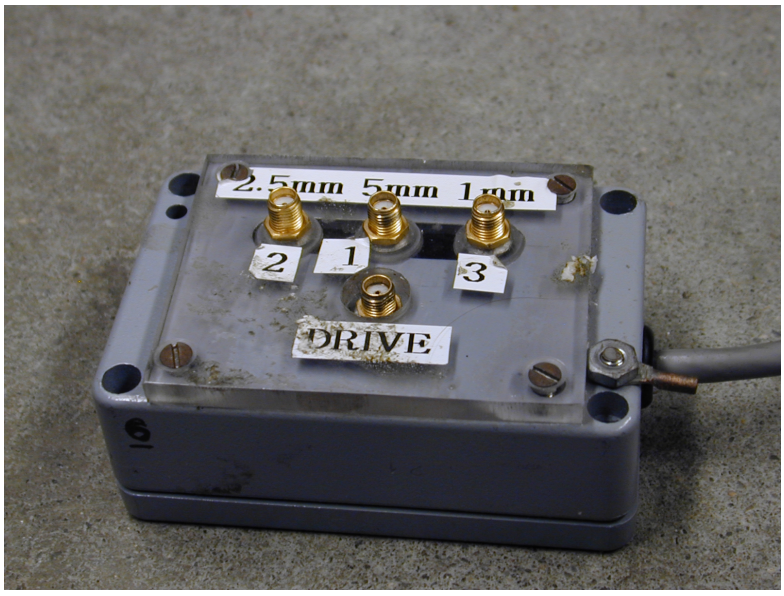

Figure 5-5: *The interface box has only one driving output, but three sensing inputs, corresponding to the three channels of a three wavelength sensor.*

Figure 5-6: *The SCCM system assembled and measuring a shoe with a three wavelength sensor.*

Required Equipment:

- Controller Box (labelled {A,B,C,D,E})
- Interface Box (SCCM's labelled {1,2,3,4,5})
- A two electrode dielectrometry sensor, such as the one built by SeongHwa Kang in 1998
- Controller Box to Serial Port cable
- Controller Box to Interface Box cable
- Takedata.exe (preferred) or a terminal program such as Kermit or Hyperterminal

Setting up the Equipment

To use the equipment, follow this procedure:

Clear a desk near the PC that you plan to use for logging data. Make sure the PC has a free serial port, and note which one it is if it has multiple serial ports. Plug the PC-to-controller box cable into the serial port. This is the only connection from the PC to the sensing equipment. Place the controller box, the interface box, and the sensor on the cleared desk in such a way

that they are accessible for debugging but won't be damaged by heavy samples or weights. Plug the circular connector end of the serial cable into the controller box. Attach the controller box to the interface box with the appropriate cable making sure to use the two rightmost bulkhead circular connectors on the controller box as shown in Figure 5-7. Be sure also to screw the interface box side of the cable, a Dsub connector, into its socket, to ensure a reliable connection that will not cause weeks of frustration. Finally, check the feedback capacitance of each amplifying board in the interface box by unscrewing and removing the bottom cover and reading the ID number on each board. The measured feedback capacitance of each board can be found in Table 5.1. Exchange the boards for ones with different values of feedback capacitance if desired, or if a board with the capacitance you want does not exist, modify one of the boards by carefully desoldering the feedback capacitor from it and installing your own that has been precisely measured. Be sure to record which boards you are using and the modifications you have made. Replace the bottom cover of the interface box. Screw the gold SMA coaxial connectors of the sensor into the corresponding driving and sensing electrode receptacles of the interface box. Place your sample on the sensor. Finally, plug in the controller box to a power outlet. Note that it is sometimes useful when using a single wavelength sensor (as opposed to a three wavelength sensor) to have several amplifying boards with different feedback capacitance values in the interface box, and to try each one separately for debugging purposes.

Using weight, and grounding the top layer

When setting up your specimen to be tested, weigh it down with a ∼20lb mass to reduce the air gap between your specimen and the sensor traces. The air gap can cause significant errors in the data because it is where the electric field is strongest. This will also make the setup more reproducible if you take your specimen off and put it back on. Ground the mass if it is metal or include a grounded metal plane as the top layer of your specimen. The parameter estimator GETGP3 assumes this to be the boundary condition.

The discharge switch

The bat switch on the SCCM Interface Box shown in Figure 5-9 interrupts the signal that causes a relay to short the feedback capacitor in one position and passes it in the other position. The

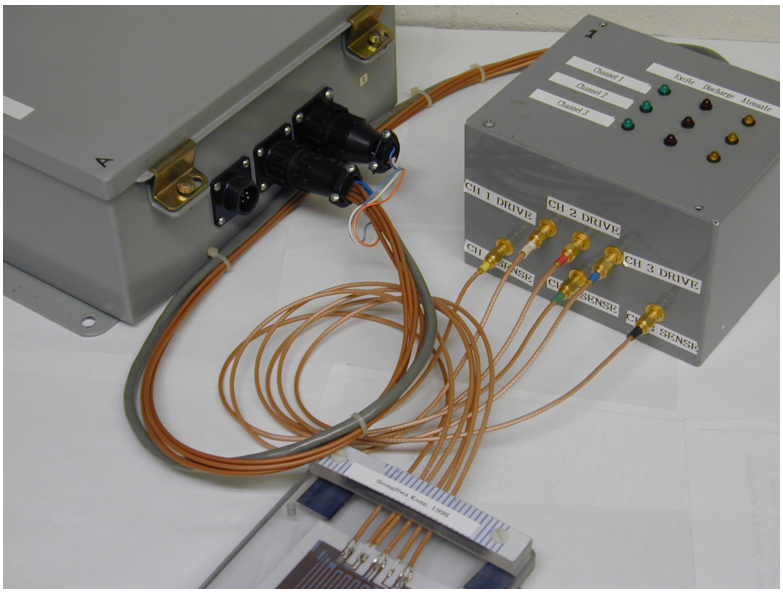

Figure 5-7: *The cables connecting the various components of the short circuit current mode system.*

Figure 5-8: *The connection to the PC's serial port via a regular serial cable that has been refitted with an AMP circular connector on the controller box side. Use a 9 to 25 pin cable converter to use the cable on a 9 pin serial port.*

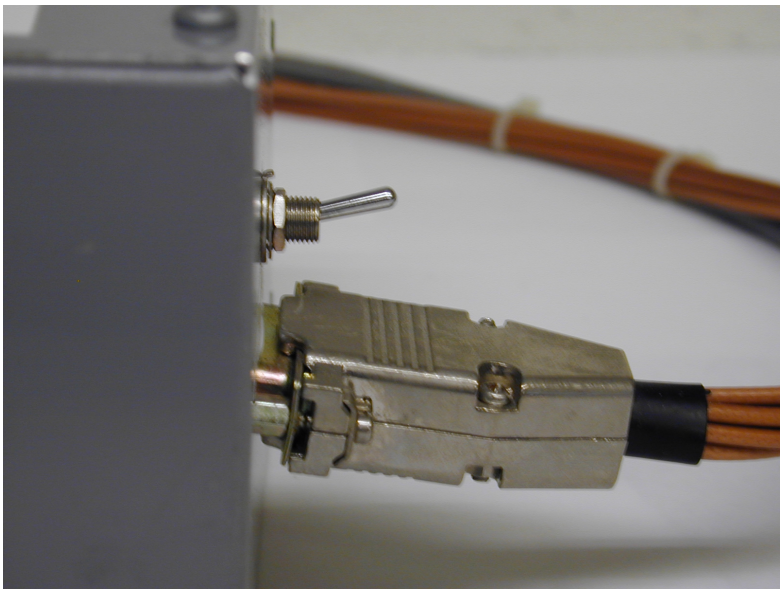

Figure 5-9: *The bat switch that controls discharge in the interface box sense boards in the up position. Table B.2 gives the enabling and disabling positions for each box's switch.*

feedback capacitor is shorted between frequencies of a measurement series to remove residual charge build up, known as *discharging*. It seems that this was implemented because the bits that should enable/disable discharge are ignored by a logic circuit in the interface box. Since the hole for the bat switch is not keyed, it's possible for the switch to rotate upside-down. You may have to try it in both positions to figure it out. A clicking noise between frequencies during a measurement indicates that the discharge relays are operating. There seems to be no reason to disable discharging, while phase readings can be adversely affected if discharging *is* disabled.

Opening the Takedata Software Application

This procedure is adapted from [26].

1. Specify the serial port you are using on your PC. Pressing 'P' toggles it.

2. Set the baud rate. Pressing 'B' scrolls the choices.

3. Specify the frequency range limits with 'U' and 'L', typing in the $\log_{10}$ of the desired limits. 4 to -2.3 corresponding to 10 kHz to 0.005 Hz is the acceptable range.

4. Open communication by pressing 'O'. Often you will have to do this three times before the link opens and the green word 'Connected' appears.

5. Press 'S' to open a command-sending dialogue box. Type in a command to send, such as [de,001001001] or [ve]. These two commands are basically all you will ever need. The command [de] is explained in the next subsection. After pressing 'enter', the controller box's reply will appear.

6. Press 'F' to specify the output file name. The file will be saved in the same directory as the file GetGP3.exe is in. The file name will be truncated to 8 characters.

7. To start taking data, press 'T'. After the test is done you can press 'C' to attach a comment to the specific test run. The data is then saved in the output file that you specified. Before viewing the output file, however, you must release it from GETGP3 control by specifying a new output file name.

Excitation and Discharge

An explanation of the role of discharge is given in ([10], pp. 552). Before Triggering a measurement series in the SCCM mode, send the command [**DE**, 3A, 3D, 3E, 2A, 2E, 2D, 1A, 1D, 1E] to the controller box, replacing 3A,3D,... etc with 0 (for off) or 1 (for on). This command sets the Attenuate (A), Discharge (D) and Excite (E) states of each channel 1 through 3. After sending the command, the corresponding LED's will be lit on top of the interface box. For example, the most common command to send will be [DE,001001001], which will cause all of the green LED's to turn on, and all of the channel drives to pass the sine wave from the controller box at -10x amplification. The Discharge bits are ignored by the interface box; it always produces the discharge gating signal. To disable discharge, use the discharge switch, discussed in this section. The Attenuate bits cause a second capacitor to be switched into the integrator's feedback loop, increasing the feedback capacitance and thus decreasing the gain.

Offset

The offset function is described in ([10], pp. 516). It's not clear how offset affects the gain and phase measurements. However, enabling discharge decreases the magnitude of the offset

voltage. (e.g., without discharge, offset ranges from 0.084 to 0.104, while with discharge, offset ranges from 0 to 0.026 in particular trials)

Expected Data from measurements

The first thing to remember when you actually take a measurement in the short circuit current mode is that the interface box has an inverting opamp on each driving channel with a gain of -10 or equivalently 10∠180. This means that the gain measurement will be increased by 20 dB and the phase measurement will be off by 180 degrees. GETGP3 does not know about the -10 gain opamp, so you will have to adjust your measurement values before comparing them to the output of GETGP3.

You might start by making a measurement in air with the short circuit current mode. To calculate by hand the gain you expect to see, use Equation 5.7 with a modification for the -10 gain opamp, yielding Equation 5.10.

$$gain = 20\log_{10}\left|\widehat{G}\right| = 20\log_{10}\left|10\frac{G_{12} + j\omega C_{12}}{j\omega C_F}\right| \ [dB] \tag{5.10}$$

Note that for air, $G_{12} = 0$. To do the calculation, find the appropriate values for $C_{12_{air}}$ in Table B.4 and for C_F in Table B.2. For the floating voltage with guard plane mode, modify Equation 5.4 to get Equation 5.11.

$$gain = 20\log_{10}\left|\widehat{G}\right| = 20\log_{10}\left|\frac{j\omega C_{12} + G_{12}}{j\omega C_{12} + j\omega C_L + G_{12}}\right| \ [dB] \tag{5.11}$$

Because air is a very good insulator, the phase you measure should be within a degree of zero for the whole frequency range from 0.005 Hz to 10 kHz in either mode. Measurements that do not match your expected gain and phase, or that have absolutely no variance (e.g., gain∠phase = -62.4∠0 for all frequencies), or that have large variance (greater than roughly 2∠5 [dB∠degrees]), or with gain and phase values unaffected by the presence of a sample material other than air indicate that the system is not working properly.

Using Hyperterminal

It is most convenient to use Takedata.exe to log dielectrometry runs. However it is possible to communicate with the controller boxes in Hyperterminal or Kermit, and this makes the communication a little less abstract for the user. The following procedure opens a Hyperterminal session to the controller box:

1. On some computers, first close all MS-DOS windows and any programs that access comports.

2. Pick Hyperterminal from the Accessories menu. A list of available programs will appear. Select hypertrm.exe. Hyperterminal will start up and automatically present the Connection Description options screen. If it presents a Location Information screen for you to input telephone options, select Cancel to move onto the next option screen, which will be thte Connection Description screen.

3. Select any phone icon and type in a name. Select OK. The Phone Number options screen will appear.

4. From the "connect using:" pulldown, choose direct to COM1, or whichever comport you have plugged the cable into. All other options turn grey. Select OK. The COM1 Properties options screen will appear.

5. Set: Bits per Second: 9600; Data Bits: 8; Parity: None; Stop Bits: 1; Flow Control: None. Select OK. The option screen disappears to leave the terminal window with a flashing cursor.

6. Type the command [ve] or [VE] (the Controller Box recognizes ']' as the end of a command, so don't type $\hookleftarrow$). Nothing you type will appear in the terminal window if local character echoing is disabled. Echoing can be enabled under the menu File/Properties/Settings/ASCII Setup. If the connection is working, the reply `[VE,1.7,97,2,12,LEES GPM/ACS Controller]` will show up in the terminal window. If the connection is not working, there will be no change to the terminal window.

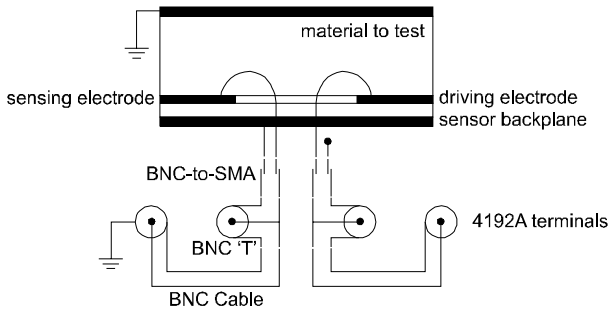

Figure 5-10: *A convenient apparatus for connecting the sensor to the HP 4192A impedance analyzer terminals. A capacitor or resistor connecting one of the sensor electrodes to ground does not affect the reading, because the impedance analyzer automatically cancels the admittance from the terminals to ground by way of a bridge circuit.*

Once a connection is established, you can initiate a measurement series right from the terminal window using the commands described in [28].

5.2.3 The Hewlett-Packard 4192A Impedance Analyzer

The Controller Box has a maximum frequency capability of 10 kHz. It is possible that some materials of interest have salient permittivity and conductivity features at frequencies above 10 kHz. New equipment is required to perform tests above this limit. The Hewlett-Packard 4192A Impedance Analyzer in LEES has a bandwidth of 13 MHz, and can be used to directly measure the transimpedance and transcapacitance of a single wavelength of the three wavelength sensor. A convenient apparatus for connecting the sensor to the 4192A terminals is given in Figure 5-10. It is at first counter-intuitive that this set up should provide accurate readings. Since none of the terminals of the 4192A is virtually grounded, the sensing electrode is not virtually grounded as it is in SCCM mode. At the same time, the guard plane and guard electrodes are hooked to real ground in the configuration of Figure 5-10, just as they are in SCCM mode. Thus there should be a capacitance between the sensing electrode and the guard plane and guard electrodes, that does not exist in either the SCCM or FVGPM modes. This extra capacitance should result in a larger measurement value, but it does not. The explanation is suspected to be the following: the terminals of the 4192A form a Wheatstone or similar style bridge that requires current to be conserved. Thus any current that is lost from the sensing electrode to the guard electrodes

(which are grounded), even reactive current, is regained by the driving electrode. The theory is corroborated by the evidence that a capacitor or resistor connecting either the sensing or the driving electrode to ground does not affect the reading. Even connecting either electrode to ground via a wire only changes the capacitance reading a little, showing that the 4192A measurement terminals have extremely high input impedance.

With the sensor connected as indicated in Figure 5-10, the measurement procedure is:

- Turn on the machine, and let it warm up for half an hour to stabilize.
- Using the up and down arrow keys, select:
  - Display A option: C
  - Display B option: R/G
  - Circuit Mode Option: Series or Parallel
- Select the frequency to measure by pressing the keypad digits and specifying the range (Hz, kHz, MHz), or specify a logarithmic sweep by pressing Blue then Log Sweep. Keep the sweep on Manual and adjust the frequency with the arrow keys on the right side of the panel. The conductance and capacitance and their units are displayed on the screens.

5.2.4 Phase Conventions

The phase of measurements can be a confusing issue because of the 180 phase shifts from the -10 gain opamp and the integrator in the SCCM interface box. Also, although the sensing electrode potential usually lags the driving electrode potential, which results in a negative phase measurement, there are instances where the equivalent conductance G_{12} is negative and thus the sensing electrode potential *leads* the driving electrode potential, resulting in a positive phase measurement. Knowing precisely what quadrant you expect the measured phase to lie in is vital and fairly simple. The convention is described below for each method.

SCCM

The -10 gain opamp phase shift cancels the integrator's phase shift. Thus for a non-conductive material, phase $\simeq 0$. For a mildly conductive material, phase $\leqslant 0$.

FVGPM

This circuit has neither an inverting amplifier nor an integrator. Thus for a non conductive material, phase $\simeq 0$. For a mildly conductive material, phase $\leqslant 0$.

GETGP3

When applied to the SCCM method, GETGP3 computes the phase considering only the inversion from the integrator and outputs a phase value in the range $-180 \leq \phi < 180$. A perfect insulator will have phase of $\phi \simeq -180$. A mildly conductive material will have a phase of $\phi < 180$. To find the phase that will be measured by SCCM subtract or add 180. For example, if GETGP3 says the phase will be 167, you will actually measure -13.

When applied to the FVGPM method, GETGP3 computes the correct phase with no shifts. The output of GETGP3 is the expected phase you will measure.

ESTLSQ

The rules of phase are interpreted by GETGP3 when it is called by ESTLSQ, so the same rules should be followed as for GETGP3. ESTLSQ can tolerate phase $\phi < -180$ and treats it as equivalent to $\phi + 360$.

5.3 Inventory of Equipment

Previous students working under Professor Zahn had produced dielectrometry equipment that can be used as a foundation for future work. The equipment includes Controller Boxes, Short Circuit Current Mode (SCCM) Interface Boxes, Floating Voltage with Guard Plane (FVGPM) Mode Interface Boxes and Three Wavelength Sensors. This equipment had been stored in shelving cabinets between graduate student projects. Before the equipment could be used again with confidence in actual experiments its condition was evaluated. Each item was tested for proper working order, and the values of the characterizing parameters were determined. The resulting specifications are summarized in Appendix B. Different tests were conducted to evaluate each type of equipment.

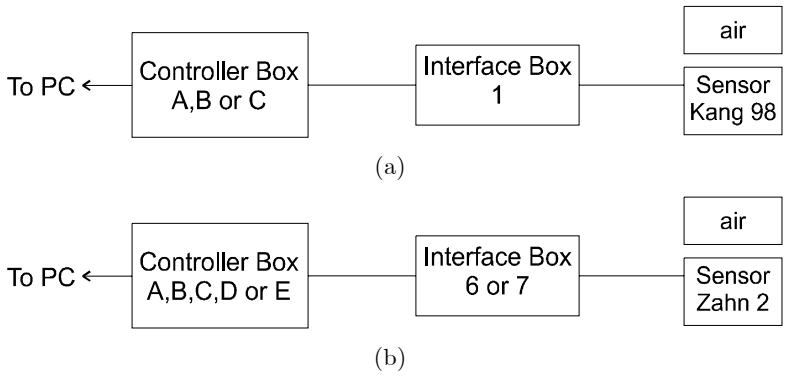

Figure 5-11: *The configuration of the dielectrometry equipment as the controller boxes were tested in a) SCCM mode b) FVGPM mode.*

5.3.1 Testing the Controller Boxes

The controller boxes were tested to make sure that they responded to commands from the serial port, and that they logged precise data. A measurement series was conducted using each controller box hooked up to an interface box and a three wavelength sensor measuring an infinite half space of air. The configuration is illustrated in Figure 5-11.

For the Short Circuit Current Mode the configuration used to test the controller boxes can be completely described as:

- Software: Takedata.exe
- Controller Boxes: {A,B,C}
- Interface Box: 1
- Sensor: Kang 98
- Connector Config:
  - Channel 1: 1mm sense, 1mm drive
  - Channel 2: 5mm sense, 5mm drive
  - Channel 3: 2.5mm sense, 2.5mm drive
- Mode: Short Circuit Current Mode (3)

- Test Material: Air

For the Floating Voltage with Guard Plane Mode the configuration used to test the controller boxes can be completely described as:

- Software: Takedata.exe
- Controller Boxes: {D,E}
- Interface Box: 7
- Sensor: Zahn 2
- Connector Config:
  - Channel 1: 1mm sense
  - Channel 2: 5mm sense
  - Channel 3: 2.5mm sense
- Drive: Drive
- Mode: Floating Voltage with Guard Plane Mode (2)
- Test Material: Air

If the controller box being tested replied with its version information to the serial command [VE] sent using Takedata.exe, then the microcontroller in the controller box was deemed to be working. The command [DE, 001 001 001] was then sent, with the expectation that the Excite LED's of the interface box would turn on, to make sure that the digital output ports were functioning. Next, a measurement series was initiated over the frequency range from 1 kHz to 10 kHz on all three channels by sending the Trigger command from Takedata.exe. If the gain and phase reported in the file were in the expected range for a measurement with air, and there was some small variance inside that range (on the order of $0.1\angle 1$ [dB$\angle$degrees]) then the controller box was deemed to be working properly. The expected measurement values for air can be calculated using the known capacitances of the interdigital electrodes in air, and

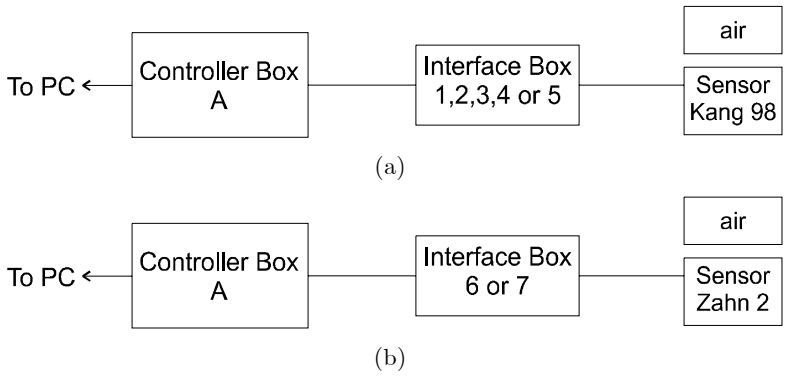

Figure 5-12: *The configuration of the dielectrometry equipment as the interface boxes were tested in a) SCCM mode and b) FVGPM mode.*

the known feedback capacitances of the amplifier boards in the interface box, with Equation 5.10 for the short circuit current mode and with Equation 5.11 for the floating voltage with guard plane mode. These equations have been repeated below for reference, with G_{12} set to zero because air is a very good insulator.

$$gain_{air} = 20\log_{10}\left|10\frac{C_{12air}}{C_F}\right| \text{ [dB] for short circuit current mode} \tag{5.12}$$

$$gain_{air} = 20\log_{10}\left|\frac{C_{12air}}{C_{12air}+C_L}\right| \text{ [dB] for floating voltage with guard plane mode} \tag{5.13}$$

$$phase_{air} = 0 \tag{5.14}$$

This calculation is described in Section 5.2.2. Measurements with absolutely no variance (e.g. gain$\angle$phase $\equiv$ -66.22$\angle$0 [dB$\angle$degrees] for all frequencies) or with large variance (greater than roughly 2$\angle$5 [dB$\angle$degrees]) indicate a system that is not working properly, although the controller box is not necessarily at fault.

5.3.2 Testing the Interface Boxes

The interface boxes were first tested to make sure they transmitted the driving and senses signals properly. The configuration for these tests is illustrated in Figure 5-12.

For the Short Circuit Current Mode the configuration used to test the interface boxes can be completely described as:

- Software: Takedata.exe
- Controller Box: A
- Interface Boxes: {1,2,3,4,5}
- Sensor: Seong Hwa Kang 1998
- Connector Config:
  - Channel 1: 1mm sense, 1mm drive
  - Channel 2: 5mm sense, 5mm drive
  - Channel 3: 2.5mm sense 2.5mm drive
- Mode: Short Circuit Current Mode (3)
- Test Material: Air

For the Floating Voltage with Guard Plane Mode the configuration used to test the interface boxes can be completely described as:

- Software: Takedata.exe
- Controller Box: A
- Interface Boxes: {6,7}
- Sensor: Zahn 2
- Connector Config:
  - Channel 1: 1mm sense
  - Channel 2: 5mm sense
  - Channel 3: 2.5mm sense
- Drive: Drive
- Mode: Floating Voltage with Guard Plane Mode (2)

- Test Material: Air

Again, a measurement series was initiated over the frequency range from 1 kHz to 10 kHz on all three channels by sending the Trigger command from Takedata.exe and saving the data file on the PC. For the interface box to be deemed in working condition, the gain and phase reported in the file were required to be in the expected range for a measurement with air, and to have some small variance around a typical value (on the order of 0.1∠1 [dB∠degrees]). Furthermore, the gain must increase several decibels when a Lexan slab is placed directly on the sensor (Lexan is General Electric's brand name for polycarbonate). Measurements with absolutely no variance (e.g. gain∠phase≡-66.22∠0 [dB∠degrees] for all frequencies) or with large variance (greater than roughly gain∠phase≡2∠5 [dBdegrees]) or with gain∠phase values unaffected by the Lexan slab indicate a system that is not working properly, although the interface box is not necessarily at fault.

The channel feedback capacitances of the SCCM interface boxes and channel load capacitances of the FVGPM interface boxes were then measured. To do this, each wavelength of the three wavelength sensors was replaced by a reference capacitor of known value as shown in Figures 5-13 and 5-14 and a measurement was taken at 1 kHz using Takedata.exe. The reference capacitors were 100 pF nominal tantalums, with SMA pins soldered onto their legs. The true values of their capacitances were measured using the HP 4192A impedance analyzer at 1 kHz and 10 kHz. In the SCCM interface boxes, three reference capacitors could be used simultaneously because each channel has its own drive circuit. In the FVGPM interface boxes, each wavelength was replaced with a reference capacitor one at a time, because there is only one drive circuit in this type of interface box. Figures 5-15 and 5-16 show the corresponding circuit diagram of a single channel with a reference capacitor in place of the interdigitated sensor, for the respective mode. Solving each circuit yielded an expression for the feedback capacitor (Equation 5.15) or load capacitor (Equation 5.16) in terms of the measured gain and the reference capacitor's value. For the short circuit current mode, the expression is:

$$C_{feedback} = C_F = C_{reference} \cos\phi 10^{\frac{|\widehat{G}|}{20}-1} \tag{5.15}$$

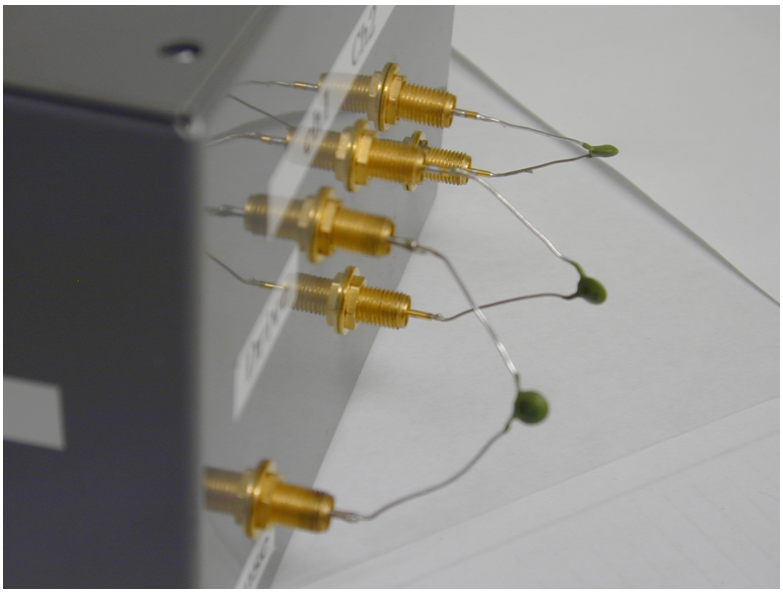

Figure 5-13: *100 nF nominal reference capacitors take the place of the interdigital dielectrometry sensors on the short circuit current mode interface box. Their values are measured precisely on the HP 4192A impedance analyzer, allowing the value of the feedback capacitor of each channel on the interface box to be solved for.*

while for the floating voltage with guard plane mode, the expression is:

$$C_{load} = C_L = C_{reference} \frac{(1 - 10^{\frac{|\widehat{G}|}{20}})}{10^{\frac{|\widehat{G}|}{20}}} \tag{5.16}$$

To be sure that the derived value for the channel feedback (load) capacitors was reasonable, the boxes were opened and the nominal capacitor values were read. The reference capacitor values and resulting feedback (load) capacitor values are listed in Tables 5.1 and 5.2.

5.3.3 The Three Wavelength Sensors

The three wavelength sensors do not contain active components and this makes them easier to examine in some respects. The sensors were first inspected for obvious damage, and some was found. In particular, the coaxial leads are vulnerable to damage by kinking and at the solder attachment to the sensor pad. The lead for the 1 mm wavelength sensor of Zahn 2 was suspected of having an internal short and was replaced. Subsequently, in some measurements

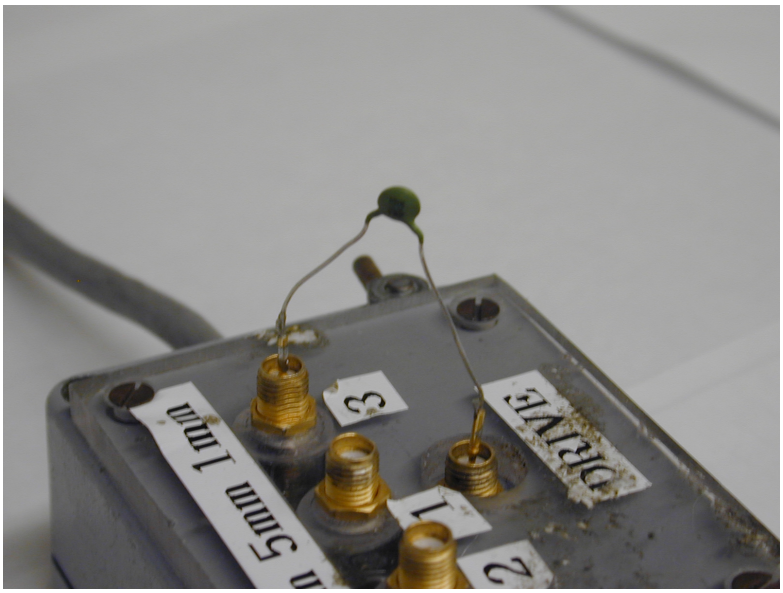

Figure 5-14: *A single 100 nF nominal reference capacitor is used in place of an interdigital dielectrometry sensor on each channel of the interface box one at a time. The channel load capacitance values are then determined.*

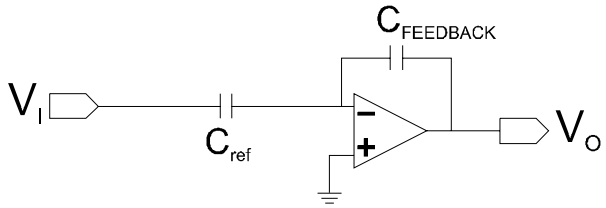

Figure 5-15: *The simple circuit that results when the interdigital dielectrometry sensor is replaced by reference capacitor in the SCCM interface box. The explicit solution of the feedback capacitance C_F is given in Equation 5.15.*

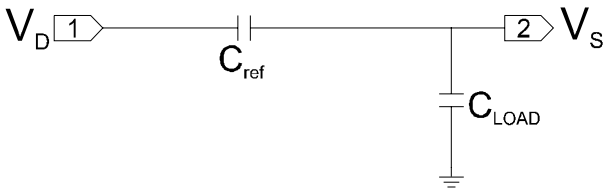

Figure 5-16: *The simple circuit that results when the interdigital dielectrometry sensor is replaced by reference capacitor in the FVGPM interface box. The explicit solution of the load capacitance C_F is given in Equation 5.16.*

		$C_{reference}$[nF]					
	Freq [kHz]	Channel 1	Channel 2	Channel 3	$C_{feedback} = C_{reference} \cos\phi 10^{\frac{\lvert\widehat{G}\rvert}{20}-1}$		
	1	92.8	92.9	90.4			
	10	91.7	91.9	89.4			
		$C_{feedback}$ [nF]			measured gain $\lvert\widehat{G}\rvert \measuredangle\phi$		
box	Freq [kHz]	Channel 1	Channel 2	Channel 3	Channel 1	Channel 2	Channel 3
1	1	9.807	2.887	2.905	-20.48∡-0.40	-9.85∡-0.60	-10.14∡-0.64
	10	9.758	2.889	2.909	-20.54∡-0.46	-9.95∡-0.68	-10.24∡-0.64
2	1	0.987	0.968	2.980	-0.55∡-0.35	-0.36∡-0.48	-10.36∡-0.56
	10	0.986	0.971	2.950	-0.63∡0.35	-0.48∡0.21	-10.37∡0.03
3	1	9.955	12.589	3.000	-20.61∡-0.21	-22.64∡-0.31	-10.42∡-0.44
	10	9.905	12.297	2.998	-20.67∡0.39	-22.53∡0.27	-10.51∡0.18
4	1	0.480	-	-	5.73∡-0.44	-	-
	10	0.479	-	-	5.64∡-0.58	-	-

Table 5.1: *The feedback capacitor values calculated from measured complex gain with reference capacitors of known value in place of the interdigital sensor.*

this sensor displays two modes: the first mode corresponds to the expected operation of the sensor; the second mode suggests a short between sense and drive electrodes. It seems the modes can be toggled by slightly shifting the sample under test. Thus the problem may be on the sensor pad itself rather than in the lead, making it difficult to fix.

Next, some of the important physical dimensions of the sensors were verified by direct measurement, including substrate thickness, sensor wavelength and meander length. Other parameters that are not so easily measured were found in the literature of past students, and include substrate permittivity, normalized interelectrode spacing and electrode thickness. All of these parameters are summarized in Table B.4.

		$C_{reference}$[nF]					
	Freq [kHz]	Channel 1	Channel 2	Channel 3	$C_{load} = C_{reference}\frac{(1-10^{\frac{\widehat{G}}{20}})}{10^{\frac{\widehat{G}}{20}}}$		
	1	92.8	92.8	92.8			
	10	91.7	91.7	91.7			
		C_{load} [pF]			measured gain $\widehat{G}\angle\phi$		
box	Freq [kHz]	Channel 1	Channel 2	Channel 3	Channel 1	Channel 2	Channel 3
6	1	12.41	12.53	12.41	-1.09∠0.25	-1.10∠0.25	-1.09∠0.25
	10	12.26	12.50	12.38	-1.09∠2.76	-1.11∠2.90	-1.10∠2.90
7	1	49.94	102.0	222.0	-3.74∠0.11	-6.44∠0.06	-10.61∠-0.01

Table 5.2: *The load capacitor values calculated from measured complex gain with a reference capacitor of known value in place of the interdigital sensor.*

Chapter 6

Experimental Results

6.1 Introduction

The experimental research began with the existing three-wavelength sensors that had been developed by former students for transformer pressboard moisture profiling. These sensors were used to learn about the dielectrometry method. Measurements were made with these sensors on common dielectric materials such as sugar, salt, sand, teflon, paper, wood, and rubber eraser. Both the Short Circuit Current Mode and the Floating Voltage Guard Plane Mode, which use different signal processing circuits, were used.

Next, a Hewlett-Packard impedance analyzer was used to directly measure the transadmittance of the sensor, essentially performing the same task as the signal processing electronics. These measurements were compared to the measurements made by the signal processing electronics to verify that all experiments had been accurate.

New sensors were designed to improve the performance of the interdigital dielectrometry system as it applies to measuring shoes. The new sensors were scaled in wavelength to have sufficient penetration depth for sensing the entire thickness of a shoe sole and in planar dimensions to have sufficient area to cover the heel of a shoe. A new method of accurately placing the shoes on the sensor was developed to deal with the irregular shape of shoes.

Various shoe types were purchased from a discount clothing store to serve as the samples for the next experiments. One shoe of each pair had a cavity machined in the sole in which samples of other materials could be placed. This would recreate the modified shoe that a suspect might

attempt to wear into a secure location.

Finally a novel sensor design was built and tested with the hypothesis that it would be more sensitive than the regular interdigital sensors. The new sensor was composed of one single driving electrode finger and one single sensing electrode finger on the top of a Teflon substrate with a ground plane on the bottom of the substrate. The centerlines of the two electrodes were spaced apart by 25 mm, giving the sensor an equivalent wavelength of 50 mm. This new design, however, did not have greater sensitivity to materials inserted into the heel cavity than the conventional 20 mm wavelength sensor.

6.2 Measurements with three-wavelength sensors

The three wavelength sensors with wavelengths of 1 mm, 2.5 mm and 5 mm were used for measurements on common dielectric material samples.

6.2.1 The dielectric material samples

Readily available dielectric materials were used as samples. Air is the easiest material to measure because it contacts the sensor pad perfectly so there is no uncertainty in the contact quality, and because it's relative permittivity is accurately known to be almost exactly 1. Lexan, with an accurately known permittivity of $\varepsilon_r = 3.17$, was used as a convenient test dielectric to verify instrument operation. Sugar ($C_6H_{12}O_6$) is known to have similar properties to common explosives such as HMX (High Melting eXplosive, also known as octogen), cyclotetramethylene-tetranitramine ($C_7H_5O_6N_3$) and TNT (2, 4, 6 – trinitrotoluene, $C_7H_5O_6N_3$) because of their common organic composition. Both granular and powder forms of sugar were used, to show the effect of particle size on the measurements. Table salt was used as another example of a granular material. The sugar and salt were measured first while contained in a white Delrin box, and then while inside a polyethylene Ziploc bag. The Delrin box and the Ziploc bag were each measured empty to compare to the measurements that were made when they contained sugar or salt. The Ziploc bag was measured empty by inflating it and setting the weight on top to ensure good contact quality.

The samples were placed on the sensor pad so that they uniformly covered all three of

the sensors. A grounded steel plate was set on top of the sample to set the upper boundary condition and to eliminate stray fields from other sources in the room. A 20 lb lead block was set on top of the steel plate to ensure a small air gap that was consistent between measurements. All of the samples were thick enough (much greater than 5 mm) that almost none of the field lines originating from the driving electrode terminated on the ground plane above the sample. Therefore the samples could be assumed to be approximate infinite half spaces.

6.2.2 Equipment

Controller box A and interface box 1 were used in the measurements. Channels 1, 2 and 3 used sensing boards 1.1, 1.2 and 1.3 with feedback capacitances of 9.81 nF, 2.89 nF and 2.91 nF and were connected to the 2.5 mm, 5 mm and 1 mm wavelength sensors, respectively. The interface box channels were set to excite but not attenuate, and the discharge mode was enabled by leaving the discharge switch in the up (on) position.

6.2.3 Experimental Results

Figure 6-1(a) shows the voltage gain for the 5 mm wavelength sensor, including the 20 dB of preamplification provided by the interface box. All of the samples except paper exhibit constant gain as the frequency of excitation changes. The measured gain for paper is typical of conductive materials, increasing at low frequencies due to the current passing through the paper. Since paper is very hydrophilic, its measurements were affected by the ambient air humidity. Air has the lowest gain because it has the smallest real dielectric constant. The Ziploc bag by itself has only a slightly higher gain, because it is only a very thin layer of polyethylene under an infinite layer of air. The Delrin box has the highest permittivity and thus the highest gain. We can see the effect of filling it with various materials: its gain is increased by filling it with granular sugar or salt, and decreased by filling it with powdered sugar, which has a higher air content than granular sugar and thus a lower gain. The gain for all of the materials shows a glitch at 63 Hz which is known to be caused by a bug in the driving electronics as they cross from high frequencies to low frequencies. It may be possible to eliminate this glitch by using the controller box command [FP,parameters] that sets a time delay compensation for measurements above 100 Hz. The command is described in [28].

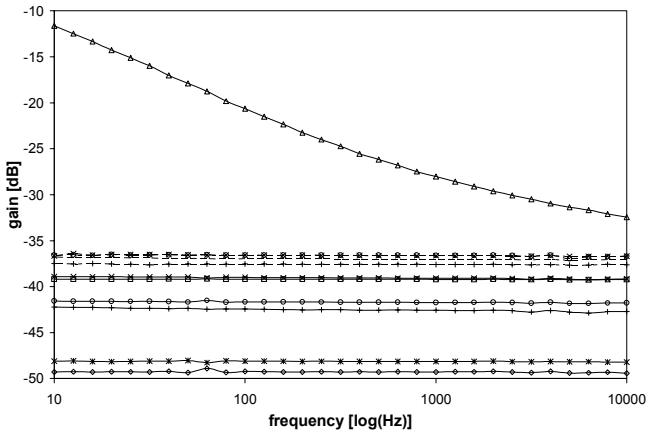

(a) Gain for $\lambda = 5$ mm.

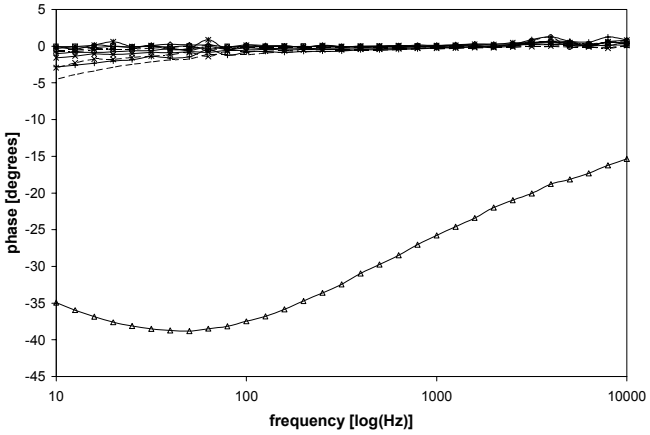

(b) Phase for $\lambda = 5$ mm.

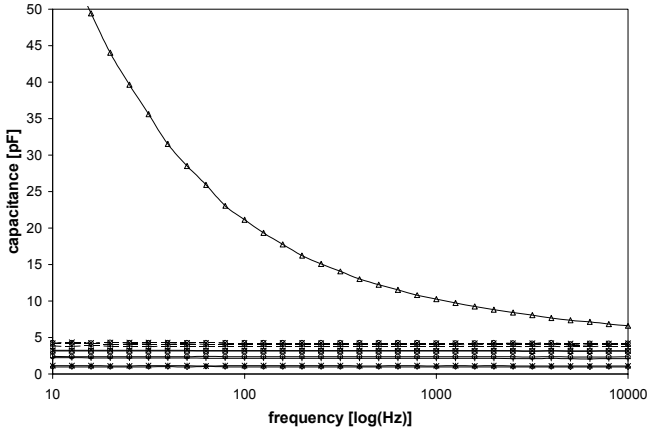

(c) Capacitance for $\lambda = 5$ mm.

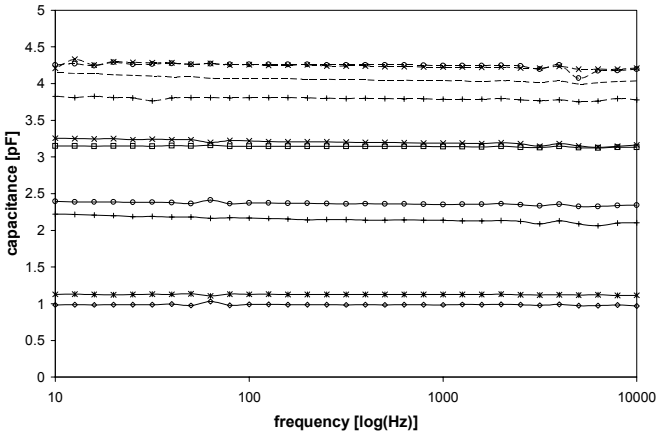

(d) Capacitance closeup for $\lambda = 5$ mm.

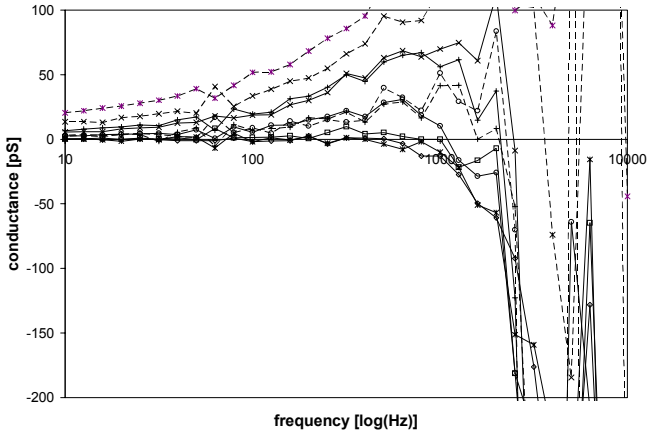

(e) Conductance for $\lambda = 5$ mm.

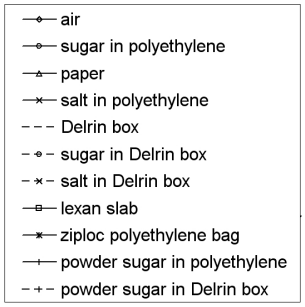

(f) legend

Figure 6-1: *Measured gain and phase and derived capacitance and conductance for the 5 mm wavelength sensor with various materials using the SCCM method.*

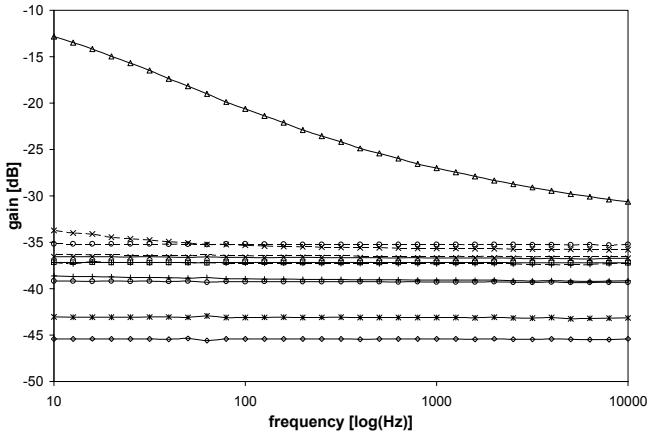

(a) Gain for $\lambda = 2.5$ mm.

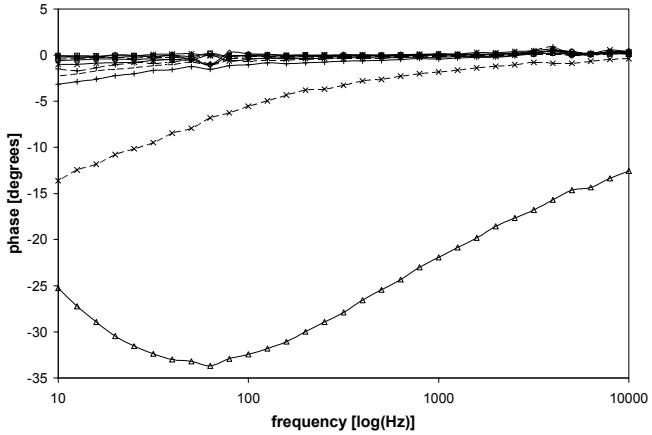

(b) Phase for $\lambda = 2.5$ mm.

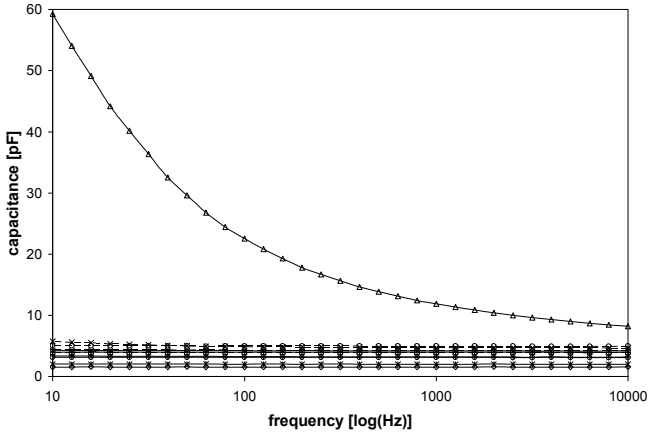

(c) Capacitance for $\lambda = 2.5$ mm.

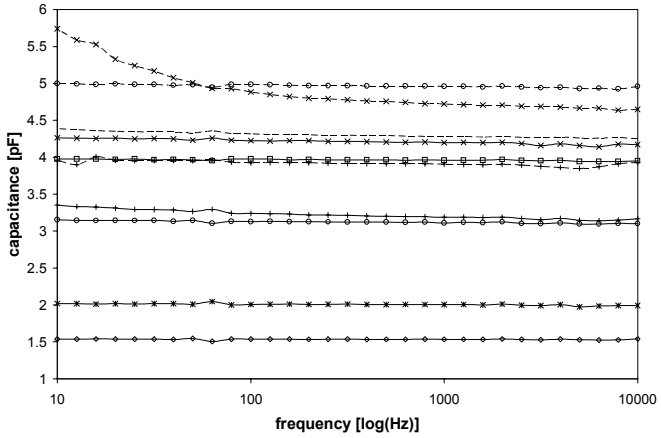

(d) Capacitance closeup for $\lambda = 2.5$ mm.

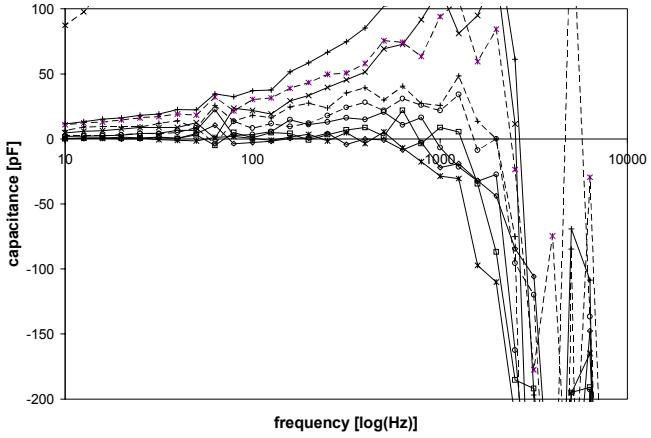

(e) Conductance for $\lambda = 2.5$ mm.

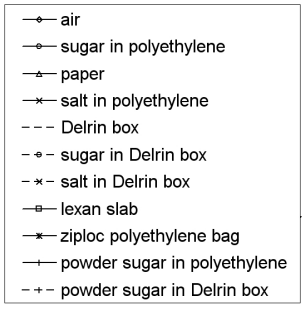

(f) legend

Figure 6-2: *Measured gain and phase and derived capacitance and conductance for the 2.5 mm wavelength sensor with various materials using the SCCM method.*

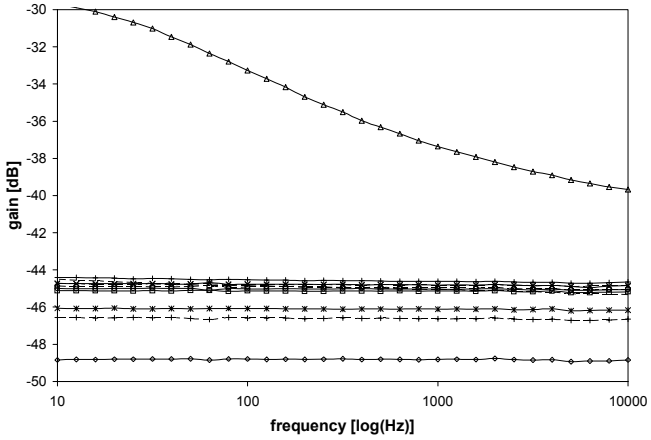

(a) Gain for $\lambda = 1$ mm.

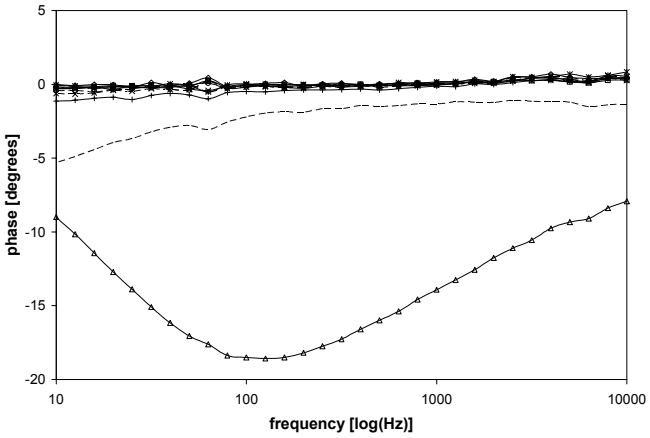

(b) Phase for $\lambda = 1$ mm.

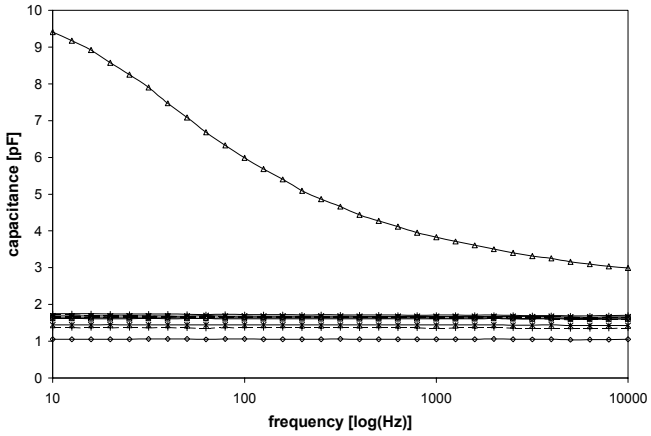

(c) Capacitance for $\lambda = 1$ mm.

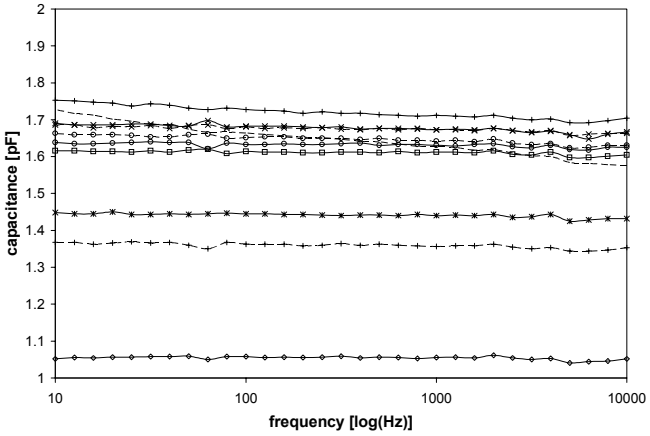

(d) Capacitance closeup for $\lambda = 1$ mm.

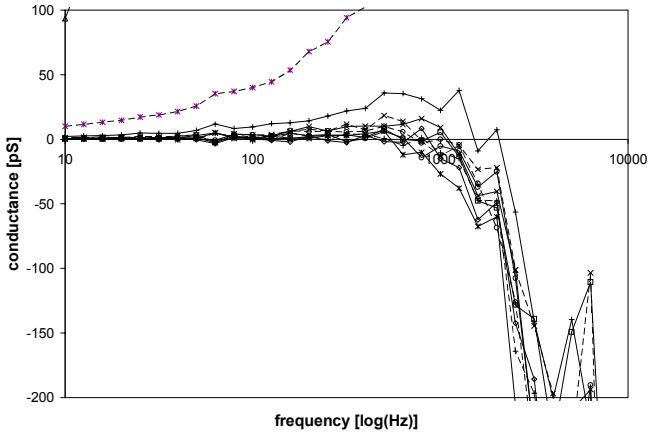

(e) Conductance for $\lambda = 1$ mm.

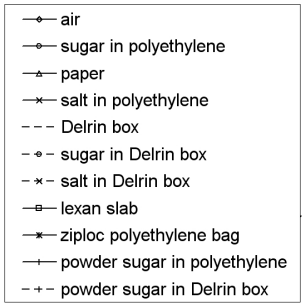

(f) legend

Figure 6-3: *Measured gain and phase and derived capacitance and conductance for the 1 mm wavelength sensor with various materials using the SCCM method.*

Figure 6-1(b) shows the phase for the 5 mm wavelength sensor. The phase is always less than zero because the system is purely capacitive. Noise at higher frequencies causes some of the measured phases to be greater than zero. Again, paper exhibits a curve that is quite distinct from the other materials and is typical of conductive materials. The frequency breakpoint that occurs at around 1000 Hz is proportional to the ratio of imaginary to real parts of the dielectric constant and is also dependent on the dielectric properties of the other materials in the system, including the Teflon substrate. The phase for all the other materials is only beginning to decrease at 10 Hz, showing that they are at least 4 orders of magnitude less conductive than paper.

Figures 6-1(c) and 6-1(d) show the transcapacitance of the 5 mm wavelength sensor calculated from measured gain and phase and known frequency using Equations 5.8 and 5.9. The transcapacitance of paper increases at low frequencies. It is not constant because the topology from which C_{12} is extracted does not reflect the real topology of the system, which has conductive paths to ground at all points between the driving and sensing electrodes. For the homogeneous non-conductive materials, the capacitance is proportional to the materials' dielectric constants. Since we know that the relative dielectric constant of air is approximately 1, the dielectric constants of the other homogeneous materials can roughly be picked off the plot if we neglect the affect of the Ziploc bag (a thin polyethylene layer). Determining the dielectric constants of the empty polyethylene bag and the empty Delrin box, which are not homogeneous samples because they contain air, requires a more detailed calculation. The calculation of the sample material's complex dielectric constant from gain and phase measurements is discussed in detail in Chapter 4.

Figure 6-1(e) shows the conductance of the 5 mm wavelength sensor. The conductance becomes very sensitive to phase at high frequencies and is affected by noise in the readings. Measurements above 1000 Hz are not reliable. Again, the conductance for paper increases at higher frequencies due to the topological representation of the system by G_{12}.

Figures 6-2(a) to 6-3(e) present the gain, phase, capacitance and conductance for the 2.5 mm and the 1 mm sensors measuring the same materials that had been measured by the 5 mm wavelength sensor. It is interesting to note that the difference in gain between the measurement of the thin polyethylene bag and the measurement of air increases at small wavelengths, because

the polyethylene fills a greater portion of the volume that contains the electric field. Likewise, the affect of adding sugar or salt to the Delrin box decreases, because the field penetrates less into the space where material changes and is instead occupied mostly by Delrin.

Although the frequency breakpoints for paper are proportional to the ratio of conductivity to permittivity, they are also dependent on the presence of other materials in the system. The normalized thickness of the Teflon substrate is greater in the 1 mm wavelength sensor and this shifts the breakpoint higher.

6.3 Measurements with an Impedance Analyzer

The Hewlett Packard impedance analyzer was used to measure the capacitance and conductance of the three wavelength sensor with the some of the same sample materials as had been used with the Short Circuit Current Mode and the Floating Voltage Guard Plane Mode in Section 6.2. The sensor was attached to the impedance analyzer with SMA-to-BNC connectors in the configuration discussed in Section 5.2.3. The samples were placed on the sensor in the same manner as they had been in the SCCM and FVGPM measurements, including a grounded plate and a 20 lb lead weight on top. The gain and phase values were converted to the capacitance and conductance between the sensing and driving electrode terminals so that they could be compared directly to the output of the impedance analyzer. Recall that for the SCCM method the capacitance and conductance are given by Equations 5.8 and 5.9 which are repeated here for reference.

$$C_{12}(\omega) = -\left|\widehat{G}\right| C_F \cos\phi = -\operatorname{Re}\left\{\widehat{G}\right\} C_F \tag{6.1}$$

$$G_{12}(\omega) = \omega C_F \left|\widehat{G}\right| \sin\phi = \operatorname{Im}\left\{\widehat{G}\right\} \omega C_F \tag{6.2}$$

which simplify to Equations 6.3 and 6.4 for non-conductive materials and at high frequencies for slightly conducting materials:

$$C_{12}(\omega) = -\left|\widehat{G}\right| C_F \tag{6.3}$$

$$G_{12} = 0 \tag{6.4}$$

For the FVGPM method the capacitance and conductance are given by Equations 5.5 and 5.6:

$$C_{12}(\omega) = -\frac{C_L \left|\widehat{G}\right| (\left|\widehat{G}\right| - \cos\theta)}{1 + \left|\widehat{G}\right|^2 - 2\left|\widehat{G}\right| \cos\theta} \tag{6.5}$$

$$G_{12}(\omega) = -\frac{\omega C_L \left|\widehat{G}\right| \sin\theta}{1 + \left|\widehat{G}\right|^2 - 2\left|\widehat{G}\right| \cos\theta} \tag{6.6}$$

which simplify to Equations 6.7 and 6.8 for non-conductive materials and at high frequencies for slightly conducting materials:

$$C_{12} = \frac{C_L \left|\widehat{G}\right|}{1 - \left|\widehat{G}\right|} \tag{6.7}$$

$$G_{12} = 0 \tag{6.8}$$

Figure 6-4 shows the capacitance of the 5 mm wavelength sensor for all three methods. In the overlapping frequency range from 1 kHz to 10 kHz, the capacitance for all materials except Teflon^{TM} is the same for all three methods within acceptable tolerances. The capacitances of sugar and teflon are so close when measured by the impedance analyzer that they are nearly indistinguishable, illustrating one difficulty of identifying materials by their dielectric character. Here we have only four insulating materials whose dielectric constants are spread by nearly a factor of four. Two of them are virtually indistinguishable across six decades of frequency measurements. The level of precision required of the equipment to allow the identification of individual materials from a possible set of hundreds or thousands will have to be carefully evaluated and will likely be quite high.

The capacitance values from the impedance analyzer drops suddenly for all materials between 100 kHz and 158.4 kHz. This is not a fault of the impedance analyzer, nor a feature of all of the materials' dielectric character. It is likely caused by a stray capacitance in the sensor coupled with a weak conductance that exhibits a frequency break point in that particular frequency range. Above 1 MHz there is a further attenuation in the capacitance of all the materials that is probably also due to a stray capacitance and conductance interaction. The glitch in the data from both the SCCM and FVGPM methods at 63 Hz is due to a bug in the

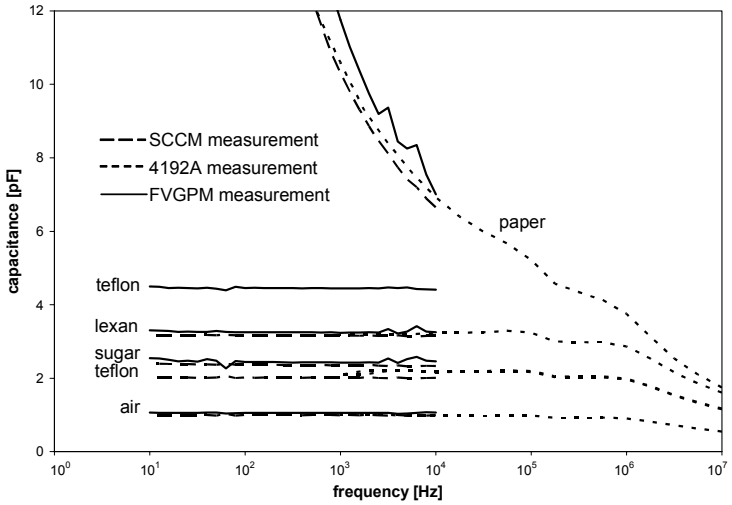

Figure 6-4: *Capacitance of the 5 mm wavelength sensor under various dielectric materials, determined using three different measurement methods.*

voltage signal driving hardware.

Figure 6-5 shows the measured capacitance of the 2.5 mm wavelength sensor for all three methods while Figure 6-6 shows the capacitance for the 1 mm wavelength sensor. The fit of the data between all three methods is best for the 5 mm and worst for the 1 mm sensor. This indicates that the contact quality and thus the air gap between the sample and the sensor pad was slightly different for each method. The 1 mm wavelength sensor was most affected because the air gap contains the greatest portion of the electric field energy for this wavelength. A change in the thickness of the air gap, then, has the greatest affect on the signal of the 1 mm wavelength sensor.

The Short Circuit Current Mode was used exclusively thereafter for all research in this thesis because there was no need for a higher frequency range, because the SCCM equipment logs data expediently, and because it is available for exclusive use in building N10 whereas the Impedance Analyzer is shared by all the students of LEES.

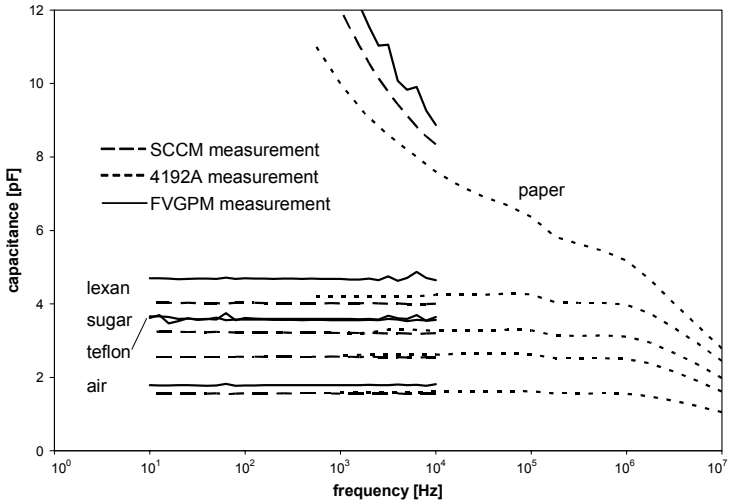

Figure 6-5: *Capacitance of the 2.5 mm wavelength sensor under various dielectric materials, determined using three different measurement methods.*

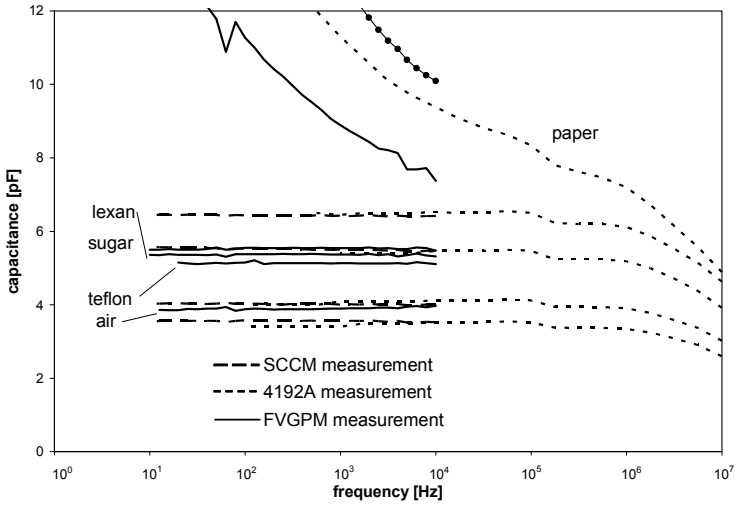

Figure 6-6: *Capacitance of the 1 mm wavelength sensor under various dielectric materials, determined using three different measurement methods.*

6.4 Measurements on Common Shoe Materials

Preliminary testing was done on common shoe sole materials to roughly determine their behavior in dielectrometry experiments. A black rubber replacement heel and a leather replacement sole were used. The black rubber heel was initially 1.4 cm thick and had a tread pattern of features with an average depth of 0.5 mm. The largest wavelength sensor in the lab at the time was the 5 mm section of the three wavelength sensor. A sugar sample would have to be within 2 mm of the sensor surface, the penetration depth of the 5 mm sensor, to be able to show the affects of having sugar inside the rubber heel. This would require a cavity in the heel of a shoe to penetrate to within 2 mm of the bottom of the sole. For a first mock-up, a thin layer of shoe sole was simply prepared that would be used without the rest of the shoe attached. A layer of average thickness 1 mm was made from the rubber heel by sanding off the tread pattern, cutting a layer off the bottom of the heel with a razor blade, and sanding smooth the cut surface of the removed layer. The layer of rubber was then tested alone and with a thick sugar sample on top, as is shown in Figure 6-8. The gain and phase response in Figures 6-7(a) and 6-7(b) respectively show that the rubber-only sample can be distinguished from the rubber in combination with sugar sample. Further analysis of the data could extract the dielectric constants of the two materials, allowing them to be more precisely identified. Inverse parameter estimation is discussed in Section 4.3.

The leather heel is much more conductive than the rubber, exhibiting the typical gain and phase curves of slightly conducting materials. The response of the leather was sensitive to humidity and changed from day to day. The rather high conductivity of leather allows it to overpower weaker signal features in the gain and phase responses of other materials that might be measured at the same time as the leather. As well, the fact that its complex dielectric constant changes with ambient moisture means it has a broad range of legitimate dielectric identities. These factors make leather a difficult candidate for dielectrometry. The leather sole is 6 mm thick and could not be thinned down to allow for a measurement with the combination of sugar and leather.

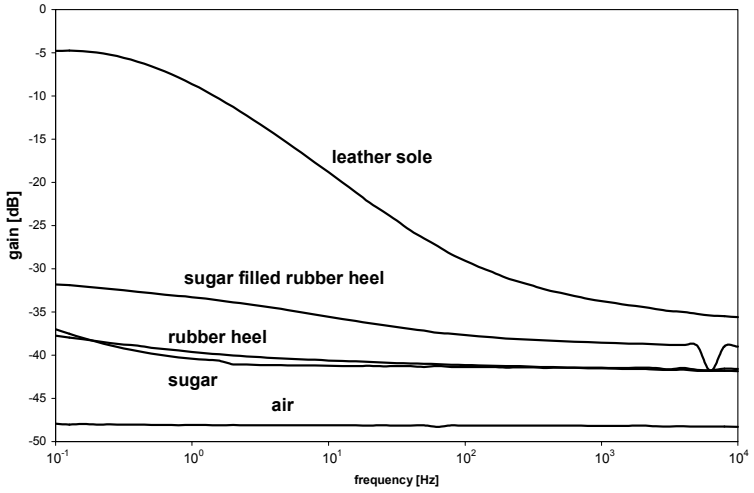

(a) Gain of the rubber heel measured alone and in combination with a sample of sugar.

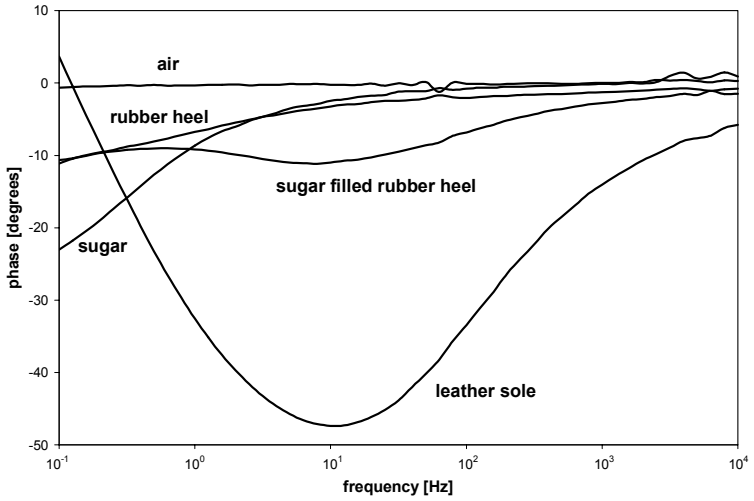

(b) Phase of the rubber heel with and without the sugar sample above it.

Figure 6-7: *SCCM measurements of the modified rubber heel with and without a sugar sample show that the difference can be detected.*

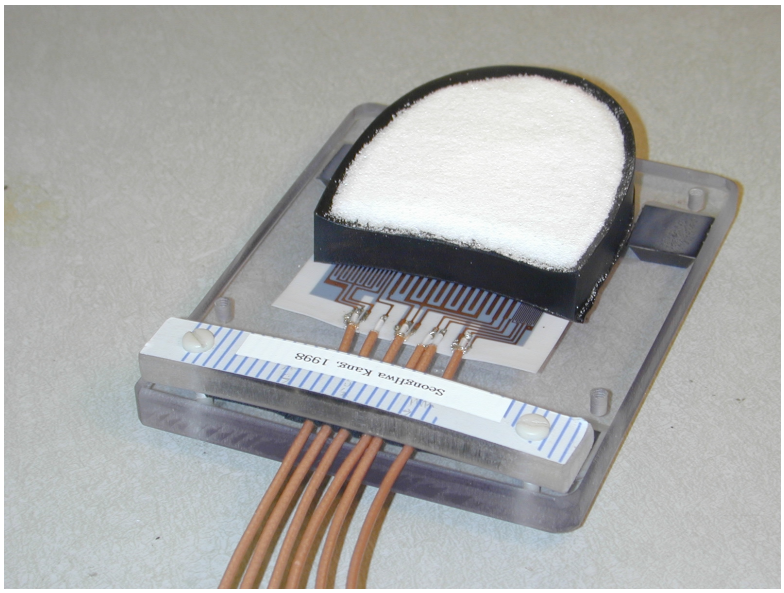

Figure 6-8: *The rubber heel being measured while filled with sugar. Because the heel is so thick, the actual measurements had to be done by slicing off the majority of the heel to leave on a 1 mm thick layer, then setting the sugar on top of that layer.*

6.5 New Long Wavelength Sensors

While the 5 mm wavelength sensor could distinguish between the rubber heel with and without sugar measurements, it would not have the penetration depth or the surface area to accomodate real shoes. New sensors were designed with wavelengths of 10 mm, 20 mm and 40 mm and with large enough areas to cover most of a shoe's sole. The sensor electrode pattern was adapted from the three-wavelength sensor design. Each sensor has two guard electrodes on each side of the sensing electrode array, a back plane on the bottom, and unplated through holes to allow a connection to the back plane from the top. Scaled down drawings are shown in Figure 6-9 of the small and large area 10 mm wavelength sensors and the 20 mm wavelength sensor and in Figure 6-10 of the 40 mm wavelength sensor. The sensors were manufactured by Polyflon [25] on one of their proprietary Cuflon microwave substrates, a 254 μm thick Teflon^{TM} sheet with a 35.5 μm thick (1 oz) copper layer on each side. The rectangular outline that surrounds the drawings was intended to represent the outline of the 12" by 18" Cuflon sheets that the sensors were made from. The sheets actually measured slightly larger than 12" by 18" so these

rectangular frames were printed. Note also the small alignment markings that were included to help in cutting the sensors apart at the right place.

While the sensors were being manufactured, the ideal feedback capacitances for each new sensor were estimated. The capacitances were chosen to be as small as possible so as to avoid saturating the integrator, while still keeping the signal above the noise region of about -35dB. Figure 6-11 plots the gain that would result for each sensor if it were measuring air versus the feedback capacitance. The data was calculated by GETGP3 using the expected sensor parameters and a 1 nF feedback capacitor. All other values of gain were extrapolated using the relation between gain and feedback capacitance of Equation 5.7.

$$\widehat{G} = \frac{V_S}{V_D} = -\frac{G_{12} + j\omega C_{12}}{j\omega C_F} = \left|\widehat{G}\right| \cos\theta + j \left|\widehat{G}\right| \sin\theta$$

For the small 10 mm and the 20 mm wavelength sensors, both having shorter meander lengths, a 0.5 nF feedback capacitor would be required to keep the signal above -35 dB. For the large 10 mm and the 40 mm wavelength sensors, which have longer meander lengths, a 1 nF capacitor was suitable. These capacitances matched feedback capacitances on amplifying boards 4.1 (0.48 nF) and 2.2 (0.97 nF), so these boards would be used in conjunction with the new sensors.

After the sensors were fabricated, an attempt to clean them was made following the recommendations in ([10], pp. 497-504). It was suggested that ultrasonic cleaning removed a brown conductive residue that was left over after manufacturing, and that bleaching would not sufficiently clean the sensor. However, the 40 mm wavelength sensor would be too large to fit in any ultrasonic cleaner that was available. A test on two small 10 mm sensors was made to see if ultrasonic cleaning had any effect on the phase measurement, which is indicative of conductivity at low frequencies. The sensor that was cleaned by merely wiping with alcohol performed just as well as the sensor that was cleaned in the ultrasonic bath. Figure 6-12 shows a comparison of the phase measurement in air of the two sensors, going down to 0.005 Hz, and illustrates that the variance of each sensor's phase at low frequency is much greater than the difference between them. Both cleaning methods adequately removed conductive residue that was left after manufacturing. Thus the 40 mm wavelength sensor was prepared by wiping with alcohol and soldering on the leads, saving a lot of trouble in finding a large ultrasonic bath.

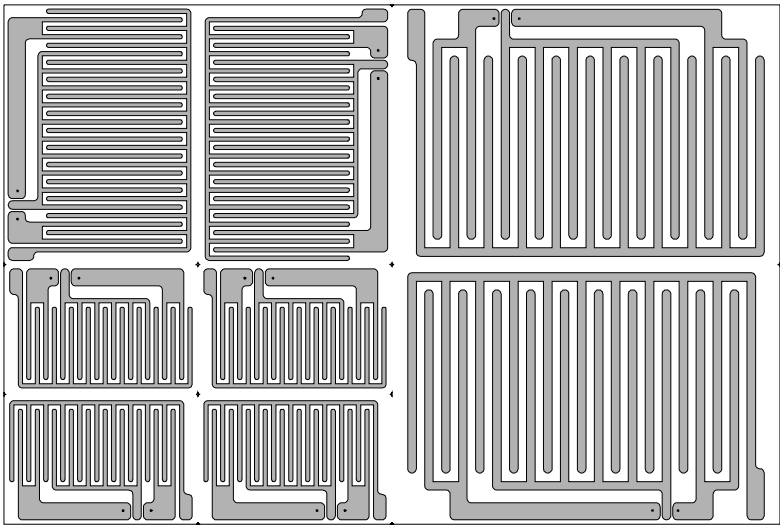

Figure 6-9: *The CAD drawing that was sent to Polyflon as the plan for the production of the 10 mm and 20 mm sensors. A separate drawing was required showing where the holes should be drilled. Note the cross hairs which are helpful when cutting the sensors apart with a shear.*

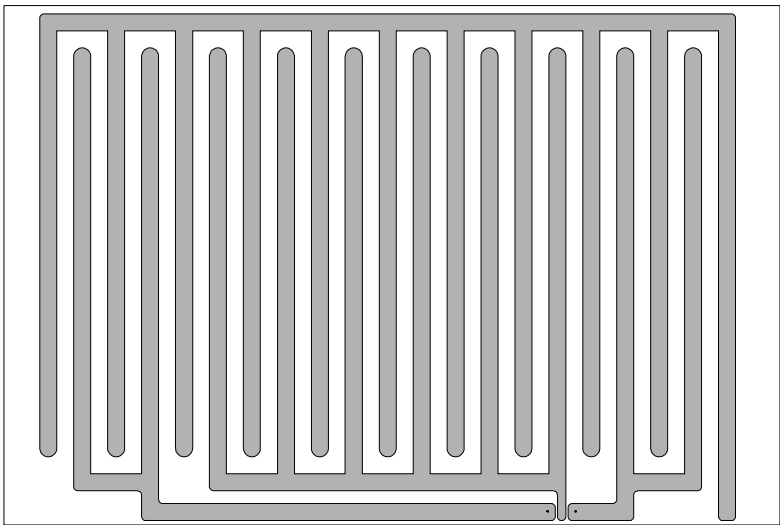

Figure 6-10: *The plan for the 40 mm wavelength sensor.*

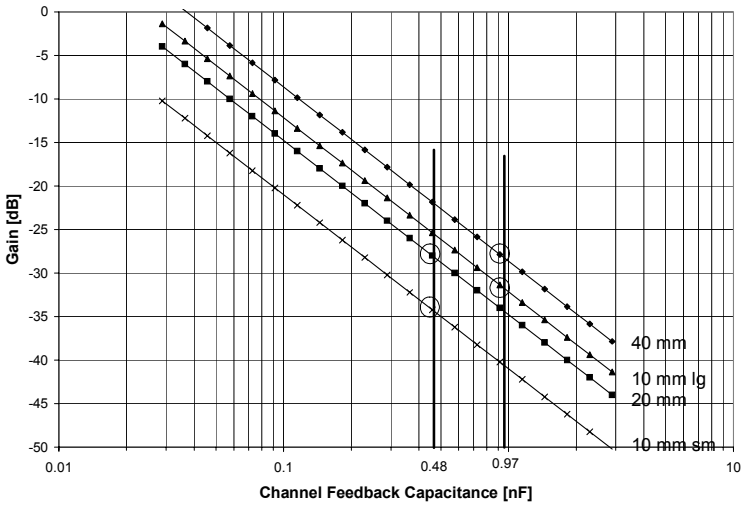

Figure 6-11: *The calculated gain that would result in the SCCM mode if each new sensor measured an infinite half-space of air versus the particular feedback capacitance. The integrating opamp used in the SCCM method saturates more readily at low frequencies for conductive materials than for air, so feedback capacitors with values of 0.48 nF and 0.97 nF were chosen to keep the signal above the noise region of about -40 dB but still avoid saturation of the integrating opamp for any material under test.*

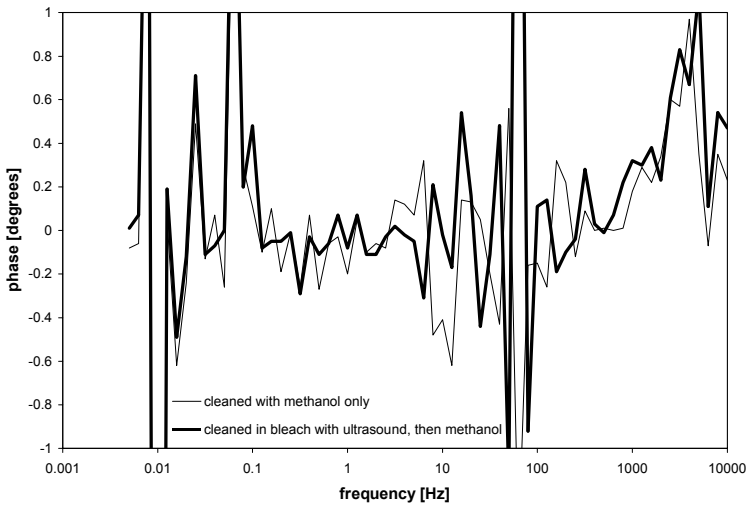

Figure 6-12: *Phase of new small 10mm sensors, comparing one that has been bleached in ultrasound to one that has only been wiped with methanol.*

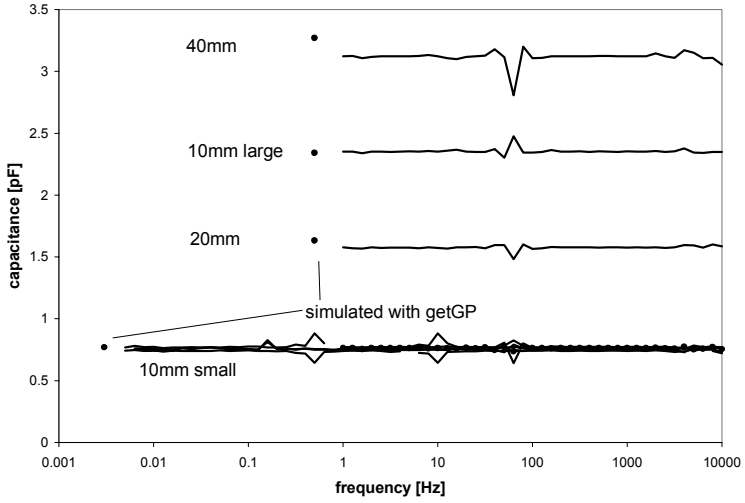

Figure 6-13: *The capacitance of the new sensors when measuring an infinite half-space of air compared to their capacitances calculated by GETGP3 have very good agreement. Multiple passes for the small 10 mm wavelength sensor show that ultrasound cleaning did not affect the sensor's performance.*

The sensors were measured to confirm that they had been fabricated according to the specifications. The capacitance of each sensor array was measured using the 0.48 nF feedback capacitor and compared to the expected capacitance that had been calculated previously using GETGP3. Figure 6-13 shows the measured capacitance for each sensor from 0.005 Hz to 10 kHz compared to the calculated capacitance, which is not a function of frequency for non-conductive sample materials. There was very good correlation between measured and simulated results.

The expected gain for various thicknesses of Lexan^{TM} on top of each of the new sensors was also calculated with GETGP3, but using the 2.98 nF feedback capacitor that was currently inside the interface box. Figure 6-14(a) shows that the 2.98 nF capacitor would be unsuitable for the new sensors, because the gain would be below -47 dB and the signal would suffer from too much noise. No equivalent measurement for comparison was made because none of the required thicknesses of Lexan^{TM} were readily available.

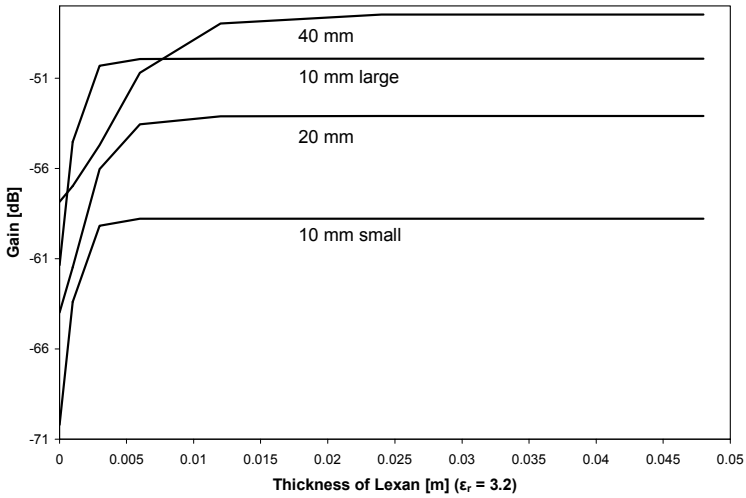

(a) Calculated gain of new sensors with various thicknesses of Lexan using the existing feedback capacitance of Channel 2 of Interface Box 1 (Cf = 2.89nF).

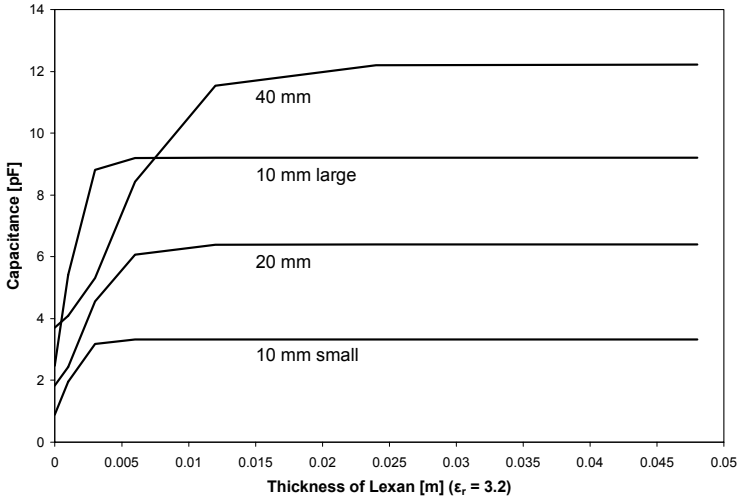

(b) Simulated capacitance of the new large wavelength sensors when measuring various thicknesses of Lexan.

Figure 6-14: *Simulations using GETGP3 of the performance of the new large wavelength sensors when measuring various thicknesses of Lexan.*

6.6 Measurements on Shoes

The new 10 mm, 20 mm and 40 mm wavelength sensors were designed specifically to accommodate shoes. They have a large enough area to cover at least the heel portion of a shoe, and a wide enough electrode spacing to penetrate into a cavity that might be hidden inside the sole of a shoe.

6.6.1 Preparing Sample Shoes with Hidden Cavities

Used pairs of various types of shoes were purchased from the Salvation Army. As the shoes' uppers would not be within the penetration depth of the sensors, they were removed to make the insole more accessible. The shoe bottom was clamped softly to the bed of a milling machine. It was then frozen with liquid nitrogen rendering the rubber and foam stiff. A pocket was milled using a good quality 1" end mill to reduce the chance of destroying the brittle shoe. The pocket was milled 4.0 cm by 7.0 cm and down to about 1 mm of remaining sole. The chips resembled those that are produced when machining steel, but would quickly soften after being removed. The surface finish was smooth and neat which would make modeling the shoe much easier and result in closer correlation between measurements and simulations. The modified and unmodified shoes are illustrated in Figure 6-15.

Shoes are inherently irregularly shaped. The specific placement of the shoe on the sensor pad would be both difficult and more likely to affect the outcome of measurements than would a solid rectangular sample such as a slab of Lexan^{TM}. A method to eliminate variation in contact quality between the sensor pad and the shoe was desired to make the measurements reproducible. First, all the equipment was moved to a laser table. The table has screw holes on a grid pattern all over its surface which allow equipment to be bolted down securely. The relative position of the sensor, the sample and the weight on top would be maintained accurately. Posts were screwed down that would serve as stops for placing the sensors, and the sensors were pushed up against these posts each time a measurement was made. A right angle optical sliding bed was mounted in such a way that it would position a horizontal plate accurately above the laser table surface. The plate could be pushed higher by turning a micrometer, but was spring loaded so that the micrometer could not pull it lower. The 20lb lead weight was bolted to the

Figure 6-15: *A pair of sneakers. The right shoe had a cavity machined into its heel from the inside that might resemble what a terrorist would make to conceal explosives. The left shoe had only the uppers removed so that it could be more easily weighted down when being measured.*

horizontal plate to provide the downward force that would press the sample to be tested onto the sensor pad. Because the plate was held truly horizontal, the weight distribution on the sample would be reproduced exactly every time it was placed on the sensor. Finally, the shoe was fitted with an accurately machined right angled rectangle of plastic that could be lined up with a square grid pattern on the sensor platform, so that the shoe would be placed in the same place on the sensor everytime. It would also allow the effect of moving the shoe across the sensor surface to be determined. Photographs of the laser table setup are given in Figure 6-16.

6.6.2 Experimental Results of Shoe Measurements

Measurements with each of the new sensors (10 mm, 20 mm and 40 mm) were made. The samples were sugar in a ziploc bag, an unmodified shoe, the shoe with its heel cavity empty, and the shoe with its heel cavity filled with the sugar in a ziploc bag. The effect on penetration depth of the sensor wavelength is evident in Figures 6-17(a) to 6-17(f). The 10 mm wavelength sensor response is dominated by the layer of rubber that is left on the sole of the shoe after the

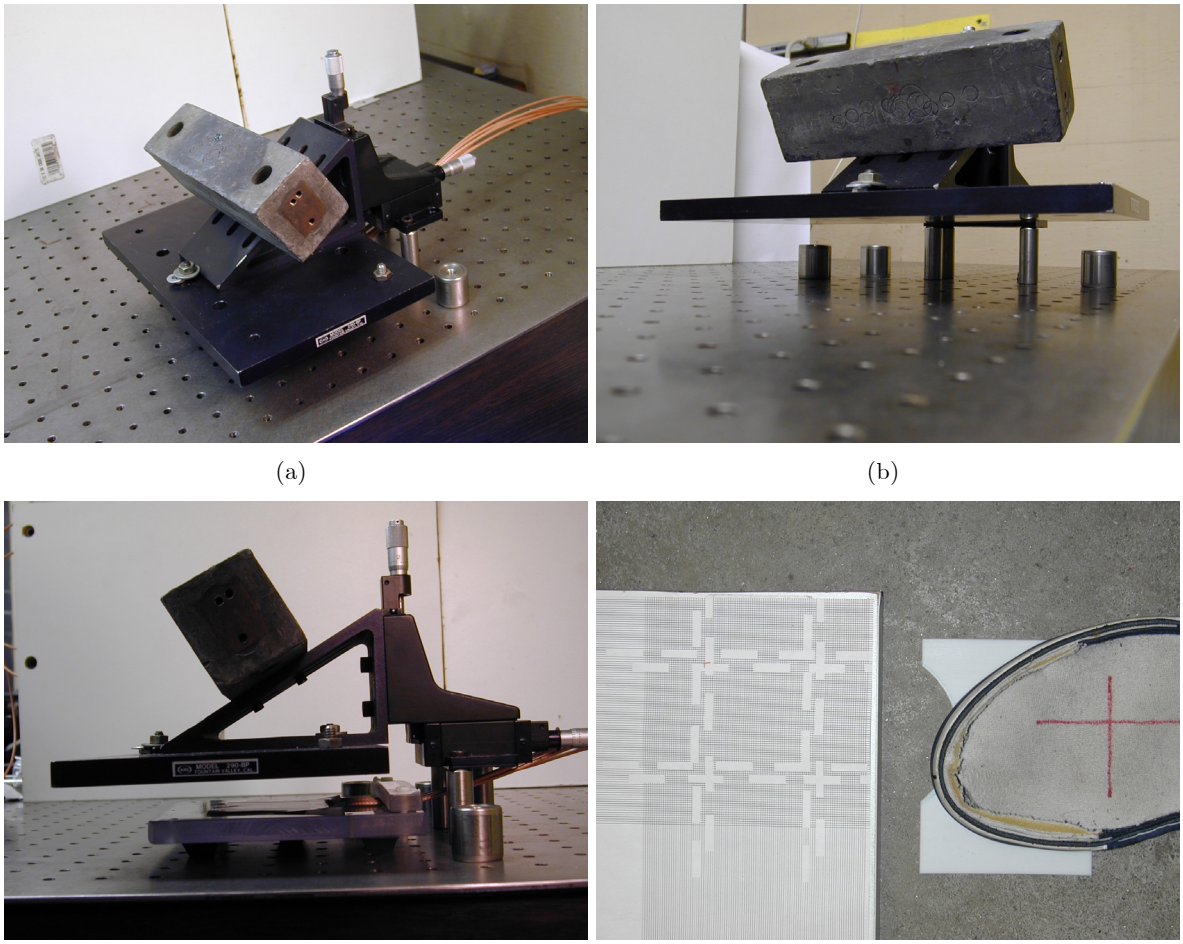

(a) (b)

(c) (d)

Figure 6-16: *Photos of the laser table equipment ensuring a horizontal top ground plane and consistent pressure on irregularly shaped samples such as shoes. (a) The large grey block is a lead weight that provides the downward force. The vertical micrometer barrel provides vertical adjustment of the large grounded horizontal aluminum plate that presses down on the sample under test. (b) The short posts visible below the large horizontal plate serve as stops to aid in positioning the sensors in the same place every time. (c) A side view shows the sensor in place without a sample on it. (d) The shoe is attached to a right angled piece of plastic that can be lined up with the grid on the sensor platform to ensure accurate placement.*

cavity is machined. For this sensor, the difference in gain and phase curves for the shoe with an empty cavity compared to those for a shoe with a sugar filled cavity are small because most of the electric field passes through the rubber layer, which is common to both sample setups. The 20 mm wavelength sensor response has a greater difference in the gain and phase between the empty and sugar filled shoe. It penetrates twice as far as the 10 mm one and therefore produces a signal that is strongly affected by the cavity. The 40 mm wavelength sensor has such a large surface area that the shoe covers only a fraction of its surface. Most of the electric field passes through the air surrounding the shoe or through parts of the shoe other than the cavity, weakening the effect that the cavity has on the signal.

6.6.3 A Novel Sensor Design and Fabrication Technique

A combination of the 40 mm wavelength sensor's longer penetration depth with the heel-sized area of the 20 mm wavelength sensor can be achieved by reducing the number of fingers on the driving and sensing electrodes, and shortening them. For modeling purposes this is not desirable because it violates the approximation that the sensor is two-dimensional with negligible edge effects. Nonetheless, an extreme simplification of the interdigital sensor is one with a single driving electrode finger next to a single sensing electrode finger. The space between the centers of the fingers is nominally the wavelength, and edge effects must be taken into account when modeling the sensor.

A two strip sensor as described above, and pictured in Figure 6-18 was built in the lab. A sheet of 0.5mm thick Teflon was used as the substrate. A 5.0 cm wide strip of aluminum shielding tape was applied to the back to serve as the grounded backplane. Two parallel 13.0 mm wide strips of copper shielding tape were applied to the front with a 13.0 mm gap between them, to serve as the driving and sensing electrodes. The sensor was attached to an aluminum plate with double sided tape, and cables were soldered to each conductor to allow the sensor to be connected to the Short Circuit Current Mode signal interface box. An amplifier channel with a 0.48nF feedback capacitor was used.

The new sensor was tested by using it to measure combinations of the shoe with the dielectric materials Teflon^{TM}, sand, wood and sugar. For each respective material, Figures 6-19(a), 6-19(c), 6-20(a) and 6-20(c) show the frequency and magnitude shift of the gain response between

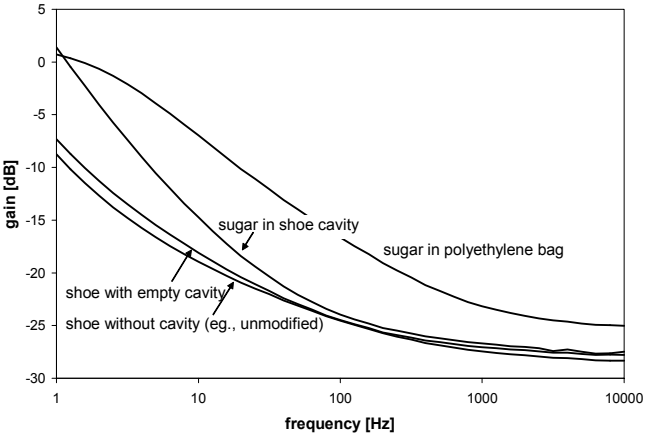

(a) Gain of large $\lambda = 10$ mm sensor.

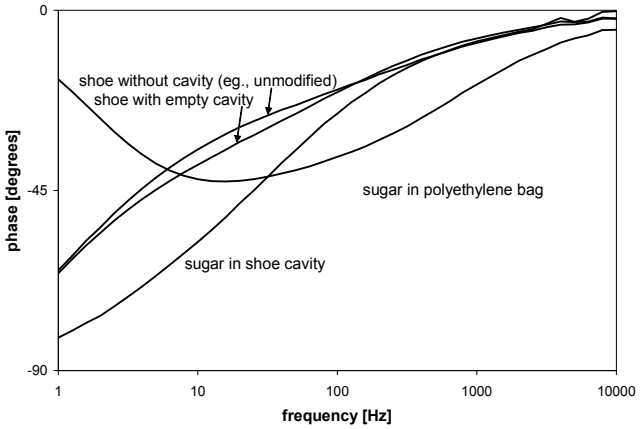

(b) Phase of large $\lambda = 10$ mm sensor.

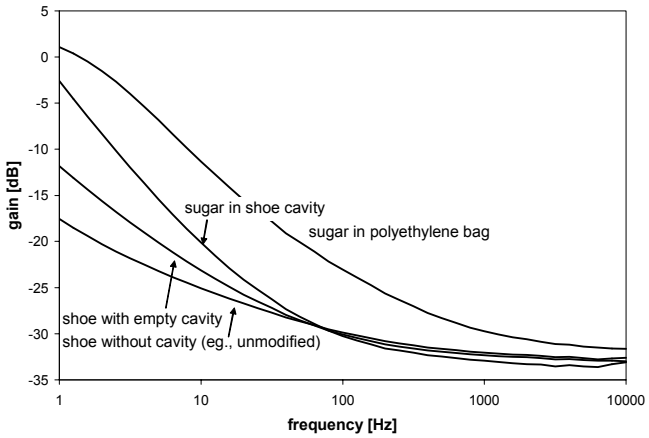

(c) Gain of $\lambda = 20$ mm sensor.

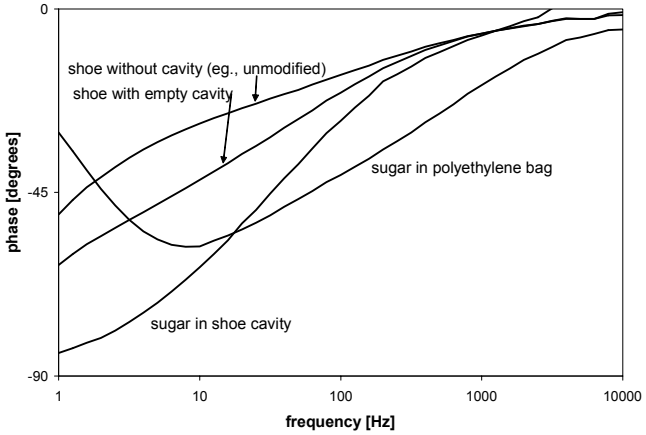

(d) Phase of $\lambda = 20$ mm sensor.

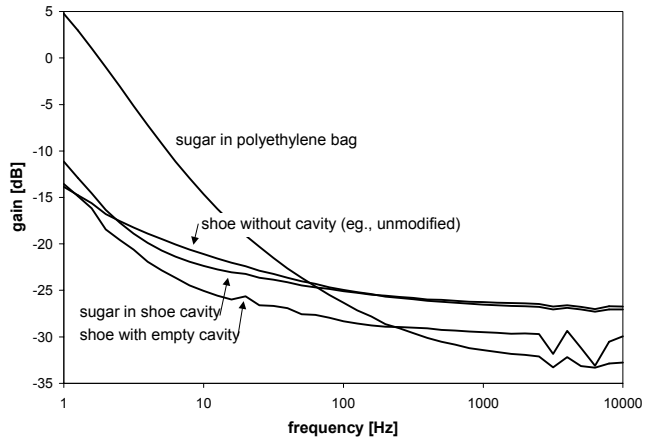

(e) Gain of $\lambda = 40$ mm sensor.

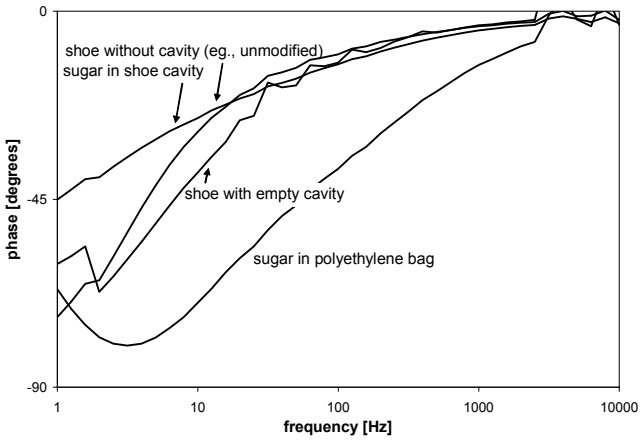

(f) Phase of $\lambda = 40$ mm sensor.

Figure 6-17: *Gain and phase measurements using the large wavelength sensors (10 mm, 20 mm and 40 mm wavelengths) for shoe heels that are unmodified, have an empty cavity, or have a cavity filled with sugar. Each sensor's response depends on its electric field penetration depth into the shoe. Figures (a) and (b): 10 mm wavelength response is dominated by the 3 mm thick rubber beneath heel cutout; Figures (c) and (d): 20 mm wavelength response is the desired combination of rubber and air or sugar in heel; (e) and (f): 40 mm wavelength response is dominated by air and rubber region surrounding sugar.*

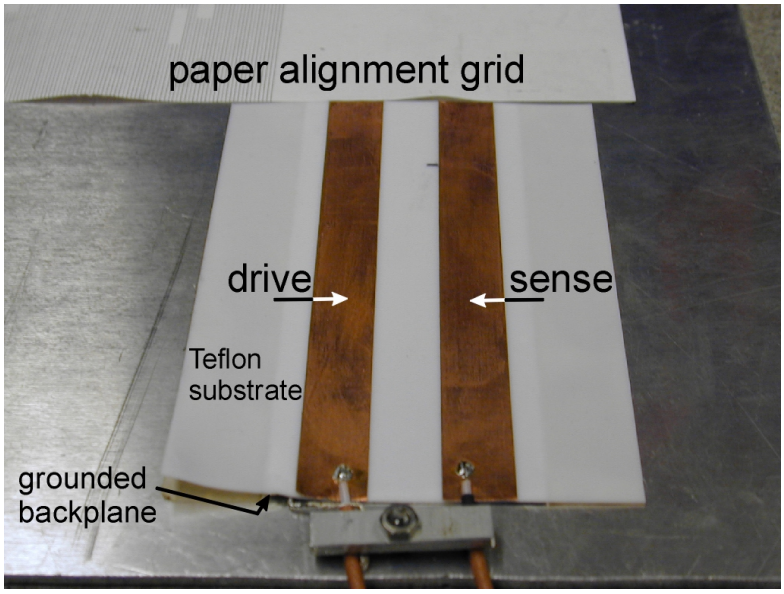

Figure 6-18: *The two strip sensor, consisting of one single driving electrode finger (left) and one single sensing electrode finger (right) with the guard electrode wire attached to the 50 mm wide section of aluminum shielding tape that is on the bottom of the Teflon substrate, in electrical contact with the aluminum plate that supports the sensor. A sheet of paper with a fine grid printed on it serves to align materials under test at the same position every time they are measured, for repeatability.*

the unmodified shoe measurement compared to the shoe with a sample-filled cavity. An upwards frequency shift is indicative of an increase in conductivity, while higher signal gain is caused by an increase of the dielectric constant, as discussed in Section 2. While this simplified sensor shows in Figure 6-20(c) only a 2dB gain difference and no phase difference between the unmodified shoe and the shoe with a sugar-filled cavity, the 20 mm wavelength sensor was able to detect a frequency shift of half a decade and a 1dB increase in gain (Figure 6-17(c)). The measurement data from the 20 mm wavelength sensor is more likely to distinguish the sugar sample hidden in the shoe when it is analyzed by the inverse model solver, and this makes the 20 mm wavelength sensor more effective. On the other hand, the simplified sensor did perform better than the 40 mm wavelength sensor (Figure 6-17(e)) when judged by the same criteria. This is probably an advantage due to its smaller surface area.

Although the simplified sensor did not improve on the 20 mm wavelength classical interdigital dielectrometry sensor, it does show that tailoring the sensor to the sample to be tested can be an important factor in the design of the dielectrometry system. Since shoes are quite variable in their dimensions and material composition, it may be necessary to develop a sensor with reconfigurable geometry. One example is the segmented sensor discussed and studied in detail in Section 3.3.1.

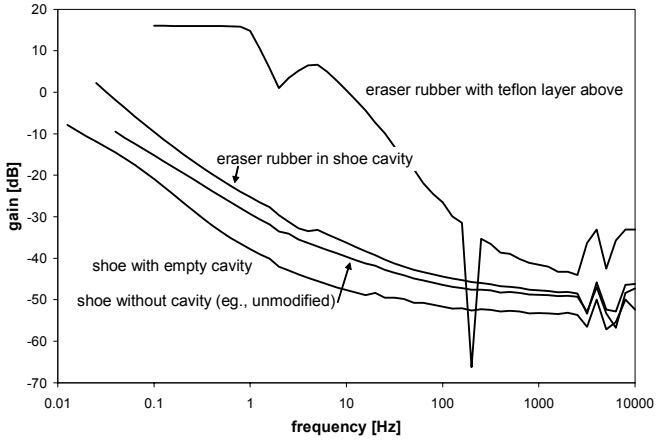

(a) Gain of eraser samples.

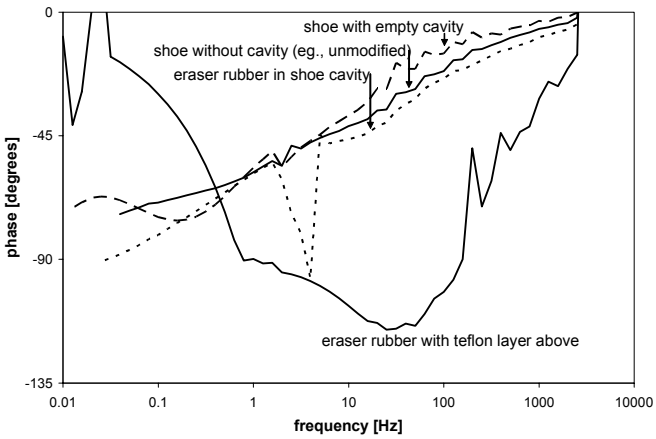

(b) Phase of eraser samples.

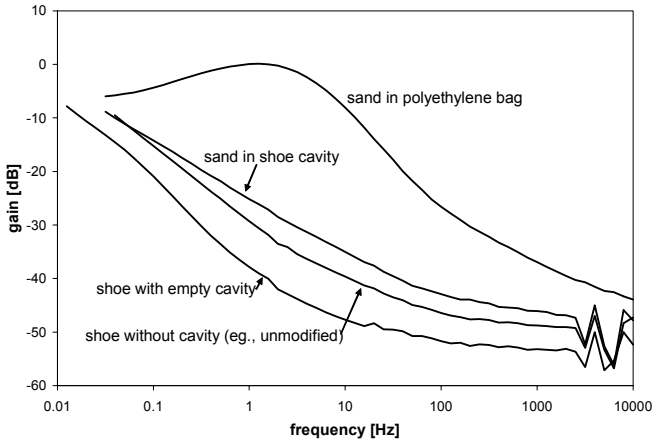

(c) Gain of sand samples.

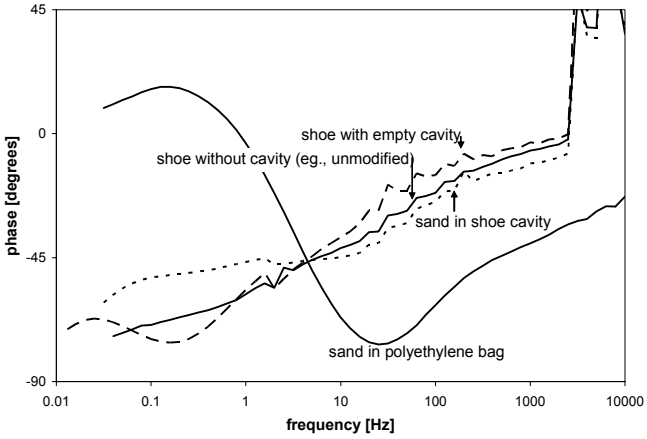

(d) Phase of sand samples.

Figure 6-19: *Measured gain and phase of two-strip sensor for a Staedtler rubber eraser and sand, materials that may be explosive simulants. The feedback capacitance was 0.48 nF for all measurements.*

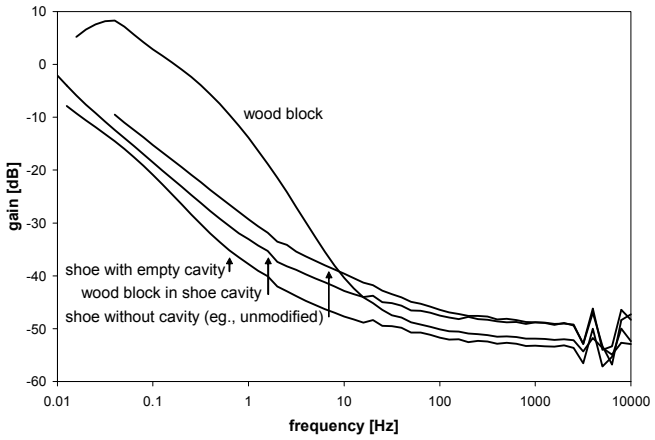

(a) Gain of wood samples.

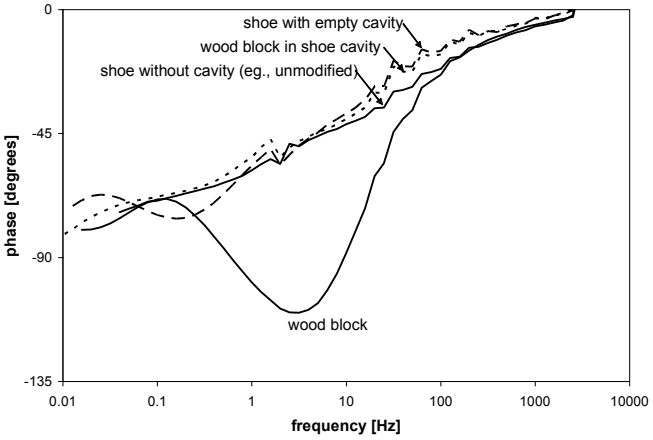

(b) Phase of wood samples.

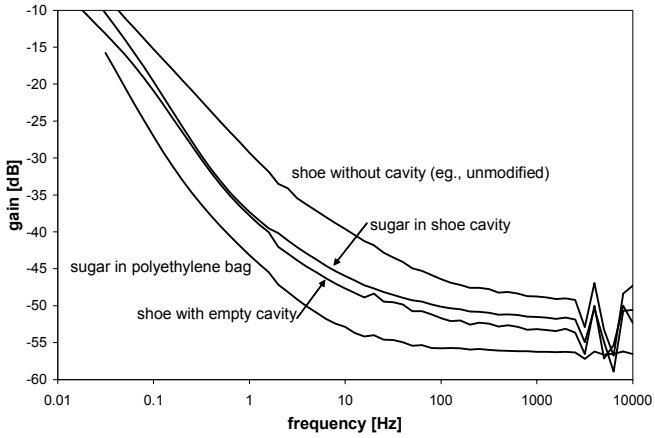

(c) Gain of sugar samples.

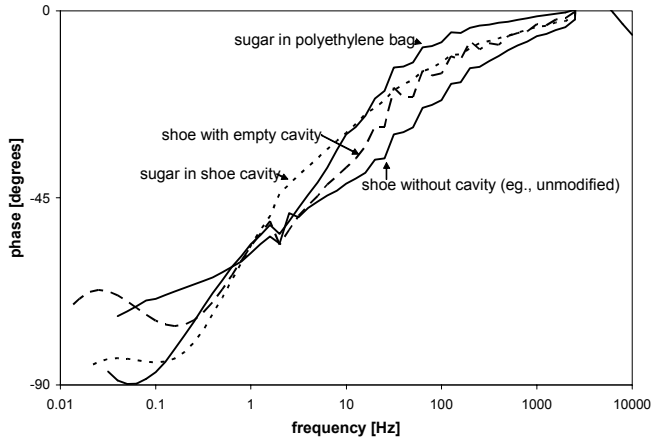

(d) Phase of sugar samples.

Figure 6-20: *Measured gain and phase of two-strip sensor for wood and sugar, materials that may be explosive simulants. The feedback capacitance was 0.48 nF for all measurements.*

Part IV

Summary, Conclusions, and Future Work

Chapter 7

Summary and Conclusions

Theoretical modeling of the sensor and the material under test was conducted with the finite element analysis package Maxwell 2D and the analytic/numerical mathematical models GETGP3 and ESTLSQ for material property estimation. Maxwell 2D and GETGP3 both solve the parameter estimation problem in the forward direction: that is, they calculate the expected response of the sensor given all electrical property and geometry information about the material under test and the sensor parameters. These programs were shown to converge for four sample cases of layered materials under test. Maxwell 2D was used to calculate the capacitance of a differential segment of the sensing electrode for the purpose of designing a next generation segmented interdigital sensor that could be optimized for a variety of penetration depths. It was found that segmenting the sensing electrode increases the penetration depth of the sensor but reduces the signal strength. GETGP3 was shown to reasonably converge to the results of actual measurements for four sample materials, proving its ability to distinguish between materials with moderately different dielectric constants. ESTLSQ was also shown to reasonably converge to the known dielectric constant of air, Lexan and Teflon but was sensitive to thickness of the air gap between the sensor and the material under test. The exercises show that dangerous material hidden in the sole of a shoe could be detected and identified if it lies within the penetration depth of the sensor and if it is sufficiently different in its complex dielectric nature from the legitimate shoe material.

The operation of existing dielectrometry equipment in the lab, including sensors, controller boxes and interface boxes, was verified. Any equipment that was not functioning properly was

repaired, except for controller box B which still requires a new AD711KN chip. The important parameters of the sensors and interface boxes were measured and confirmed. Experiments using interdigital sensors with wavelengths ranging from 1 mm to 40 mm in the frequency range of 0.005 Hz to 10 kHz first on homogeneous materials such as air, sand, sugar, salt, wood, Lexan, Teflon, and paper and later on actual shoes and representative materials that simulate explosives, such as sugar, show that the materials can be recognized based on their complex dielectric properties as extracted from experimental data using an inverse parameter solver for material property estimation. Three methods of measuring the transadmittance of the dielectrometry sensor, including the short circuit current mode, the floating voltage guard plane mode, and a commercial Hewlett-Packard 4192A impedance analyzer, produced comparable results. The impedance analyzer extended the frequency range to 13 MHz. New sensors with wavelengths of 10 mm, 20 mm and 40 mm, in the size range that is estimated to be appropriate for measuring shoes, were able to distinguish actual shoe samples that had variously modified soles to simulate hidden materials. The new sensors performed better than the shorter wave length sensors because they had a greater penetration depth and a larger area. A simplified two-strip sensor did not perform very well in identifying materials but illustrated that sensor geometries tailored to shoes may be useful.

The ability of the dielectrometry system to precisely identify materials from a database of hundreds or thousands is presently limited by measurement noise, contact quality and sample placement inconsistency. Likewise, variations due to moisture content and other contamination present challenges to future development of the technology.

Chapter 8

Suggestions for future research

Future development and possibly commercialization of the dangerous material detection system requires continued research. New researchers in this technology require a solid understanding of the physics and theory of dielectrometry before serious measurements and equipment design are undertaken.

The first step should be an in depth analysis of the error in the material property estimates due to signal noise and contact air gaps. The inverse parameter estimator ESTLSQ is sensitive to signal noise and inaccuracies in poorly known quantities such as the air gap and surface roughness between the sensor and the material under test. The analysis should follow from preliminary work in ([10], pp. 307-320) and concentrate on the combined effect of multiple layers, discontinuity in the directions parallel to the sensor surface, unknown air gaps, surface roughness, and signal noise. Error margins should be found for the estimated dielectric properties of materials in realistic sample cases, and these error margins will have to be accomodated during the material identification process. The maximum allowable size of error margins for the material identification process will define the limit for all un-modelled variables, such as air gap thickness, signal noise, and the extent to which the sample under test is not continuous in the directions parallel to the sensor surface. The question of non-unique solutions to the inverse problem is contained in this task. Ultimately this analysis will tell whether dielectrometry detection of hidden explosives in a shoe is actually feasible, and if it is, how reliable it can possibly be.

Concurrently, accurate knowledge of the material properties of both legitimate shoe ma-

terials (leather, rubber, cardboard, etc.) and target dangerous materials (explosives) should be composed from published data and from in-house measurements where necessary. This knowledge is necessary for applying the results of the error analysis to sample cases. A crucial component of this step is to discover the sensitivity of all the materials to moisture, temperature and other factors and to assess whether the dielectric properties of distinct materials overlap when these variables are taken into account. If the properties of legitimate and target materials do overlap, a method to account for these factors will be necessary.

After considerable theoretical analysis, real measurements should begin on idealized "shoes under test" such as machined blocks of Teflon, leather, rubber, Lexan and other plastics. The first step will be to reduce the predicted un-modelled variables, and any others that arise, to the limits set by the error analysis. Confirmation that the error margins of material dielectric property estimates do lie within their acceptable ranges when these limits are met should be made using real measurement data as the input to ESTLSQ. For example, when a stack of three sheets of different materials is measured, the complex dielectric constants and thicknesses of the sheets estimated by ESTLSQ should be closer to the true values for these materials than to any other material in the list of both legitimate and target materials so that a positive identification can be made with confidence.

Once measurements on idealized shoes-under-test are successful, the experimentation can move to real shoes and eventually to real shoes with real dangerous materials hidden in them. The same criteria as for the idealized shoe will have to be met at each step: that is, for any measurement, the materials must be distinguishable from a list of all possible legitimate and target materials by the property estimates from ESTLSQ. Segmenting the sensing electrode to increase penetration depth could be an important strategy in improving sensor performance.

Successful identification of the materials in shoes is likely to be very difficult. Significant advancements in the sensor design, the sensing and driving electronics, and possibly the mathematical models will probably be necessary. These advancements will come about when specific limitations in the present technology are identified. Thus a solid theoretical analysis of what is actually required from the technology should first be conducted; next, the technology should be tested to see whether it meets these needs; and finally, any shortfalls should be overcome by engineering design.

A student beginning research in the field of dielectrometry would benefit greatly by reading the theses [1] to [4] and especially [5] to [12], while being introduced to the dielectrometry measurement equipment but before beginning serious experimental analysis.

Appendix A

Properties of Explosives

The permittivity and conductivity of various rubber and leather materials that might be commonly found in shoes are plotted in Figures A-1 and A-2. The plots show that many of these materials are slightly dispersive and that some, such as the leather sole, are highly dispersive. The dispersivity of a material can be used as an identifying feature in dielectrometry tests. One disadvantage, however, is that leather's dispersivity is related to its moisture content, which is apparent when the permittivity for a leather sole is compared to that of a dried leather sole. Because the moisture content of a test shoe will not necessarily be known, a wide range of permittivity for hydrophilic shoe materials such as leather will have to be accomodated in the inverse parameter solution to identify the materials in the shoe. The relative permittivity, the loss tangent $\tan\delta = \frac{\sigma}{\varepsilon\omega}$, and the conductivity of the dry and moist explosive trinitrotoluene (TNT) are plotted in Figures A-3, A-4 and A-5 respectively. Like leather, TNT has quite different complex dielectric characteristics when dry and moist.

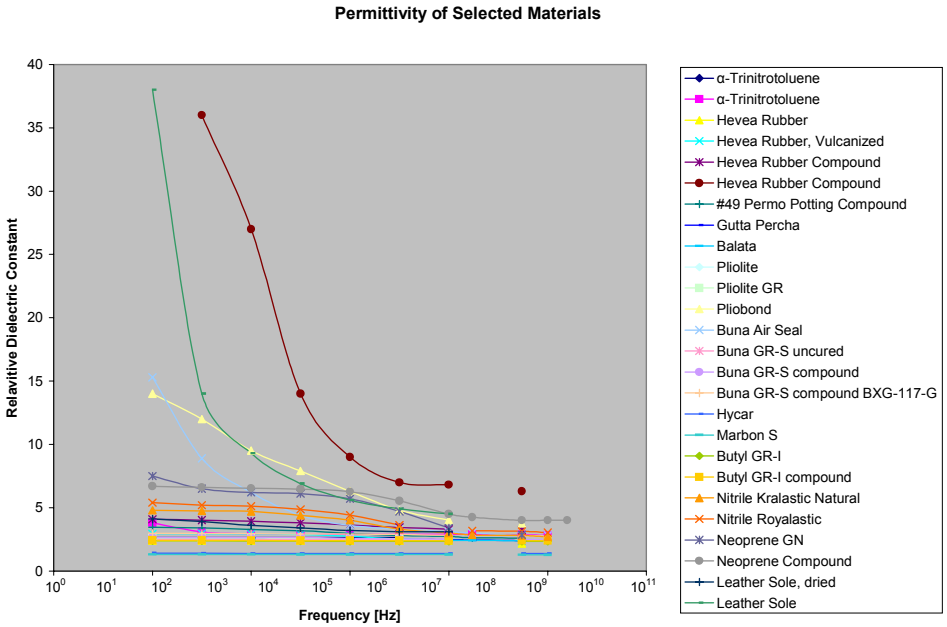

Figure A-1: *Permittivity of rubber compounds that may be commonly used in shoes, together with trinitrotoluene, a representative explosive material. Data taken from [29].*

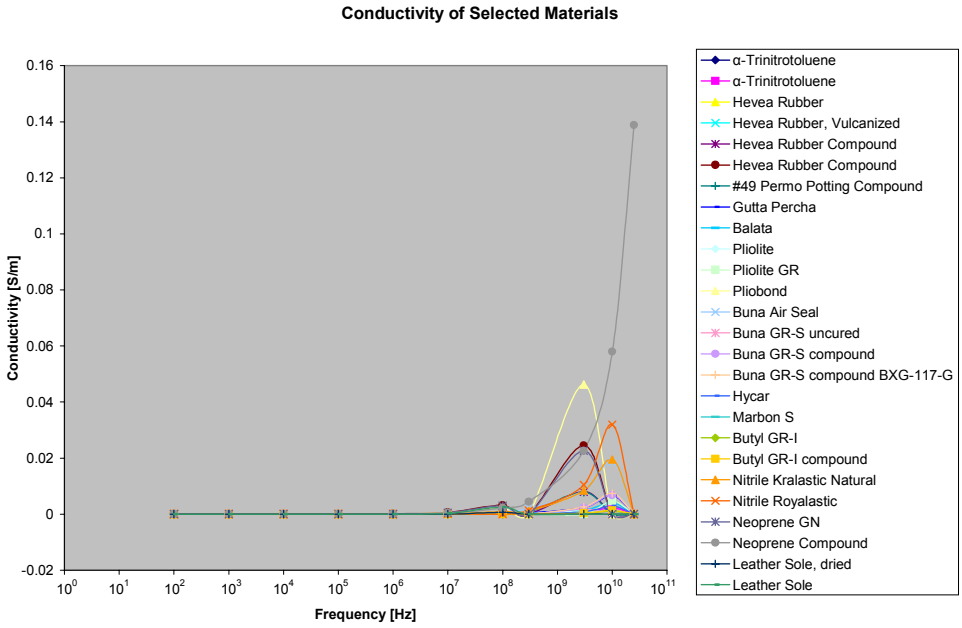

Figure A-2: *Conductivity of rubber compounds that may be commonly used in shoes, together with trinitrotoluene, a representative explosive material. Data taken from [29].*

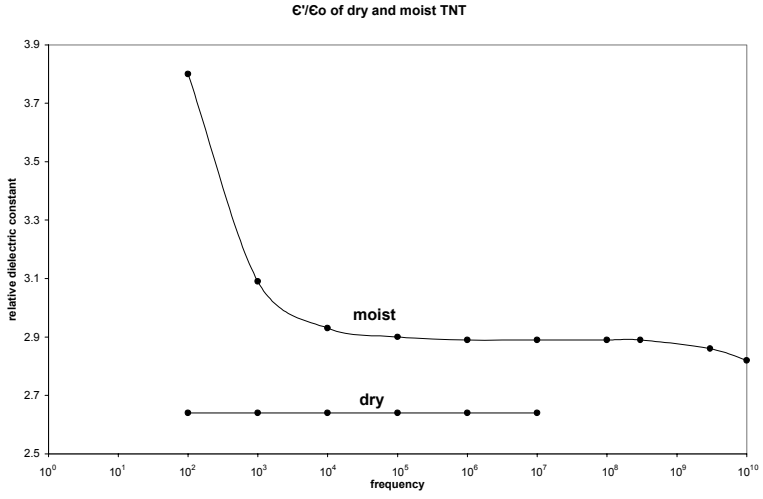

Figure A-3: *Permittivity of trinitrotoluene, dry and moist.*

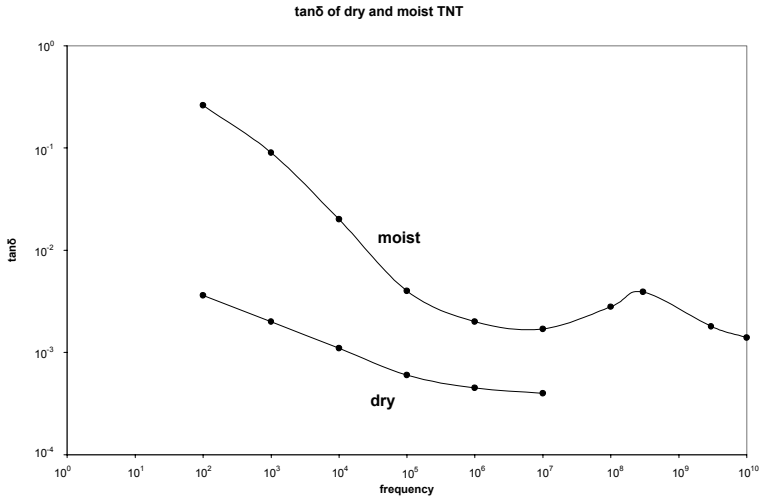

Figure A-4: *Loss tangent of trinitrotoluene, dry and moist.*

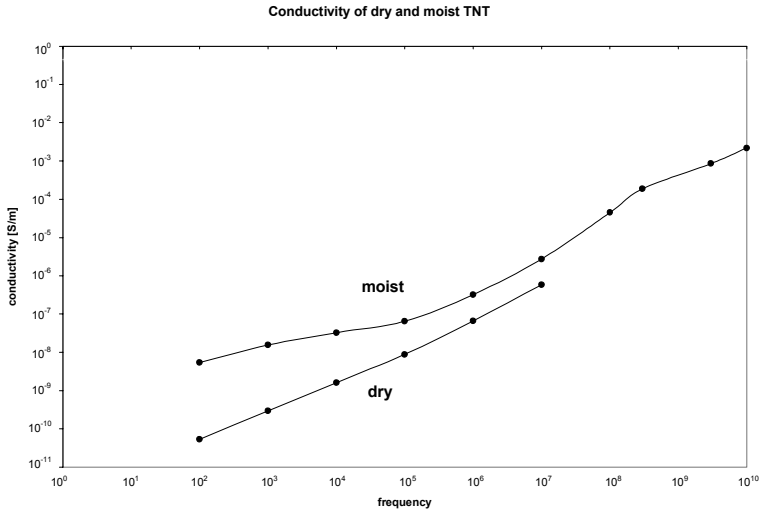

Figure A-5: *Conductivity of trinitrotoluene, dry and moist.*

Appendix B

Dielectrometry Measurement System Specifications

B.1 System Specifications and Commonly Used Constants

The specifications of the equipment after it was thoroughly tested are listed. Table B.1 lists the specs for the controller boxes; Tables B.2 and B.3 list the specs for the short circuit current and floating voltage interface boxes, respectively, Table B.4 lists the sensor parameters, and Table B.5 lists common constants that are used in the research.

ID	Baud Rate	Response to [VE]	comment
A	9600	[VE,1.7,97,2,12,LEES GPM/ACS Controller]	works
B	9600	[VE,1.7,97,2,12,LEES GPM/ACS Controller]	requires new AD711KN chip
C	9600	[VE,1.7,97,2,12,LEES GPM/ACS Controller]	works
D	9600	[VE,1.5,91,9,5,LEES GPM/ACS Controller]	use only for FVGPM mode
E	4800	[VE,1.5,91,9,5,LEES GPM/ACS Controller]	use only for FVGPM mode

Table B.1: *The condition of the controller boxes. The version 1.5 boxes cannot be used for Short Circuit Current Mode measurements because they do not have the necessary digital outputs that send the excite, discharge and attenuate signals at the beginning of a measurement run.*

	$C_{Fmeasure}$ ($C_{Fnominal}$) [nF]			
ID	Channel 1	Channel 2	Channel 3	comment
1	9.81(10)	2.89(3)	2.91(3)	switch=down to disable discharge
2	0.99(1)	0.97(1)	2.98(3)	switch=up to disable discharge
3	9.95(10)	12.59(13)	3.00(3)	switch=up to disable discharge
4	0.480(0.47)	x(1)	x(3)	switch=up to disable discharge

Table B.2: *The feedback capacitance of the channels of the Short Circuit Current Mode interface boxes. The board for each channel resides at the bottom of the box, and is marked with a number x.y, where x represents the box number and y the board number. For example, board 1.2 has a feedback capacitance of 2.89 nF. The boards can be freely interchanged.*

	$C_{Lmeasured}$ [pF]			
ID	Channel 1	Channel 2	Channel 3	comment
6	12.41	12.53	12.41	works
7	49.94	102.0	222.0	works

Table B.3: *The load capacitance for each channel on the Floating Voltage with Guard Plane mode interface boxes.*

	sensor:	Zahn 2 and Kang 98			sm 10 mm	lg 10 mm	20 mm	40 mm
Substrate material	Units	teflon						
Substrate permittivity	[F/m]	1.86e-11=2.1ε_0						
Substrate thickness (h)	[m]	0.000254						
metal thickness	[μm]	17.8	17.8	17.8	35.5	35.5	35.5	35.5
wavelength (λ)	[m]	0.001	0.0025	0.005	0.01	0.01	0.02	0.04
normalized thickness ($\frac{h}{\lambda}$)	-	0.254	0.102	0.0508	0.0254	0.0254	0.0127	0.00635
interelectrode spacing	-	0.25	0.25	0.25	0.25	0.25	0.25	0.25
meander length	[m]	0.251	0.253	0.255	0.271	0.826	0.68	1.497
$\frac{1}{\varepsilon_{substrate} meanderlength}$	[nF^{-1}]	214	212.5	211	198.4	65.09	17.10	35.91
capacitance in air	[pF]	3.212	1.542	0.963	0.769	2.345	7.549	3.258

Table B.4: *Specifications for all the sensors used in the dielectrometry experiments.*

Constant	Units	Value
Air permittivity	[F/m]	8.85e-12
Teflon Permittivity	[F/m]	1.86e-11†
Teflon Conductivity	[S/m]	0
Kapton Permittivity	[F/m]	
Lexan Permittivity	[F/m]	2.81e-11†
Polyethylene (Ziploc bag) Permittivity	[F/m]	3.54e-11 to 4.43e-11†

Table B.5: *Common material property values used in dielectrometry experiments. †Data sources for material dielectric constants are: Lexan [30]; Teflon [32]; polyethylene [31].*

Bibliography

[1] S.L. Garverick, "A.C. measurements with a depletion-mode charge-flow transistor," S.M. thesis, Department of Electrical Engineering and Computer Science, Massachusetts Institute of Technology, Cambridge, MA, 1980

[2] H.L. Lee, "Optimization of a resin cure sensor," Ph.D. thesis, Department of Electrical Engineering and Computer Science, Massachusetts Institute of Technology, Cambridge, MA, 1982

[3] L. Mouayad, "Monitoring of transformer oil using microdielectric sensors," S.M. thesis, Department of Electrical Engineering and Computer Science, Massachusetts Institute of Technology, Cambridge, MA, 1985

[4] M.C.W. Coln, "A high performance dielectric measurement system," Ph.D. thesis, Department of Electrical Engineering and Computer Science, Massachusetts Institute of Technology, Cambridge, MA, 1985

[5] M.C. Zaretsky, "Parameter estimation using microdielectrometry with application to transformer monitoring," Sc.D. thesis, Department of Electrical Engineering and Computer Science, Massachusetts Institute of Technology, Cambridge, MA, 1987

[6] P. Li, "Low frequency, millimeter wavelength, interdigital dielectrometry of insulating media in a transformer environment," S.M. thesis, Department of Electrical Engineering and Computer Science, Massachusetts Institute of Technology, Cambridge, MA, 1987

[7] P.A. Von Guggenberg, "Applications of interdigital dielectrometry to moisture and double layer measurements in transformer insulation," Ph.D. thesis, Department of Electrical

Engineering and Computer Science, Massachusetts Institute of Technology, Cambridge, MA, 1993

[8] Y.K. Sheiretov, "Dielectrometry measurements of moisture dynamics in oil-impregnated pressboard," S.M. thesis, Department of Electrical Engineering and Computer Science, Massachusetts Institute of Technology, Cambridge, MA, 1994

[9] D.E. Schlicker, "Flow Electrification in Aged Transformer Oils," S.M. thesis, Department of Electrical Engineering and Computer Science, Massachusetts Institute of Technology, Cambridge, MA, 1996

[10] A.V. Mamishev, "Interdigital Dielectrometry Sensor Design and Parameter Estimation Algorithms for Non-Destructive Materials Evaluation," PhD thesis, Department of Electrical Engineering and Computer Science, Massachusetts Institute of Technology, Cambridge, MA, May 1999.

[11] A. Lu, "Model based landmine detection using dielectrometry," M.Eng thesis, Department of Electrical Engineering and Computer Science, Massachusetts Institute of Technology, Cambridge, MA, 1999

[12] Y. Du, "Measurements and Modeling of Moisture Diffusion Processes in Transformer Insulation Using Interdigital Dielectrometry Sensors," Ph.D. thesis, Department of Electrical Engineering and Computer Science, Massachusetts Institute of Technology, Cambridge, MA, 1999

[13] Mamishev, A.V. S.R. Cantrell, Y. Du, B.C. Lesieutre, and M. Zahn, "Uncertainty in Multiple Penetration Depth Fringing Electric Field Sensor Measurements," IEEE Transactions on Instrumentation and Measurements, Vol. 51, No. 6, pp. 1192-1199, December 2002.

[14] Mamishev, A.V., A.R. Takahashi, Y. Du, B.C. Lesieutre, and M. Zahn, "Parameter Estimation in Dielectrometry Measurements," Journal of Electrostatics Vol. 56, pp. 465-492, 2002.

[15] Mamishev, A.V., Y. Du, J.H. Bau, B.C. Lesieutre, and M. Zahn, "Evaluation of Diffusion-Driven Material Property Profiles Using a Three-Wavelength Interdigital Sensor," IEEE

Transactions on Dielectrics and Electrical Insulation, Vol. 8, No. 5, pp. 785-798, October, 2001.

[16] Du, Y., A.V. Mamishev, B.C. Lesieutre, M. Zahn, and S.H. Kang, "Moisture Solubility for Differently Conditioned Transformer Oil," IEEE Transactions on Dielectrics and Electrical Insulation, Vol. 8, No. 5, pp. 805-811, October, 2001.

[17] Lesieutre, B.C., A.V. Mamishev, Y. Du, E. Keskiner, M. Zahn, and G.C. Verghese, "Forward and Inverse Parameter Estimation Algorithms of Interdigital Dielectrometry Sensors," IEEE Transactions on Dielectrics and Electrical Insulation, Vol. 8, No. 4, pp. 577-588, August, 2001.

[18] Zahn, M., Y. Du, and A. Mamishev, Interdigital Frequency-Wavelength Dielectrometry Sensor Design and Parameter Estimation on Electric Charges in Non-Conductive Materials, Tours, France, 1-6 July 2001, pp. 87-95.

[19] Du, Y., M. Zahn, B.C. Lesieutre, A.V. Mamishev, and S.R. Lindgren, "A Review of Moisture Equilibrium in Transformer Paper-Oil Systems," IEEE Electrical Insulation Magazine, Vol. 15, pp. 11-20, January/February1999.

[20] Mamishev, A.V., Y. Du, B.C. Lesieutre, and M. Zahn, "Development and Applications of Fringing Electric Field Dielectrometry Sensors and Parameter Estimation Algorithms," Journal of Electrostatics, 46, pp. 109-123, 1999.

[21] Zahn, M. "Optical, Electrical and Electromechanical Measurement Methodologies of Field, Charge and Polarization in Dielectrics," IEEE Transactions on Dielectrics and Electrical Insulation, Vol. 5, No. 5, pp. 627-650, October 1998.

[22] Mamishev, A.V., B.C. Lesieutre, and M. Zahn, "Optimization of Multi-Wavelength Interdigital Dielectrometry Instrumentation and Algorithms," IEEE Transactions on Dielectrics and Electrical Insulation, Vol. 5, No. 3, pp. 408-420, June 1998.

[23] Washabaugh, A.P. A. Mamishev, Y. Du and M. Zahn, "Dielectric Measurements of Semi-Insulating Liquids and Solids," 12th International Conference on Conduction and Breakdown in Dielectric Liquids, July 15-19, 1996, Rome, Italy, pp. 381-384.

[24] Sheiretov, Y. and M. Zahn, "Dielectrometry Measurements of Moisture Dynamics in Oil-Impregnated Pressboard," IEEE Transactions on Dielectrics and Electrical Insulation, Vol. 2, No. 3, pp. 329-351, June 1995.

[25] Polyflon Company. One Willard Road Norwalk, CT 06851 USA, tel (203) 840 7555, info@polyflon.com, www.polyflon.com

[26] M. Brickman, Structural Health Monitoring of Composite Materials using Interdigital Dielectrometry Sensors, Technical report for SAAB Automobile Company, pp 7-8, 2001.

[27] Yanko Sheiretov, Multidimensional Parameter Estimation Routines, User's Manual, LEES, Massachusetts Institute of Technology, Cambridge, MA pp 93-94, May 1997

[28] Moisture Meter Reference Manual, version 1.4 Laboratory for Electromagnetics and Electronic Systems, Massachusetts Institute of Technology, Cambridge, MA, pp 1-14, 1991.

[29] A. R. Von Hippel, editor, *Dielectric Materials and Applications*, MIT Press, 1954.

[30] Lexan permittivity data: http://www.pg-usa.com/raw%20material.PDF

[31] Polyethylene permittivity data: http://www.able.co.uk/dielectric.htm

[32] Teflon Permittivity data: http://www.sftc.co.kr/r&d/r&d%20center_k_3.html